Photo-induced reversible assembly of colloidal polymer nanoparticles

Dissertation

Zur Erlangung des Grades

Doktor der Naturwissenschaften

Am Fachbereich Chemie,

Pharmazie und Geowissenschaften

der Johannes Gutenberg-Universität Mainz

vorgelegt von

Carlos Cárdenas-Daw

geboren in Celaya, Mexiko.

Mainz 2011

Die vorliegende Arbeit wurde in der Zeit von Mai 2009 bis September 2011 am Max-Planck-Institut für Polymerforschung durchgeführt.

Tag der mündlichen Prüfung: 9.12.2011

to my wife

ZUSAMMENFASSUNG

In der vorliegenden Arbeit wurden Polymernanopartikel mit photoresponsiven Markern synthetisiert. Zunächst wurden Nanokugeln mit terminalen Hydroxygruppen (~ 60 nm Radius) in Miniemulsion über die Copolymerisation von Styrol mit dem Vernetzer Divinylbenzol sowie Poly(ethylenglycol)acrylat hergestellt. Im folgenden Schritt wurden diese mit einem photoresponsiven Marker funktionalisiert. Hierfür wurden zwei verschiedene photoaktive Moleküle verwendet: Anthracen, welches bekannt ist für seine kovalent-gebundenen Dimere im angeregten Zustand, sowie Pyren, welches im angeregten Zustand nur kurzlebige Dimere (Excimere) bildet. Die Anbindung der photoresponsiven Marker erfolgte über eine Veresterungsreaktion ihrer korrespondierenden Säurederivate (9-Carboxyanthracen, 4-(Pyren-2-yl)butansäure) mit den terminalen Hydroxygruppen der Nanopartikel über eine intermediäre Bildung des entsprechenden Säurechlorids.

Die erhaltenen photomarkierten Nanopartikel scheinen hoch hydrophobe Strukturen auszubilden. Die Analyse der in wässriger Lösung ausgebildeten lyophoben Strukturen mittels *dynamischer Lichtstreuung* (*DLS*) und *ultramikroskopischer Partikelverfolgung* deutet auf ein Ensemble aus einzeldispergierten Nanopartikeln und einigen wenigen Nanopartikelaggregaten hin. Die relative Anzahl der Aggregate nimmt mit steigender Konzentration des Tensids Natriumdodecylsulfat (SDS) ab. Dies bestätigt die Theorie, dass die Aggregation einem Gleichgewichtszustand entspricht, welcher eine Folge der Lyophobizität der Nanopartikel ist. Die Ausbildung dieser Aggregate wurde mittels rasterelektronenmikroskopischen Aufnahmen bestätigt. Die Bestrahlung von wässrigen Suspensionen der lyophoben, Anthracen-markierten Nanopartikel mit Licht geeigneter Wellenlänge führte zur verstärkten Ausbildung von Aggregaten, die sich mittels DLS und Ultramikroskop verfolgen ließen. Durch eine Ultraschallbehandlung ließ sich der Aggregationszustand wieder aufbrechen. Daraus ergibt sich die Möglichkeit, das System auf reversible Aggregation durch aufeinanderfolgende Zyklen von Bestrahlung mit Licht und Ultraschallbehandlung einzustellen. Analog dazu, führte die Bestrahlung mit Licht von wässrigen, lyophoben Suspensionen der Pyren-markierten Nanopartikel zur verstärkten Ausbildung von Aggregaten. DLS und Ultramikroskopanalysen deuten darauf hin, dass die NP aufgrund von hydrophoben Wechselwirkungen aggregieren. Dieses System konnte ebenfalls reversibel redispergiert werden durch aufeinanderfolgende Zyklen von Bestrahlung mit Licht und Ultraschallbehandlung.

ABSTRACT

Polymer nanoparticles functionalized on the surface with photo-responsive labels were synthesized. In a first synthetic step, polystyrene was copolymerized with the cross-linker divinylbenzene and poly(ethylene glycol) acrylate in a miniemulsion, to produce nano-sized spheres (~ 60 nm radius) with terminal hydroxyl groups, which were functionalized in a subsequent synthetic step with photo-responsive labels. For this purpose, two photo-active molecular structures were separately used: anthracene, which is well known to form covalently bonded dimers upon photo-excitation; and pyrene, which only forms short lived excited state dimers (*excimers*). Acid derivatives of these labels (9-anthracene carboxylic acid and 1-pyrene butyric acid) were bonded to the hydroxyl terminal groups of the nanoparticles through an esterification reaction, via the intermediate formation of the corresponding acid chloride.

The obtained labeled nanoparticles appeared to be highly hydrophobic structures. They formed lyophobic suspensions in water, which after analysis by *dynamic light scattering* (DLS) and *ultramicroscopic particle tracking*, appeared to equilibrate as a collection of singly dispersed nanoparticles, together with a few nanoparticle aggregates. The relative amount of aggregates decreased with increasing amounts of the surfactant sodium dodecyl sulfate (SDS), thus confirming that aggregation is an equilibrated state resulting from lyophobicity. The formation of such aggregates was corroborated using scanning electron microscopy (SEM). The photo-irradiation of the lyophobic aqueous suspensions of anthracene labeled nanoparticles (An-NP) resulted in the formation of higher aggregates, as evidenced by DLS and ultramicroscopy. The obtained state of aggregation could be reverted by sonication. The possibility to re-aggregate the system in subsequent photo-excitation and sonication cycles was established. Likewise, the photo-irradiation of lyophobic aqueous suspensions of pyrene-labeled nanoparticles (Py-NP) resulted in the formation of higher aggregates, as evidenced by DLS and ultramicroscopy. These appeared to remain aggregated due to hydrophobic interactions. This system could also be re-dispersed by sonication and re-aggregated in subsequent cycles of photo-excitation and sonication.

TABLE OF CONTENTS

1 INTRODUCTION

'Smart' is an adjective commonly given to those materials in which certain physical properties can be markedly altered in a controlled manner through changes in the environment. Alterations in shape, conformation, or mechanical properties like viscosity or strength, can be triggered by temperature changes, chemical signaling, force fields, etc. These responsive systems are of particular interest for a variety of practical applications, spanning from simple sensors and actuators to more complex systems like artificial muscles or self-healing materials. A significant feature for these materials is full reversibility, which defines the limits for its continuous operability. This indicates that the modification of a system should fade away either after the stimulus is ceased or as a result of a complementary signal. Complete reversibility implies that after a cycle is concluded and the arrangement goes back to its initial state, there should be no new components in the system. Under this consideration, non-invasive stimulation tools such as force fields or electromagnetic radiation are particularly appropriate. Additionally, those signals can be delivered with convenient modulation in time and high spatial precision.

Nanoparticles represent an exciting field of research. At such dimensional scales, certain 'traditional' materials present novel physical properties which notably differ from those in the bulk (i.e. quantum dots). Heterogeneity based on the combination of different substances at such scales represents a strategy for the creation of new materials with properties strategically resembling those of the precursor components (i.e. magnetic fluids). The size range itself opens the door for ambitious applications like miniature machines or chemical reactors which operate without major disruptions in otherwise inaccessible spaces, such as a living body.

The facile and scalable assembly of nanoparticles at the following mesoscale is a milestone to put into practice their potential benefits. The fabrication of sophisticated systems, such as microscopic electronic or optical circuits, relies on the controlled arrangement of the nano-sized components. Frequently, the properties which define the performance of engineering materials, such as yield strength, ultimately depend on the interaction between collections of homogenous domains of nanometer size scales. The

strategic and fully controlled ordering of nanoparticles up to the macro-scale thus appears as a strategy for high performance materials.

Self-assembly refers to the facile arrangement of components into desirable architectures of higher complexity without direct human intervention. Building blocks are mixed together and, as the name of the process implies, are spontaneously arranged into more complex structures. Such a process is the ultimate approach for the efficient mass production of supra-molecular architectures. The instructions code for the assembling process is dictated by the physical properties of the building blocks which govern their interactions with the continuous medium and between each other. This implies limitations, as not any material will hold the characteristics which are necessary for the assembling procedure to result in the desired architecture. While a broad assortment of nanoparticles has been developed, the possibility to self-assemble them into useful arrangements is limited. There is an inalienable link between the material of which a nanoparticle is composed and its physical properties, which govern the interactions with its surroundings and consequently, the way in which it will arrange in a self-assembly process. It is not always the case that the properties necessary for a preferred arrangement correspond to those of the building blocks desired for its composition. On this regard, composite nanoparticles present a smart strategy to broaden the possibilities. Nanospheres with a hybrid composition of materials can be produced by creative variations of the miniemulsion polymerization technique.[1] A component of interest can be conveniently encapsulated in a polymer nanoparticle. The interactions of such nanostructures with the surroundings are ultimately dictated by the surfacing polymeric material, which has a versatile functionality that can be conveniently modified. Overall, the miniemulsion technique may concede, within a spectrum of possibilities, the preferred self-assembly code to the desired components.

The process of self-assembly can be directed and controlled by the inclusion of responsive functionalities on the building blocks, which modify the interactions governing the assembly process as a result of external stimuli.[2] In this order of ideas, it is of interest to develop *smart* nanoparticles which can be reversibly assembled into mesoscale architectures in a controlled manner. For this purpose, light stands as a convenient method of control, as it is non-invasive and deliverable with time and spatial precision.

1.1 Objective of this project

The reversible aggregation of colloids has attracted attention due to its potential implementation as a responsive functional system. Such systems have been achieved using diverse signaling methods including temperature, pH, solvent polarity, or light.[3] As previously discussed, this last method is a particularly attractive stimulation technique due to the precision with which it can be delivered, and the fact that it is not invasive and does not change the composition of the system, making it particularly fit for the purpose of continuous operation over several response cycles.

The reversible aggregation of colloids through photo-excitation has been achieved by triggering mechanisms which compromise the colloidal stability of the suspended particles.[4] In such systems, the extent of aggregation and the resultant size of the aggregates are not directly controlled by the stimulation signal, but rather pre-established by the interplay of certain parameters related to the construction of the system, which include the type and amount of surface functionalization of the particles, and the resultant compatibility with the selected solvent.

A more direct control of the size of the aggregates has been achieved with the light-induced formation of inter-particle bridges. This has been possible through the incorporation to the surface of the suspended particles, of molecular structures which can be reversibly dimerized through photo-excitation. This approach has been explored for lyophilic colloids, in which not only the colloidal particles are compatible with the solvent, but also the photo-active functionalities. Suspensions in THF of polysiloxane nanoparticles labeled with cinnamate and coumarin photo-dimerizable dyes were successfully aggregated by photo-excitation and subsequently re-dispersed by irradiation at lower wavelengths. A subsequent aggregation cycle was not achieved with these systems, apparently due to the photo-degradation of the labels during the reversion step. [5]

A great number of colloidal systems which are of technological interest are indeed lyophobic, that means, the suspended objects are not compatible with the solvent, which commonly is water. That is the case of several biological systems and industrial

products. After all, colloids represent in several scenarios an alternative for the fluidization of insoluble materials of interest. The extension of photo-induced colloidal aggregation studies to aqueous lyophobic systems remains unexplored and of high interest.

It is the purpose of this work to develop and study a novel system for the controlled and reversible photo-induced assembly of colloidal nanoparticles over multiple cycles, based on polymer nanospheres labeled on the surface with photo-responsive molecular structures. For this purpose, two photo-active molecules are investigated: anthracene, which is well known to form covalently bonded dimers upon photo-excitation; and pyrene, which only forms short lived excited state dimers (*excimers*).

It is intended to produce a versatile model system of responsive nanoparticles which could be conveniently adapted to diverse hybrid compositions of materials. Attention is centered in the controlled formation of aggregates, the reversibility of the process, and its operability over consecutive cycles.

2 THEORETICAL SECTION

2.1 Nanotechnology

Nanotechnology is frequently defined as the manipulation of matter atom by atom and molecule by molecule for functional purposes. Indeed, the deliberate manipulation of matter at the atomic level is by no means a new discipline. Over the course of centuries, a vast body of knowledge has been gathered to comprise the scientific discipline of chemistry. The transformation of matter to fulfill needs of our society is an everyday practice which has reached a high level of sophistication. For instance, oil can be transformed into plastic materials or synthetic drugs, which are designed at the molecular level to emulate natural products. On the other side, the manipulation of matter at the macroscopic scale has also reached high levels of intricacy. Machining techniques to shape all kinds of materials have been developed as part of the engineering sciences. The level of control has reached micrometer scales, which has allowed for instance the emergence of the microchip. Current research in nanotechnology seeks the control of matter at the dimensional scale that lies in between those two *bottom-up* and *top-down* approaches. Thus, the development of this field can be understood as the completion of the missing gap for a comprehensive manipulation of matter from the atomic to macro scale. This is a reason that makes nanotechnology such a multi-disciplinary field of research. Chemists use their synthetic knowledge to arrange atoms into molecules, and push further into the creation of supra-molecular arrangements. Physicists study along the principles and properties of such arrangements of matter. On the other side, engineers continue to push the limits of top-down manipulation of matter through the development of lithographic techniques, while biologists contribute their understanding of living systems, which operate in a high level of complexity at the nanoscale, and can be manipulated for functional purposes.

Full control of matter at the nanoscale represents a very promising strategy to boost the properties of materials and to develop novel functional systems. In the last years, research has resulted in the emergence of exciting applications. An overview of some relevant topics of intense study in the area of nanotechnology is presented in the following section.

Biomedical applications

Relevant applications of nanotechnology in biomedicine include the development of biosensors and targeted delivery systems. These appear as a potential tool to fight cancer, which is one of the greatest threats to human health. Benefits are expected in diagnosis and therapy. Traditional treatments like chemotherapy and radiation are based on killing malignant cells. Adversely, these therapies are not specific enough so the damage of healthy tissues is unavoidable. A strategy to prevent this negative outcome is the development of nano-sized drug carriers which selectively target cancerous cells. In the search for such functional devices, diverse nanostructures have been considered, such as nanotubes, micelles, dendrimers, liposomes, and polymeric shells. Passive targeting based on the *enhanced permeability and retention* (EPR) effect, leads to the accumulation of carriers in the tumor. EPR seems to result from the abnormally accelerated metabolism of cancerous cells. Many nano-carrier therapies based on passive targeting are already in the market. Active targeting on the other side is based on carriers labeled with molecules which bind to overexpressed antigens and to receptors present on the targeted cancerous cells. Such molecules may consist of antibodies, peptides, vitamins, or carbohydrates. The study of an adequate choice is nevertheless difficult due to the multiple factors which may affect the intake of the nano-carriers and their bio-distribution.[6]

The external control of biological systems by force fields based on nanotechnology is also being developed. For instance, the internalization of magnetic nanoparticles in cells is being studied as a tool to control biological processes inside the cell by the application of magnetic fields. This is leading to the investigation of cellular functioning mechanisms like ion channel signaling. In addition to cell research, there are also a number of technological applications, such as the control of cell deposition on substrates for the development of biocompatible interfaces. In this regard, the controlled adhesion and conditioning of cells on synthetic substrates leads to the development of engineered tissue, for which mechanical stimuli are also important to promote its formation, in addition to biological signaling.[7] Moreover, the production of synthetic tissues benefits from nanotechnology also in the development of the necessary growth substrates, which can be constructed out of composite nano-materials which incorporate

biomolecules into the structural scaffolds which direct the binding and growth of the transplanted cells.[8]

Novel electronics and optics

The structuring of materials at the nanometer scale can result in certain cases in the tuning of electrical conductivity properties. The inherent promise for the miniaturization of electronics has emerged as a very active field of research. Examples are radiofrequency transistors based on carbon nanotubes, which are being developed for the amplification of power with low noise levels. This aims to the miniaturization of advanced wireless communication systems, foreseeing the emergence of nano-radios.[9]

Much attention has been centered in the last years to the development of transistors based on graphene, a two dimensional material consisting of graphitic sheets with the thickness of a single atom. Due to its excellent mobility, graphene appears as an adequate option for post silicon electronics, which are prone to reach soon their miniaturization limit. Strips of graphene with nano-sized widths, known as nano-ribbons, have a conductive bandgap which makes them usable as switching transistors.[10] Currently, research efforts are strongly centered in the challenging fabrication of graphene nano-ribbons with well-defined dimensions. The strategies being explored for this purpose include the *unzipping* of carbon nanotubes[11] and the defined synthesis out of polyphenylene precursors, which promises optimal structural definition.[12] A key aspect being investigated for the application of graphenes in electronics and photonics is the development of techniques for its supra-molecular ordering to improve the charge carrier mobility.[13] A milestone in this regard is the possibility to have scalable processes for facile mass fabrication. An approach being actively investigated for the production of materials composed of graphene is the formation of colloidal suspensions of precursors, such as graphite oxide.[14]

Opotoelectronics is another field of interest being expanded through nanotechnology. It refers to the development of devices which function as transducers of electricity to light or vice versa. The functionality of optoelectronic devices like organic solar cells and organic light emitting devices is based on the formation of *excitons* in nanostructured materials.[15] When a photon is absorbed, the excited electron goes to the conduction

band and a positive whole is formed. However, the electron and the hole remain electrostatically bound by Coulomb forces, thus constituting an exciton. The subsequent dissociation into free carriers, the unbound electron and a positive hole, is fundamental for the functioning of photovoltaic devices. This is the step where the structuring of organic opotoelectronic devices at the nanoscale is important. For instance, organic solar cells consist of a mixture of two materials, an electron donor and the acceptor, which form a heterojunction. In order to create a current, the exciton needs to migrate to this heterojunction. Nevertheless, it is globally neutral and nothing drives its diffusion. Therefore, the migration of excitons is random, so a given point where it is generated should have a nearest hererojunction within the distance it diffuses without decaying, thus making nanoscale confinement and delocalization a fundamental aspect for the adequate operation of such systems.[16]

Nanomachines

Nanometer scale machines are perhaps one of the most sophisticated foreseeable outcomes of nanotechnology. Current research is focused on the study of biological systems which convert chemical energy to effective and controlled linear or rotational motion. Bio-motors working as sensors, transport and assembly tools may someday confer materials with properties currently attributed particularly to biological systems, such as self-repair and self-replication. The studied systems include enzymes such as DNA polymerase, and scaffold proteins which transport cargo along neurons.[17]

Synthetic motors inspired in bio-machines are also being developed. Their advantage resides in a higher tolerance for diverse environmental conditions. Conversely, they are still far from the level of sophistication in self-repair and maintenance observed in the biological model systems. A key feature is the molecular arrangement which converts fuel into motion, i.e., potential energy into kinetic energy. The source of energy can be chemical or solar. Photo and electrochemically fueled machines are a main topic of research. Their advantage resides in the possibility to control the systems externally with relative ease, without by-products which pollute the system. Intense research has resulted in the production of systems which are able to transform molecular motion into macroscopic work.[18]

Nanocomposite engineering materials

A composite material results from the physical combination of two or more materials of distinct properties, maintaining an identifiable interface in the final state. A nano-composite results when one of the combined components has dimensions in the nanoscale. With this approach, it is possible to obtain materials with improved properties performing beyond the simple "addition" of those of the components.[19] The field of nano-composites is rather broad and is commonly classified according to the continuous phase.

Polymer matrix composites are the most common form in which engineering plastics are actually put into use. For nano-composites, it is generally the case that the integration of low loads of high performance nanoparticles brings significant improvements of the properties. For instance, the incorporation of carbon nanotubes to a polystyrene matrix at a low content of only 1% weight of filler (aprox 0.5% vol) has resulted in the improvement of elastic stiffness by 36-42% and tensile strength by 25%.[20] The benefits of nano-composites are not only in the mechanical performance, but also in other functional aspects such as gas barrier behavior, electrical properties and charge dissipation. Continuous research is carried in order to improve the properties without sacrificing their ease of processing. The focus is centered in those aspects which directly define the performance, such as the distribution and dispersion of the filler, and the nature of the produced interface. For their fabrication, fillers are incorporated either to a monomer mixture or to the polymer blend by mechanical mixing.[20]

Metallic matrix nano-composites can be fabricated by the in-situ generation of a second nanoscale phase. The formation of ceramic particles by a reaction between the elements in the mixture during processing results in the improvement of the mechanical properties. This approach increases the cleanliness of the interface, the thermodynamic stability, and the homogeneity of the distribution of the nano-phases. Alternatively, when the filler cannot be produced in such a way, metal-matrix nano-composites can also be generated by the addition of available nano-fillers, mixed with the metal matrix either in powder or the molten state. An active field of research is the integration of carbon nanotubes to metallic matrices for structural and functional applications. This is expected to improve the mechanical performance, as well as the enhancement of the

thermal and electrical properties. The key aspects being investigated are the processing techniques to procure an adequate dispersion and interface, with chemical and structural stability of the nanotube. Although not yet commercially available, the potential applications are foreseen in the automotive and aerospace industries for high strength structural components and breaks, and functional application as heat sinks for thermal management.[21]

Ceramic matrix composites are generated with the intention to improve the limitations of ceramic materials, like fracture toughness, creep, fatigue, and thermal shock. In the past, the incorporation of micro-sized fillers has been mostly unsuccessful. Nevertheless, the incorporation of metal nanoparticles has resulted in the improvement of some properties. The filler accumulates in between the grains of the ceramic material, as well as within grains, creating dislocations which contribute to the improvement of strength. Magnetic and electric properties can as well be incorporated this way. A common approach for the incorporation of nano-fillers to ceramic materials is by "mechanical alloying" using ball millers.[19]

Applications in process engineering

Nanofluidic devices represent an application of relevant economic impact due to the potential reduction of costs in industrial energy consumption. The flow of substances through structures smaller than 100 nm increases the interactions between the fluid and the stationary phase, with an overall escalation of the interface per fluid volume, which can be used for more efficient processes, such as separations. For instance, the use of polymer gel for DNA electrophoresis could ultimately be dismissed. Studies of fluid transport phenomena are being carried out, with a potential impact in chemical engineering, analytical chemistry, or energy conversion.[22]

Environmental and health concerns

The development of nanotechnology in numerous fields of prospective applications has raised concerns regarding the potential damage on the environment and public health. The definition for legal purposes of what is a nanoparticle is a milestone in this issue.

The debate is centered around a definition based on size vs. a definition based on the emergence of special size-dependent properties not observed in the bulk material.[23] Potential threats being considered include the disruption of biological processes leading to environmental oxidation.

2.2 Nanoparticles

Nanoparticles are basic elements of nanotechnology for the formation of functional materials. Nanoparticles are widely recognized as particulates in a range from 1 to 100 nm in the three dimensions. The International Organization for Standardization defines a *nanoparticle* as a "Nano-object with all three external dimensions in the nanoscale" (ISO/TS 27687:2008), and *nanoscale* as a "Size range from approximately 1 nm to 100 nm" (ISO/TS 27687:2008). In the following sections an overview is presented of available nanoparticles in the broader sense of the definition.

Semiconductor and metallic nanoparticles

When metals and semiconductors are delimited in nanoscale dimensions, special physical properties emerge which differ significantly from the bulk material. At such sizes, the electronic properties are predominantly governed by quantum mechanics, in contrast with the laws of classic physics for the bulk. Quantum mechanics describes the movement of electrons in a material as waves with wavelengths in the nanometer range. When a conducting or semiconducting material is of size comparable to the wavelength of the confined moving electrons, the quantization of energy becomes more evident. In such a case the electrons behave like the quantum mechanical model of "the particle in a box", in which changes in energy are quantized depending on the dimensions of the box and the allowed wavelengths of the particle which determine the kinetic energy.

A semiconductor particle with all dimensions within a few nanometers and presenting quantization effects is called a quantum dot. It can be excited optically or electrically and emit photons. Quantum dots have applications in light emitting devices, like energy

efficient displays. Other potential applications range from diode lasers to quantum computation.

Colloidal metal nanoparticles have peculiar absorption spectra with bands emerging as a result of surface plasmons. Metals are rich in electrons, which move collectively over the surface. The plasmon bands appear at the resonance frequency for such a movement. The dependence of the resonance frequency on the size of the particle is however not as dramatic as that observed in quantum dots, where small size changes have a marked effect on the spectra.[24]

The methods for the synthesis of metallic and semiconductor nanoparticles are diverse. A few representative examples are described here. Quantum dots can be prepared by the pyrolysis of organometallic precursors which are injected in a hot coordinating solvent, providing discrete coordination which results in the growth of the particle. For instance, CdSe nanoparticles can be prepared through the injection of dimethylcadmium and bis(trimethylsilyl)selenium into the solvent tri-n-octylphosphine oxide (TOPO) or tri-n-octylphosphine (TOP). Another approach is the use of micro-heterogeneous systems, i.e. vesicles, as reaction compartments. Thiols are widely used to stabilize and produce mono-disperse sized particles. For instance, quantum dots of CdSe, CdTe, or HgTe can be produced from the aqueous solutions of precursor metal salts in the presence of stabilizing thiols, such as 1-thioglycerol or thioglycolic acid. The growth of the particle can be initiated by heating the system.[24]

Nanoparticles of noble metals have been well known for some time already. To benefit from their special properties, it is important to get mono-disperse sizes.[25] The reduction of salts is applicable for the production of nanoparticles of several metals, such as platinum and silver. Importantly, sols must be protected by repulsive or steric forces to prevent coagulation. This protection may result from the production method itself, such as in the reduction of $[AuCl_4]^-$ with sodium citrate, which produces nanoparticles stabilized by Coulomb repulsive forces from the ion layers of citrate and chloride ions. Polymers are also commonly used in the preparation of such colloids. The reduction of metal salts in solution can also be accomplished by alternative methods, like radiolysis, which produces reducing agents such as solvated electrons or free radicals upon irradiation, or photolysis, which proceeds with the reduction to zero

valence of the metals under a slow controlled process which prevents the formation of bulk metal. These methods have the advantage of higher cleanliness and homogeneity.

Carbon-based nanoparticles

Graphenes are single layers of carbon atoms arranged in a hexagonal lattice with sp2 hybridization, making and extended pi conjugated system.[26] Great expectations were raised by early measurement on a few layers of graphene which showed charge transport characteristics that make them a promising material for electronic and magnetoelectronic novel applications.[27] Graphene can be produced by simple micro exfoliation of graphite through the adhesive tape peel off method. Other methods include chemical vapor deposition and epitaxial growth. As previously described, novel synthetic methods have been developed to produce graphenes with well-defined dimensions through the cyclo-dehydrogenation of polycyclic aromatic precursors.[12-13] Graphene can be understood as the parent material of fullerenes and nanotubes.[26]

Fullerenes are molecular closed cages formed by carbon atoms arranged in a semi-graphitic curved plane composed of a combination of hexagons and pentagons, although less classic forms may consist as well of heptagons and octagons. C^{60} is the most abundant from and the first one to be discovered.[28] The next most common is C^{70}, which is more elongated. Fullerenes are regularly formed by carbon vapor deposition.

Carbon nanotubes consist of seamless cylindrically-shaped graphene planes.[29] They can be single-walled, or multi walled arranged concentrically. The diameters are in the order of a few nanometers, with lengths up to a few microns.[28] Nanotubes are thermodynamically stable structures formed by growth on metallic catalysts by different methods such as plasma arc discharge between graphitic electrodes, laser ablation on graphite, or chemical vapor deposition. Due to the nature of these techniques, it is difficult to produce mono-disperse populations, which complicates their commercial application. The electronic properties of carbon nanotubes, spanning from metallic to semi-conduction, depend on the chirality, i.e., the orientation in which the graphene hexagonal structure is *rolled* with respect to the axis of the tube. The diameter of the cylindrical structures determines also the optical transitions and the bandgap in semiconductor nanotubes. This explains the need for mono-disperse structures for their

application in electronics and optics. Copious research is centered on the separation and purification of mono-disperse portions. Strategies include selective chemical functionalization, electrophoresis, chromatography, ultracentrifugation, and selective destruction, such as the etching of metallic tubes with fluorine gas followed by annealing. Research efforts are also being carried on selective growth of carbon nanotubes of certain chirality and diameter. The strategies followed include the variation of the carbon source, reaction conditions, and very importantly, catalyst type. Some control on the diameter has been achieved, as well as a certain level of enrichment of the metallic nanotube portion. Another approach being investigated is the use of previously purified mono-disperse samples of nanotubes as *seeds* for the growth of an additional batch. None of the strategies in pre or post production appears so far as a definitive solution. Intensive research still continues.[30]

Carbon nano-dots are quasi-spherical carbonaceous particles with typical sizes below 10 nm. They present desirable quantum dot properties, with the advantage of being composed of abundant and non-toxic carbon. They consist of sp2 hybridized graphitic-like carbon, with a surface usually bearing carboxylic groups, which facilitates their functionalization. C-dots show characteristic light absorption in the UV regime extending to the visible, and photo-luminescence which strongly depends on the excitation wavelength. It remains unclear whether the selectivity of the excitation wavelength results from size-dependent quantum effects, or *traps of emission* on the surface. The quenching of photo-luminescence by acceptor molecules is indicative of photo-induced electron transfer processes. C-dots also quench the photo-luminescence of typical donors, showing the possibility of electron acceptor behavior. The synthesis of C-dots is inexpensive and easily scalable. Common methods include top-down approaches like arc discharge, electrochemical oxidation, or ablation of larger carbon structures with lasers. Bottom up approaches include combustion, thermal, and microwave treatment of molecular precursors such as natural gas, ammonium citrate, or natural and synthetic polymers. The potential uses of c-dots are in energy conversion and storage, drug delivery, sensors and composites. These nano-materials also appear attractive for bio-imaging due to the low toxicity compared to other quantum dots.[31] Methods of separation and mono-disperse production are also investigated.

Nano-diamonds are nanoparticles composed of sp3 hybridized carbon cores with a narrow graphitic superficial layer. Overall their elemental composition is over 98%

carbon. Their surface chemistry has been investigated, achieving non-covalent and covalent functionalization. The fabrication methods include milling, chemical vapor deposition, or detonation, during which shock waves on graphitic material produce nanometer sized diamond crystals covered by graphitic layers. This material is of interest because of the remarkable mechanical properties of diamonds. Their high strength makes them ideal for polishing, coatings, and for the formation of polymer matrix composites. Due to their biocompatibility, nano-diamonds also have potential biological applications as vehicles for targeted drug delivery, and as labeling markers due to their florescence under the adequate surface conditioning. Potential applications also include electronics, since their doping leads to semi conducting and even quasi-metallic properties. Nano-diamonds are promising materials because of their inexpensive and scalable preparation. Current research is focused on the production of batches with narrow size distributions.[32]

Organic nanoparticles

Nanoparticles composed of organic molecules are extremely diverse, ranging from low molecular weight components to macromolecules. A selection of representative examples is here presented.

Molecular nanocrystals

Nanometer sized crystals of low molecular weight molecules can be formed from solutions in organic solvents which are emulsified in water. Colloidal nanocrystals of π-conjugated hydrocarbons have been formed by this procedure. Solutions of the precursors at elevated temperatures were emulsified in water, with crystallization taking place as the system is allowed to cool down. The organic solvent was subsequently eliminated by evaporation.[33] The preparation of nano-crystals of polycyclic aromatic hydrocarbons is of interest for applications in optoelectronics.

Dye organogels

Organogels of nanometer dimensions can be prepared using large aromatic dye molecules like porphyrines or fullerenes. These have the tendency to form aggregates based on π-π interactions in one dimension. In the adequate solvent, these molecules will conform in columns and fibrous arrangements, which themselves entangle in three dimensional arrangements which trap solvent. Van der Waals and hydrogen bonds contribute to the stabilization of the organogel structure. Given the non-covalent nature of the interactions keeping them together, these structures are adequate alternatives for responsive materials depending on the component dyes, which can then induce phase transformations from gels to solutions.[34] Responses to mechanical, thermal, electrochemical, and chemical stimuli from certain ionic species can be observed.[35] Overall, such arrangements of dyes have potential applications as charge carriers.

Surfactant – dye complexes

The self-assembly of colloidal surfactants in combination with certain counterions has been used to precipitate materials with an ordered heterophase in the nanoscale.[36] The tuning of this approach has resulted in the formation of stable nano-sized complexes in colloidal suspension.[37]

Polyelectrolyte complexes

Polyelectrolytes can be combined with organic counterions to from nanostructures. The complexation of two polyelectrolyte species of opposite charge results in scrambled structures which are normally not very ordered.[38] Polyelectrolytes have also been complexed with surfactants of opposite charge, resulting in comparatively more ordered structures. Complexation is carried out from solutions of the precursors, which if combined under the adequate conditions, result in the formation of nanoparticle dispersions. It has been found that a charge stoichiometry of 1:1 is the most adequate. The resulting structures can be tuned by temperature and ionic strength of the precursor solutions.[38]

Polymer nanoparticles obtained by the Ouzo effect

Polymer nanoparticles can be conveniently produced by the so called *Ouzo effect*, which refers to the spontaneous formation of an emulsion. A mixture of a hydrophobic oil dissolved in a fully water-miscible solvent is added into water. As a result, short-lived droplets are formed, which eventually phase separate. Surfactant may be added to enhance stability, but is not always needed. The effect can also be achieved by the inverse addition of water into the oil solution. The sizes obtained depend on the concentration of the components in the mixture. More diluted initial solutions of oil before the addition into water tend to form smaller particles. Nanometer range sizes can be obtained with this technique, spanning from 100 nm to a few microns. The formation of nanospheres or nano-capsules is accessible with this technique. The oil may consist of polymers or monomers which are then polymerized. Alternatively, polymerizable oligomers can be used, and then be further polymerized after the formation of the emulsion. The Ouzo effect is a convenient alternative to other energy intensive emulsification techniques, like high-shear mixing and sonication, which are difficult to take to industrial scales. Its limitations are related to the solubility requirements of the components.[39]

Nanoparticles from polymerization in hetero-phases

The formation of polymer nanoparticles can also be approached by the use of amphiphilic assemblies to achieve nanoscale structuration. The polymerization inside surfactant "casting molds" of nanometer dimensions is an alternative for the synthesis of polymer particles with a size which can be controlled by the surfactant content. In addition, the surface composition is also controllable by exploiting the polarity gradient of the interface, where amphiphilic components will be enriched.[36a]

An emulsion is a classic example of a hetero-phase system. It consists of two immiscible liquids which are homogenized by the formation of small droplets. In general, emulsions can be destabilized and separate into two macroscopic phases by two main processes: *coalescence*, which refers to the fusion of droplets, and *Ostwald ripening*, which corresponds to the thermodynamically driven migration of molecules

from small droplets into bigger ones, which is possible by a partial solubility of the immiscible liquid in the continuous phase. This process is thermodynamically driven because it ultimately results in a decrease of the interface to mass ratio. In a *miniemulsion*, these two processes are minimized by the addition of a surfactant and a an osmotic pressure agent. The surfactant gives rise to inter-droplet repulsion, thus minimizing coalescence. This repulsion can result from Coulomb forces or steric hindrance. The osmotic pressure agent is highly insoluble in the continuous phase. It is solubilized in the droplets, raising the osmotic pressure and thus minimizing the partial solubility of the dispersed component, ultimately minimizing the Ostwald ripening process. The components are homogenized by high power ultra-sonication or high-pressure mixing. High energy homogenization and the minimization of the destabilization processes result in the adequate conditions for the equilibrated formation of metastable droplets with a narrow distribution of sizes which can be controlled by the relative content of the surfactant. The droplets can achieve nanometer range sizes. Thus, polymerizations carried inside these molds result in the formation of nanospheres.[40]

The copolymerization of a monomer which is insoluble in the continuous phase with an amphiphilic comonomer can be used as a strategy to obtain nanospheres with specific functional groups on the surface. The amphiphilic monomer will preferentially migrate to the interface. As a result, the surface of the nano-sphere will be enriched with those groups which are lyophilic with the continuous phase.

Miniemulsions are very suitable for free radical polymerizations. Ionic polymerizations can also be achieved for certain highly reactive monomers, or in inverse miniemulsions with a non-aqueous continuous phase. Polycondensation reactions are also possible even with an aqueous continuous phase, due to the highly hydrophobic environment inside the droplet. Some polymerizations are more difficult to be carried out inside the miniemulsion droplets. In those cases, solutions of the corresponding polymers previously synthesized under the adequate conditions can be dispersed in a miniemulsion. The subsequent evaporation of the solvent causes the precipitation of the polymer, leaving behind a suspension of nanospheres.

Another application of miniemulsions is the encapsulation of substances which are insoluble in the continuous phase but soluble in the droplets. Solids which are insoluble

but still lyophobic to the continuous phase and compatible with the droplets can be encapsulated provided adequate homogenization is achieved.

Heterogeneous nanoparticles can be prepared by phase-separation processes within miniemulsion droplets. *Janus* particles, named after the Roman god with two opposing faces in a single head, can be formed out of two immiscible polymers which separate to form two defined hemispheres in the resulting nanoparticle. Such phase separations take place as the polymerization inside a monomer mixture droplet proceeds. Alternatively, they can be achieved when a solution of polymers is used to make a miniemulsion and the solvent is evaporated to trigger precipitation and phase separation.[1]

2.3 Mesoscale assembly of nanoparticles

The organization of nanometer sized structures at extended length scales is a challenging condition to be met in order to benefit at the macro scale from their remarkable properties. The importance of a well-defined organization of nanostructures up to the macroscopic level is evidenced in the construction of high performance natural materials. Moreover, the construction of useful devices for microelectronics, photonics, and other emerging fields, requires the positioning of nanoscale building block into functional arrangements for the construction of useful devices. Furthermore, the collective properties of nanoparticles in many cases are markedly different from those of the isolated particles. For instance, the propagation of signals through particles with special electric and magnetic properties, will depend in their inter-particle arrangements. In other words, the planned organization of component particles is a strategy for the deliberate directionality of magnetic and electric phenomena. The fabrication of three dimensional functional microstructures, out of nanoscale building blocks, appears as an alternative to the lithographic machining of a larger block which has inherent limitations due to its 2D process nature.[41] Current uses of nanoparticle assemblies include light emitters, optical switches, plasmon waveguides, and focusing lenses. For instance, research is being conducted to use arrays of FePt and CoPt for magnetic data storage of great capacity. Nanoparticle arrangements have also been created to develop

pH meters, thermometers, and chemical sensors, which due to the nanoscale have special accessibility to otherwise inoperable spaces.[42]

Nanoparticle assembly is the next step in the generation of fully defined materials. For this purpose, nanoparticles appear as the counterparts of atoms and molecules in an analogy between chemistry and *mesoscale assembly*.

Techniques of assembly

The assembly of nanoparticles into functional arrangements can be carried by a top-down approach in which external control is taken on each component, or through a bottom-up strategy, in which particles are assembled into architectures dictated by the environmental conditions.

Direct manipulation

The direct manipulation of matter atom by atom using a scanning tunneling microscope under cryogenic and ultrahigh vacuum conditions was reported in the pioneering work of IBM scientists.[43] The direct manipulation of matter atom by atom over surfaces at room temperature has also been achieved using atomic force microscopy.[44] At the mesoscale level, it is also possible to arrange nanoparticle by nanoparticle with methods based on atomic force microscopy (AFM). It has been possible to position 100 nm gold nanospheres by contact manipulation using an AFM tip. One of the challenges of this technique resides in the difficulty to simultaneously image the process. Research efforts are also being directed towards improvements in speed and precision.[45] Optical tweezers represent another strategy for the direct manipulation of dielectric nanoparticles. This method relies on the generation of force gradients by highly focused laser beams. This effect depends on the refractive index of the particle.[46]

Self-assembly

Self-assembly is a convenient synthetic strategy which refers to the spontaneous arrangement of building blocks without direct human intervention.[2] Self-assembly has proven to be useful for nanotechnology. In comparison with top-down methods such as one by one manipulation or lithographic shaping, it allows cost-effective mass production of three dimensional structures.[47] Traditionally used as a bottom up strategy in the assembly of molecules into nanostructures, this strategy can also be used at the *meso* and *macro* scales. Several general principles of molecular self-assembly apply at these higher levels, such as the type of interactions which guide the process, like attraction or repulsion; and reversibly, which implies self-adjustment. The appropriate environment is important, such as solutions, suspensions, or interfaces which allow the displacement of the components. The mobility in molecular self-assembly is provided by heat, while at nanoscale it is provided by Brownian motion.[41]

During the assembly process, in many cases nanoparticles do not reach the thermodynamically lowest state, and remain trapped. Inter-particle forces play an important role on this regard. They may be van der Waals, electrostatic, or magnetic interactions. Another type of repulsive force results from steric hindrance, which makes particles repel due to structural features which keep them apart. Solvation is an important factor for inter-particle interactions. This takes place when the solvent makes an ordered structure around the particle, affecting other interactions like van der Waals and electrostatic ones.[48]

The anisotropy of the nanoparticles is a factor which determines the architecture of the assembly. Simple isotropic spheres result in arrangements of simple symmetry, like face centered cubic hexagonal closed packed structure in analogy with crystallography, in which atoms and molecules belong to a packed structure depending on their anisotropy. Anisotropy may result not only from the overall geometry, but also from the hybrid material composition, which can cause amphiphilicity, density or roughness gradients.[49] Self-assembly can be achieved from solution or can be directed by templating, like in interface assembly, or assisted assembly, for instance by magnetic or electric fields.

The self-assembly of colloidal nanoparticles can be *directed* by molecular interactions. The stability of a colloid is heavily dependent on the repulsion forces between particles which prevent aggregation. Those forces depend themselves on the superficial properties of the particles and their interactions at the molecular level. Thus, the surface chemistry of the particle can be used to direct their assembly into the desired architecture.[3] In several cases, this chemistry can be reversibly altered by environmental changes in pH, ionic strength, temperature, or solvent polarity. From this perspective directed assembly appears as a strategy for the development of responsive materials which may as well be reversible. An example of chemically driven directed self-assembly is the use of RNA and DNA interactions for the particle arrangement. The specificity of base pairing can be used to create ordered superstructures with a pre-programmed architecture. This can be accomplished either with nanoparticles made of RNA or DNA, or with fragments of these biomolecules attached to nanoparticles made of other materials.[50] Another example of directed self-organization of nano-sized structures corresponds to the ordering of hybrid inorganic crystals bearing superficial polymers, in which the final arrangement is directed by the organic matrix.[51]

Self-assembly directed by external fields is possible in suspension of particles which are responsive to electric or magnetic fields, and can be oriented into peculiar arrangements under their influence. These are nevertheless not the only available tools. Patterned optical traps, based on the principles of optical tweezers can also result in directed self-assembly. Directed assembly can as well be achieved using flow fields in the medium, in a process which is also understood as a form of *dynamic self-assembly*. This concept refers to the continuous input of energy, which gives rise to the resultant structures. Such an approach is a close mimic to the processes of nature, which are indeed in many cases non-equilibrium states.[2]

The *templated self-assembly* of nanoparticles is another valuable approach. The assembly of colloidal polymer nanoparticles has been achieved by templating on the interface in an emulsion. Dense-packed clusters of up to several nanoparticles have been formed by this technique. The relative content of aggregates of different sizes could be indirectly controlled to a limited extent with the alteration of the relative concentrations of the system.[52]

2.4 Responsive materials

Stimuli-responsive materials are a dynamic field of research due to their prospective applications of high technological relevance, spanning from actuators and sensor to more sophisticated systems such as healable materials. Reversibility is an important parameter to consider in the application of responsive materials, as it defines the extent of continuous operability. The following section presents an overview of the state of the art in this research field.

Mechanism of response

Responsive materials can be classified in terms of the mechanism behind the response, irrespective of the signaling method. The origin of the observed change in the properties of a material is often related to a change in the relative positioning and association of the building blocks which comprise the system, spanning from atoms and molecules to nano- and micro-scale domains. A broad range of response mechanisms can be identified. A collection of the most representative is here described (see Figure 2.1).

Phase transformations in the solid state imply a change in the periodic arrangement of a lattice. This is the response mechanism behind shape memory alloys like nickel-titanium or copper-zinc-aluminum-nickel, which recover its cold-forged shape after being deformed and heated. These alloys are used as sensors and actuators in the medical and aerospace industries.[53] Another responsive material based on lattice changes are piezoelectric crystals, which produce mechanical stress when voltage is applied on them, and vice versa. These are used as actuators, in which a desired movement can be effected in a well-controlled manner by applying voltage, which can be delivered with a high degree of control.[54] Responsive organic molecular crystals have also been identified, which change their physical conformation at the micron level as a response to light.[55]

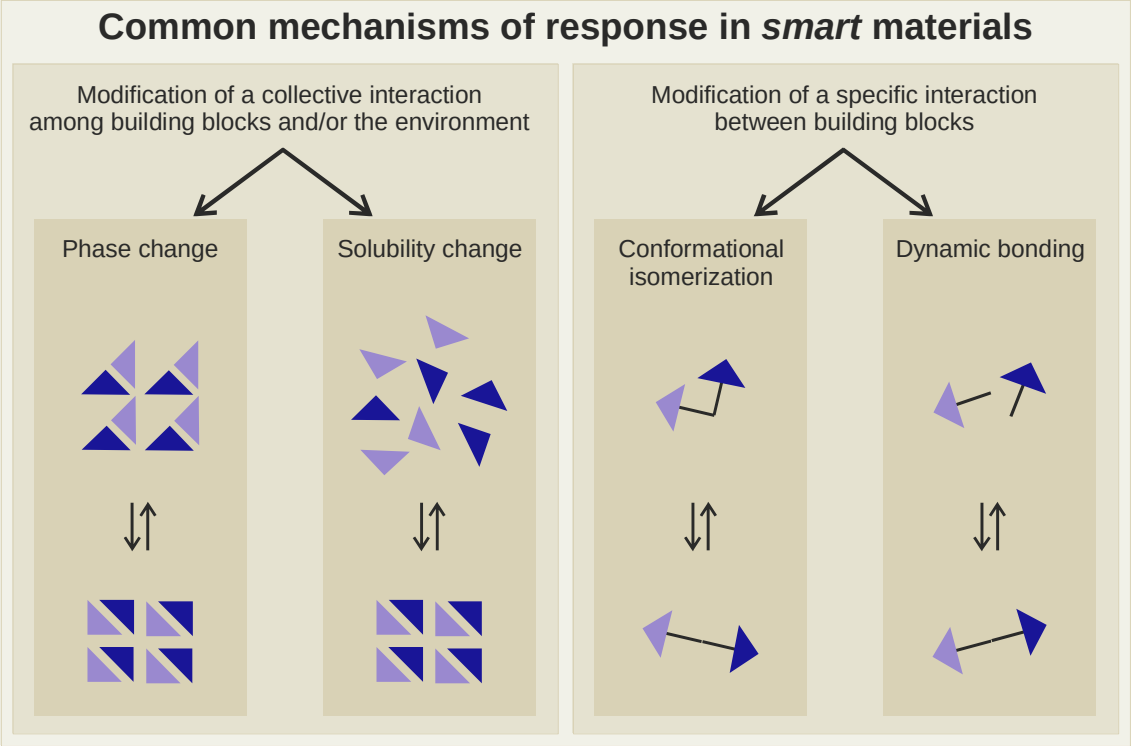

Figure 2.1. Classification of the mechanisms of response commonly observed in smart materials.

Response mechanism can also be based on changes in the solubility or the overall solvent affinity of the building blocks of a material. This has been achieved with single molecules which form responsive gels,[56] as well as polymeric molecules which have been adapted to undergo changes in their overall solubility, for instance by charge generation upon photochromic isomerization.[57] Responsiveness as a result of solubility or lyophilic changes can also be observed at the nanometer scale. That is the case for gold nanoparticles capped with random copolymers of oligo(ethylene glycol) methyl methacrylate (OEGMA) and 2-(2-methoxyethoxy)ethyl methacrylate (MEO_2MA), in which the solvent affinity has been altered by chemical signaling, resulting in the reversible transfer of the nanoparticles the between toluene and the water phase.[58]

Conformational isomerization has been widely exploited at different size ranges for the generation of responsive materials. Molecular structures undergoing *cis-trans* isomerization have been integrated to diverse building blocks.[59] Dynamic bonding is

also a powerful strategy for the preparation of responsive materials. These can be either covalent or non-covalent.[60] This approach allows the explicit linking of building blocks. The versatility of this approach is based on the variety of possible dynamic bonds. These last two mechanisms are frequently triggered by photo-excitation, and will be discussed in greater extent in the following sections.

Types of modified materials

The integration into conventional materials of active molecular structures which give rise to dynamic responses is a powerful and versatile approach for the generation of stimuli responsive materials. Several types of materials have been modified by the integration of such responsive functionalities on building blocks of different sizes. The modification of single molecules which self-assemble into supra-molecular arrangements has been reviewed,[61] also with a focus on surfactants.[62] Macromolecular units have been modified to generate responsive materials in the bulk,[63] as thin films,[64] colloidal amphiphilic polymer vesicles,[65] polymer micelles,[66] or as liquid crystalline polymers.[67] Higher level building blocks have also been modified such as nanoparticles,[3] including systems from core-shell nanoparticles[68] up to microgels.[69]

Signaling methods and responsive functionalities

Two recurrently used methods of signaling include temperature [68-69] and pH [68, 70] changes. These are commonly related to changes in solvation, which result in gelling systems. Examples of polymers bearing such functionality are presented in Figure 2.2 and Figure 2.3.

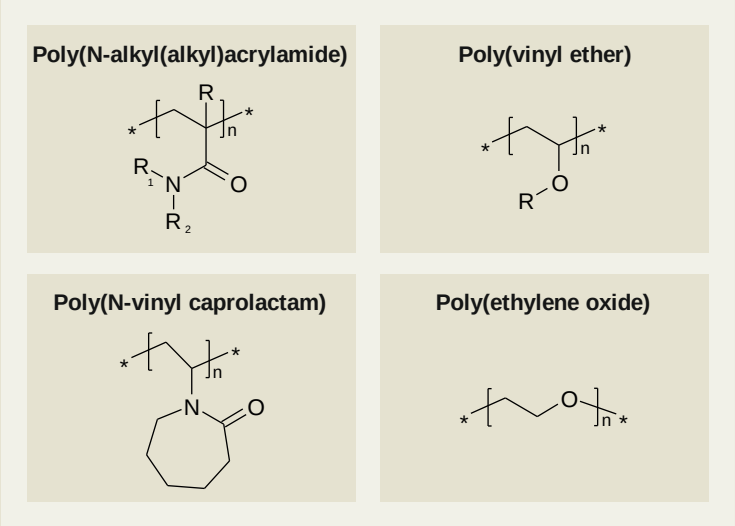

Figure 2.2. Structures of thermally responsive polymers

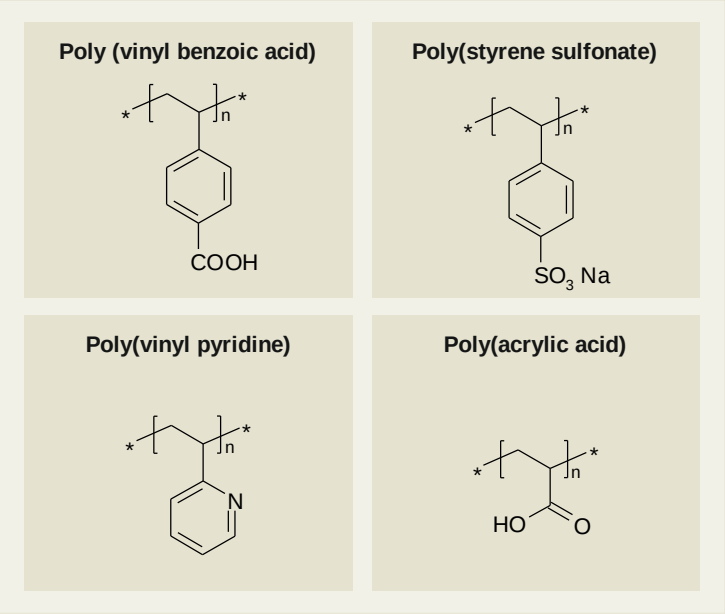

Figure 2.3. Structures of pH responsive polymers

Light signaling is a particularly convenient method. An advantage is the possibility to deliver the signals with precision. Compared to temperature changes, a light signal can be delivered and ceased within fractions of a second. On the other hand, it is a *non-invasive* signal, which makes it particularly adequate for multi-cycle response purposes along which the chemical composition of the system is not progressively altered.

The molecular structures which are responsive to light can be classified as irreversible or destructive, and reversible.

Non-reversible destructive responses based on photo-degradation are diverse. Some representative examples are shown in Figure 2.4. Derivatives of o-nitrobenzyl have been introduced as cross-linkers in microgels, which can be photo-cleaved.[71] The photo-triggered cleavage of pyrenylmethyl, coumarin and o-nitrobenzyl functional groups pending from block copolymers has resulted in overall changes in the hydrophobic / hydrophilic character, and have been used in a variety of supramolecular arrangements.[72] The UV-triggered cleavage of azo bonds by UV light has been used for the fabrication of responsive materials. Polymers incorporating such bonds have been used for the fabrication of capsules for the purpose of signal-controlled release.[73] This irreversible mechanism of photo-response has also been reported in azo-sulfonate based surfactants, which undergo degradation into sulfate salt and the corresponding uncharged hydrophobic residue, ultimately resulting in volume changes in microgels.[74] *Photo-acid generators* (PAG) integrated between polyelectrolyte layers, were used to form capsules which release its contents upon photo-stimulation. Under UV irradiation of high energy (λ = 254 nm), PAGs decompose and release protons.[75] PAGs have also been used in combination with block copolymers to reversibly flocculate clay colloidal nanoparticles.[76] Polyelectrolyte stars have been complexed with multivalent ions, such as hexacyanocobaltate(III), which undergoes non-reversible valence change upon photo-irradiation. This changes the conformation of the polyelectrolyte, making it re-solubilize.[77]

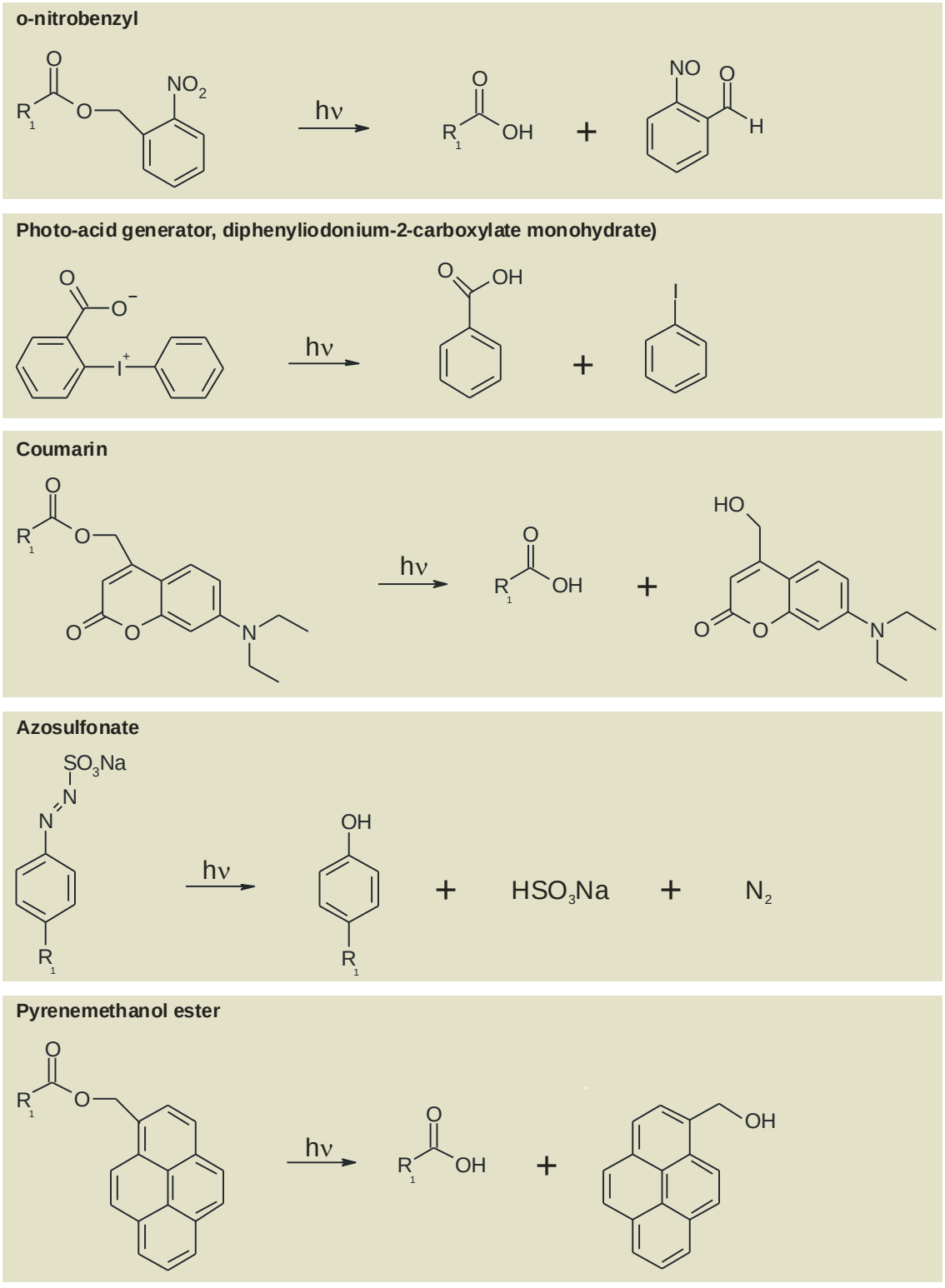

Figure 2.4. Non-reversible/destructive light-responsive molecular structures.

Reversible light-responsive systems are of great interest for the development of responsive materials which can operate for several cycles. That is the case for metallic

nanoparticles which irradiated with infra-red light transform photons into heat. This effect has been used to develop photo-responsive gels, like poly(N-isopropylacrylamide) with embedded gold nanorods, which shrink as a response to light.[78] As previously stated, the inclusion of responsive molecular structures in conventional materials is a powerful strategy. An overview of representative examples of such functionalities which are photo-responsive and reversible is shown in Figure 2.5.

Photochromic isomerizations which result in cis-trans conformational changes have been integrated into a variety of systems. As previously described, single molecules which self-assemble into supramolecular arrangements have been incorporated with this functionality. In recent work, azobenzene structures were bonded to guanosine, resulting in the reversible light-triggered formation of assemblies due to cis-trans isomerization.[79] Azobenzene functionalities have also been used for the photo-induced formation of organogels.[80] The effect of light on aqueous vesicles formed by azobenzene containing surfactants was of limited structural changes which were mainly related to size, as the formation of supramolecular structures was observed for both isomeric conformations.[81] Butadiene also undergoes cis-trans isomerizations. This functional structure has been used for the formation of liquid crystals, vesicles and organogels as well, which undergo light-induced responses and are reversible with temperature.[59b] The photo-triggered isomerization of trans-ortho-methoxycinnamic acid into the cis conformation resulted in the formation of a gel in combination with cationic surfactants in aqueous solution. Despite not being a degradation mechanism, the system appeared to be non-reversible.[82] Macromolecular units have also been integrated with this photo-responsive functionality. The cis-trans isomerization of azobenzene structures bonded as side groups of a polymer chain and bearing a terminal carboxylic group, was used to reversibly form organogels due to the conformational control over hydrogen bonding formation in DMSO.[83] The electrostatic self-assembly of PAMAM dendrimers with the sulfate-functionalized azobenzene dye acid yellow, was triggered by photo-excitation. The complexation proved to be reversible by changes in pH and subsequent heating.[84] Azobenzene structures have been integrated into biological systems, achieving the transformation of ligand-actuated biological processes into light-actuated. Ion channels which can be blocked with lipophilic cations, have been reversibly controlled with cationic azobenzenes.[85] Photo-responsive nanoscale

systems have been developed using cis-trans isomerization. The integration of azobenzene to colloidal gold nanoparticles as part of the stabilizing ligand, resulted in the reversible photo-induced formation of clusters.[4]

Photochromic isomerizations which lead to the formation of ionic charges have been found useful to develop responsive materials. Spiropyran structures have been bonded to block copolymers, achieving in combination with temperature control, the photo-induced inversion of micelles in aqueous environment.[86] Also, the integration of Spyrobenzopyran into N-isopropyl acrylamide has resulted in the generation of light-responsive gels. Very interestingly, this system uses visible blue light of λ = 436 nm,[87] which makes it better fit for biological applications. Poly(ethylene glycol) has been functionalized with a leuco dye derivative. This polymer has been used to form vesicles in aqueous medium, which can be broken with light. The re-aggregation process was spontaneous and could be controlled by temperature.[88]

Photo-dimerization reactions have been integrated into a variety of systems. Coumaryl derivatives have been integrated to polymeric materials to produce micelles which change in size and shape upon photo-excitation.[89] The photo-induced swelling and de-swelling of poly(ethylene oxide) based nanogels functionalized with coumaryl groups has been achieved for several cycles.[90] Copolymers of cynnamic acid derivatives have been prepared by polycondensation. The copolymer was used to form nanoparticles which could be cross-linked upon photo-excitation, observing a change in size. The reversibility of the process could be achieved partially.[91] Photo-dimerizable groups have also been integrated to nanoscale system. Polysiloxane nanoparticles labeled with coumaryl and cinnamoyl groups could be aggregated in organic solvent suspensions through photon excitation. The clusters were re-dispersed using light of higher energy. Nevertheless, a second aggregation cycle could not be achieved, apparently due to the photo-degradation of the photo-active labels during re-dispersion.[5, 92]

Anthracene is a photo-dimerizable molecular structure which has been widely used for the generation of responsive materials. Several polymeric systems have been functionalized with this molecule. Anthracene has been bonded to styrene for the generation of photo cross-linkable polymers.[93] Anthracene was also bonded to the free end of cross-linked star (CCS) acrylate polymer.[63] In general, reversibility was achieved only partially in most systems. The photo-triggered formation of gels was

observed in poly(ethylene glycol) star polymers labeled with anthracene at the free end.[94] The photo-induced cross-linking of mono-disperse star polymers of poly(tert-butyl methacrylate) and poly(methacrylic acid) bearing anthracene on the free ends, was achieved with the purpose of generating model polyelectrolyte networks.[95] Poly(ethylene terephthalate) (PET) was copolymerized with anthracene dicarboxylate, resulting in photo cross-linkable polymers in thin films, which nevertheless could not be cleaved back.[96] Anthracene was bonded to poly(N-acetylethylenimine) through a disulfide bond. It was possible to photo-induce the cross-linking of this polymer from an aqueous solution. The subsequent cleavage was achieved by chemical reduction of the disulfide bridge. The produced system was thus functional for only one cycle.[97] Polystyrene-*block*-poly(methyl methacrylate) block copolymers, with anthracene groups in between the blocks, was synthesized to produce films in which nano-sized phase separations could be generated through photo-excitation.[98] Amphiphilic block copolymers bearing anthracene groups were synthesized, achieving the photo-triggered formation of micelles.[99] Recently, the photo-dimerization of anthracene was used for the generation of nanoscale responsive systems. Gold nanoparticles with adsorbed anthracene groups were assembled into aggregates, and to ZrO_2 surfaces bearing also adsorbed anthracene functionalities.[100]

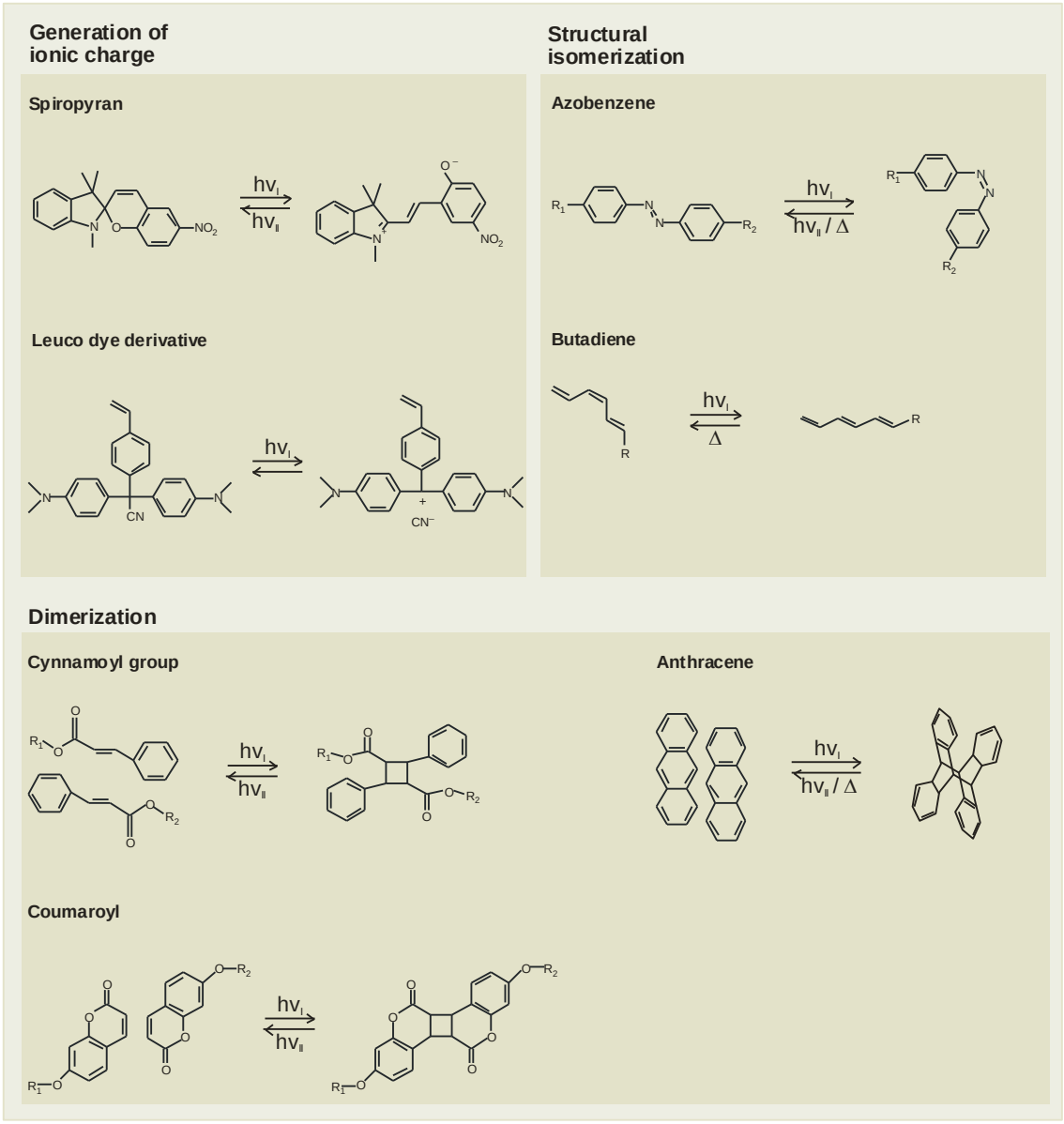

Figure 2.5. Photo-responsive reversible molecular structures.

3 ANALYTICAL METHODS

3.1 Fundamentals of colloidal systems

A theoretical overview of colloids is given in this section as a background for the subsequent discussion of the analytical techniques used for this study.

A colloid is a substance constituted by a continuous phase and a dispersed phase which appears homogenously distributed in small particulates in typical size ranges below 1 µm. Colloidal systems with a continuous liquid phase are known as *emulsions* when the dispersed phase is a liquid, or *sols*, when the dispersed phase is a solid. The term *suspension* is used in a more generic manner to describe colloidal systems with a liquid continuous phase. Colloids are generally classified as *lyophilic* (solvent loving) or *lyophobic* (solvent hating). They can also be categorized as *reversible* and *irreversible*, respectively, based on the ease with which they can be re-dispersed after drying. In reality, systems range in between these two extreme cases. Lyophobic colloids are thermodynamically unstable and remain kinetically trapped in a metastable dispersed stated. The gathering of the dispersed phase into a single portion is thus energetically favored. Nevertheless, this is avoided due inter-particle repulsions which arise either electrostatically or sterically. The destabilization of a colloid may result from changes in the electrostatic charge around the particles, thus allowing them to come into close contact and coagulate. Unlike electrostatic stabilization, steric stabilization is equally effective in non-aqueous media, generally unaffected by particle concentrations, and not very sensitive to electrolyte content. Despite of repulsive forces, destabilization may still occur when polymeric molecules act as bridges between particles, forming loose aggregates in a process known as flocculation. Flocculated aggregates are generally more easily reversible than electrostatically coagulated clusters.[101] Steric stabilization can be broken when the solubility of the stabilizing chains is changed. The system remains stable when polymer-solvent interactions are stronger than polymer-polymer interactions. Nevertheless, a critical flocculation point may be reached when changes in temperature, pressure, or the addition of a miscible non-solvent decrease the solubility of the stabilizing polymer chains in the dispersing medium. For instance, aqueous suspensions stabilized with water-soluble poly(ethylene glycol) (PEG), generally suffer

destabilization with increasing temperature due to the gradual dehydration of the polymer chains.[102]

The characterization of colloids is commonly focused on the determination of the size distribution of the suspended particles, their shape and charge. The specific surface area is a characteristic related to the size. This information enables the manipulation of the colloidal system for its practical use. Depending on the characterization method, the information regarding the size might be only available as an average, with different average values resulting from different measurement methodologies. When the distribution of sizes becomes broader, such differences become more pronounced.

The *number-average* diameter of the particles in a colloidal system responds to the following formula:

$$\langle D \rangle_n = \frac{\sum n_i D_i}{\sum n_i} = \sum f_i D_i \qquad \textbf{(3.1)}$$

where n_i is the number of particles of size D_i and f_i the corresponding fraction. Likewise, the *mass average* responds to the following formula:

$$\langle D \rangle_m = \frac{\sum m_i D_i}{\sum m_i} \qquad \textbf{(3.2)}$$

where m_i is the mass of particles of size D_i. This average results from characterization methods in which the signal is proportional to the mass, rather than the number of particles. Similarly, the *z average* is obtained from characterization methods in which the signal is proportional to the squared-mass of the colloidal particle:

$$\langle D \rangle_z = \frac{\sum m_i^2 D_i}{\sum m_i^2} \qquad \textbf{(3.3)}$$

The significance of the difference between these average values can be seen in Figure 3.1, which shows a normal distribution and the localization of the respective averages.

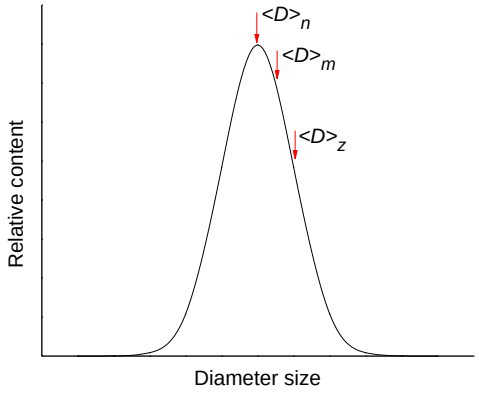

Figure 3.1. Normal distribution of sizes showing the differences between number average $<D>_n$, mass average $<D>_m$, and z average $<D>_z$ diameter size.

To evaluate the broadness of the distribution of sizes, a useful parameter is the standard deviation σ_s:

$$\sigma_s = \sqrt{\sum [f_i (D_i - \langle D \rangle_n)^2]} \qquad \textbf{(3.4)}$$

Conventionally, a system is regarded as *monodisperse*, when the relative standard deviation, ($\sigma_s/\langle D \rangle$) is lower than 0.1.[103]

The distribution of sizes is not necessarily symmetrical, and the shape can give information about the history of the colloidal system. If the current distribution is the result of a "growth" or nucleation process, the distribution will present a longer tail towards smaller sizes. On the other hand, when the current distribution is the result of a fragmentation process, the distribution will present a longer tail towards higher sizes[103] (see Figure 3.2).

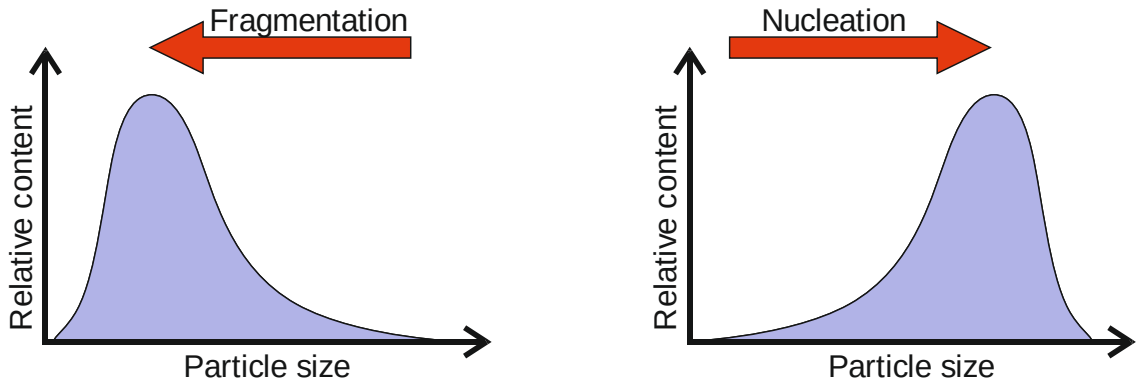

Figure 3.2. Particle size distribution asymmetry indicating the history of the colloid.

The analysis of colloids can be carried using different techniques. In some cases, an average is obtained, while in others the full distribution of sizes can be determined. The selection of the analytical method depends on the size range that is accessible to be resolved with a certain technique. Another important parameter to consider is the stability of the studied sample under the conditions of the analysis. In some cases the analytical procedure completely disrupts the colloidal state. Moreover, for some systems even the integrity of the suspended particles may be compromised.

If the size of the suspended particles results from an equilibrated colloidal state, non-disruptive methods are necessary. This is the case of self-assembled structures, like surfactant micelles and vesicles. Non-disruptive methods are also ideal for colloidal

stability studies, in which dynamic processes such as dispersion, aggregation, and precipitation are monitored. The present study makes use of non-disruptive analytical methods which are based on Brownian motion. The principles of this process are reviewed in the following section.

Brownian motion

Named after Robert Brown, the botanist who first described the microscopic observation of constantly moving pollen grains suspended in water, Brownian motion refers to the random motion in three dimensions of particles suspended in a fluid. Einstein explained the observations in terms of the molecular-kinetic theory of heat. Such explanation represented the confirmation for many skeptics of the atomistic theory of matter.[104]

Consider that free diffusion is governed by Fick's law:

$$\frac{\partial \rho(r,t)}{\delta t} = D\nabla^2 \rho(r,t) \qquad \textbf{(3.5)}$$

where ρ is the density at traveled distance r in a time lapse t, and D the diffusion coefficient. This differential equation has the following solution:

$$\rho(r,t) = (4\pi Dt)^{-\frac{3}{2}} \quad \exp\left(-\frac{r^2}{4Dt}\right) \qquad \textbf{(3.6)}$$

with the average traveled distance is expressed as:

$$\langle \Delta R(\tau)^2 \rangle = \int_0^{\infty} r^2 \ \rho(r,t) dr = 6Dt \qquad (3.7)$$

for three dimensional diffusion. Einstein's clever contribution was to relate this to the kinetic theory of heat. A suspended particle, say the pollen grain suspended in water observed by Brown, is constantly bombarded by surrounding molecules. It feels pressure and exerts back the pressure corresponding to the volume of water that it displaces. According to the kinetic theory, the pressure exerted by the solvent on the particle results from constant momentum exchange from single solvent molecules (see Figure 3.3).

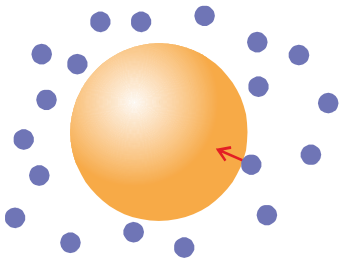

Figure 3.3. Model of a colloidal particle under constant bombardment by surrounding solvent molecules.

If a time lapse is considered, so short that during it, only one molecule hits the suspended object, then the particle should move due to an imbalance of forces around it, and due to the momentum exchange from a single solvent molecule. The motion of the particle due to this single hit is described as:

$$\Delta x = \frac{F}{2M}(\Delta t)^2 \qquad \textbf{(3.8)}$$

where *Δx* is the traveled linear distance, *F* is the force, *M* the mass of the particle, and *Δt* the time lapse.

The displacement caused by the collision of a single solvent molecule is too small to be detected. If we consider random walk statistics, the effect of a single molecule hit can be revealed when a collection of such single collision events results in a displacement which can be detected at the microscopic level. According to random walk statistics, the total squared-average displacement $\langle R^2 \rangle$ after *N* random hits in any direction with a constant step size *r* and free rotation after each step is expressed as:

$$\langle R^2 \rangle = N\Delta r^2 \qquad \textbf{(3.9)}$$

The combination of this statistical approach with Fick's law (equation (3.7)) gives an expression for the diffusion coefficient *D* in terms of the mean squared-displacement $\langle R^2 \rangle$ in a time lapse *Δt*:

$$D = \frac{\langle \Delta R^2 \rangle}{6\Delta t} \qquad \textbf{(3.10)}$$

For spherical particles, the value of the diffusion coefficient D_s can then be used to calculate the hydrodynamic radius R_h of the colloidal particle using the Stokes-Einstein equation:

$$D_s = \frac{kT}{6\pi\eta R_h} \qquad \textbf{(3.11)}$$

where k is Boltzmann's constant, T is the temperature, and η is the viscosity of the continuous medium in which the particle is undergoing Brownian motion.

This result is fundamental for the theory behind particle sizing by *ultramicroscopic particle tracking* and *dynamic light scattering*. In those two methods, the average displacement of the colloidal particles is experimentally determined. Such techniques have the advantage of measuring particle size without disrupting the colloidal state of the sample.

3.2 Dynamic light scattering

Principles of light scattering

Electromagnetic radiation is composed of oscillating magnetic and electric fields arranged perpendicularly. Its interaction with matter is related to the charged nature of atoms, which are built of a positive nucleus and surrounding negative electrons.

The electric field component induces the acceleration and displacement of charges, resulting in a dipole, which oscillates according to the frequency of the incoming light (see Figure 3.4). The generated dipole itself becomes a focus of multidirectional electromagnetic irradiation, giving rise to the phenomena of *scattering*.

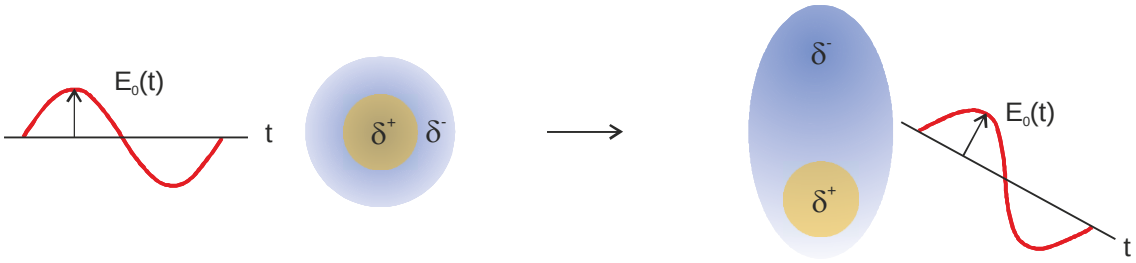

Figure 3.4. Interaction of electromagnetic radiation with matter and induction of the Hertz dipole.[105]

The strength of scattering depends on the feasibility to displace the charges of the irradiated material. This quality is described as the *polarizability*, which is an inherent property of a given material.

The application of scattering as an analytical tool is based on the effect of *interference*. Spatially superimposed waves add together, giving as a result a wave with amplitude which depends on the phase shift between the added components (Figure 3.5).

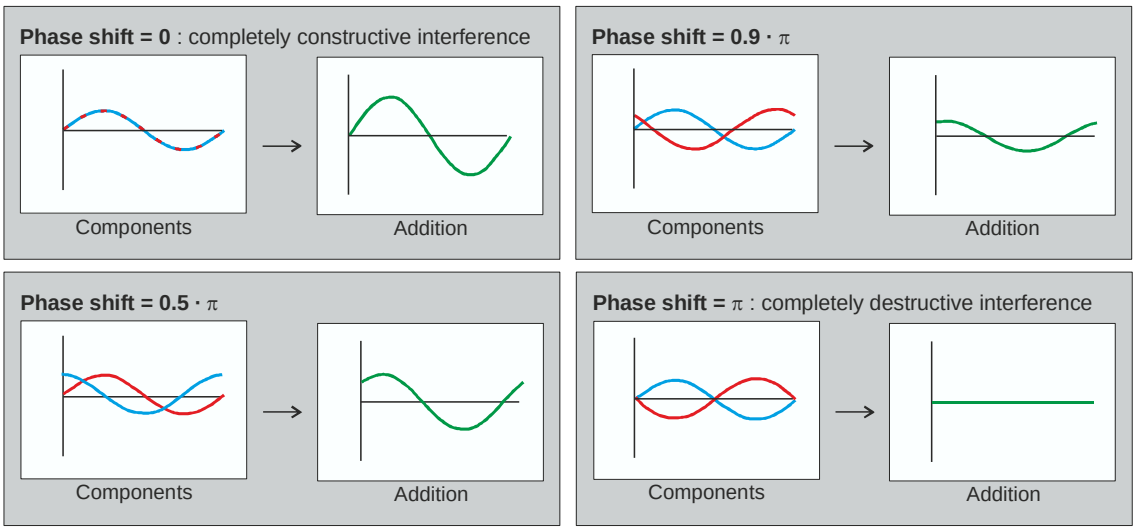

Figure 3.5. Addition of sinusoidal curves, showing the effect of phase-shift on the amplitude.

The relevance of interference relies on the dependence of the resultant intensity patterns on the separation between two in-phase emitters at a fixed observation distance, which is the case in a scattering experiment (Figure 3.6).

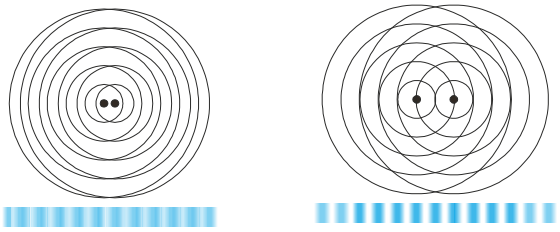

Figure 3.6. Interference pattern dependency on the distance between two scattering centers.[105]

The mathematical description of the scattering pattern is conveniently carried out with the definition of the *scattering vector q*, which results from the vector subtraction of the scattered wave $\vec{k}$ from the incident wave $\vec{k}_0$, observed at a scattering angle θ (Figure 3.7).

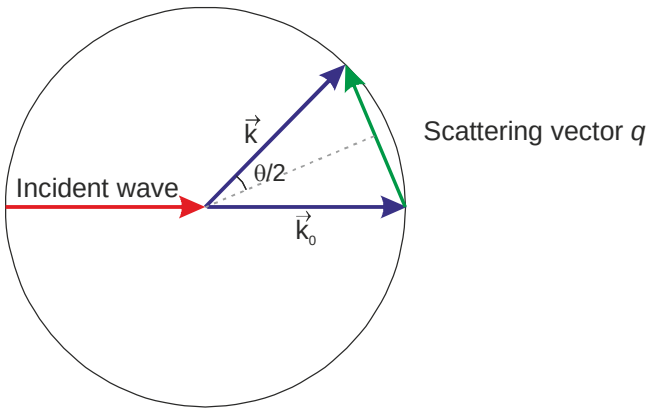

Figure 3.7. Schematic representation of the scattering intensity.[105]

which results in the following expression:

$$q = \frac{4\pi n_D}{\lambda_o} \sin\left(\frac{\theta}{2}\right) \qquad \textbf{(3.12)}$$

where λ_o is the wavelength of light in vacuum, and n_D the refractive index of the propagating medium.

Principles of dynamic light scattering

In dynamic light scattering (DLS), it is the change of the scattered intensity *I* vs. time *t* what is measured. DLS of colloidal suspensions uses this time-resolved information to determine the linear velocity of the objects traveling in Brownian motion. To determine this velocity, consider a collection of scattering bodies at a certain instant (see Figure 3.8).

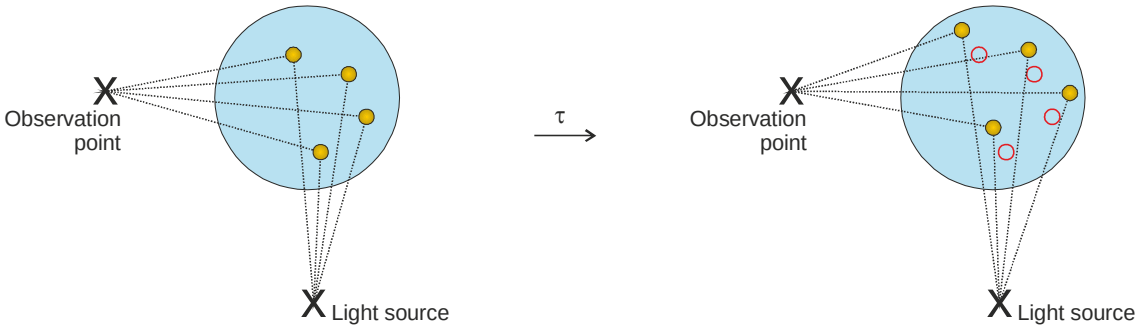

Figure 3.8. Schematic representation of the dynamic light scattering experiment.[105]

The total intensity of the scattered light at the point of observation results from the addition of the light waves emitted by each scattering point. The amplitude of such addition depends itself on the phase shift (Figure 3.5). The phase shift of these waves is determined by the total distance traveled divided by the wavelength, which results from

the exact location of each scattering point with respect to the source of light and the point of observation.

We do not have access to the information regarding the exact location of the scattering objects, which are homogenously distributed. Nevertheless, the exact instantaneous value of the intensity is not of relevance for the purpose of DLS, but rather its change vs. time. During the experiment, the location of the point of observation and the source of light are kept fixed, with only the Brownian motion of particles being the source of variation in the total length of the trajectory traveled by light through each particle.

The treatment is thus based on a statistically homogeneous distribution of the scattering centers over a fixed scattering volume, with a change in the distribution which is governed by Brownian motion random walk statistics, with an average distance R traveled in a time lapse τ.

Consider the time correlation function of the density function:

$$G_s(R,\tau) = \langle \rho(R,t)\rho(R,t+\tau) \rangle = \lim_{T\to\infty} \frac{1}{T} \int_0^\infty \rho(R,t)\rho(R,t+\tau)dt \qquad \textbf{(3.13)}$$

For a three dimensional random walk, the solution is expressed as:

$$G_s(R,\tau) = (4\pi D\tau)^{3/2} \exp\left(-\frac{R(\tau)^2}{4D\tau}\right) \qquad \textbf{(3.14)}$$

The Fourier transform to q space of this dynamic form factor leads to the electric field time correlation, which corresponds to an experimentally accessible value:

$$g_1(q,\tau) = \exp(-Dq^2\tau) = \langle E_s(q,t)E_s{}^*(q,t+\tau)\rangle \quad \textbf{(3.15)}$$

Experimentally, what is commonly measured is the scattered intensity autocorrelation function:

$$g_2(q,\tau) = \frac{\langle I(q,t)I(q,t+\tau)\rangle}{\langle I(q,t)\rangle^2} \quad \textbf{(3.16)}$$

which is related to the electric field correlation function through the Siegert relation:

$$g_1(\tau) = B\sqrt{\lfloor g_2(\tau)\rfloor - 1} \quad \textbf{(3.17)}$$

where *B* is a factor which depends on the experimental setup and accounts for the spatial coherence between the detector area and the scattered light.

Analysis of polydisperse samples

In a system composed of colloidal objects of different sizes, each element will be *represented* according to the intensity with which it scatters light. The analysis of the entire system thus gives average values in which each colloidal object is weighted by the intensity of the light it scatters according to the following formula:

$$I_i \sim n_i \cdot M_i^2 \cdot P_i(q) \qquad \textbf{(3.18)}$$

I_i is the intensity of the light scattered by particle species *i*, n_i the total number of such particles, M_i the corresponding mass, and P_i the *form factor*, which accounts for the intensity variation resulting from intra-particle interference. This takes place when the system is composed of larger particles (over 20 nm), which have more than one electric oscillator, thus resulting in interference from a single scattering object.[106] Of course, the distance between two oscillators of the same particle is always constant, meaning that the interference between them does not contribute to the intensity variation detected by DLS. Nevertheless, in systems with a polydisperse size distribution, the form factor will play a role due to the difference in the intensity of light scattered by objects of different sizes. The form factor has a value of 1 at a scattering angle of zero. To cancel its effect and to obtain a valid z average value of the diffusion coefficient, the data must be extrapolated to a squared scattering vector of zero ($q^2 \to 0$).

For polydisperse colloidal systems, the dynamic form factor is a summation of exponential functions of the different components:

$$g_1(\tau) = \int_0^\infty W(\Gamma) \cdot \exp(-\Gamma\tau)\, d\tau \qquad \textbf{(3.19)}$$

where $W(\Gamma)$ is the weighting factor of the exponential corresponding to a given *relaxation rate* Γ, which itself is defined as:

$$\Gamma = q^2 D \qquad \textbf{(3.20)}$$

Methods of data analysis

The analysis of data can be carried out by directly fitting the experimentally measured intensity autocorrelation function g_2 (equation (3.14) with model exponential functions. This is regularly accomplished using algorithms based in *least squares fitting*.

To account for broadening distributions, the intensity autocorrelation function can be fitted to an *extended exponential* function, also known as the Williams-Watts formula:[107]

$$g_2(\tau) - 1 = c_0 + \left(c \cdot \exp(-\Gamma\tau)^{\beta}\right)^2 \qquad \textbf{(3.21)}$$

The distribution is centered at the characteristic decay time Γ^{-1}, with a width determined by the parameter β, which is equal to 1 for monodisperse systems, and decreases as the width of the distribution broadens ($0<\beta\leq1$).

The average decay time value of the extended exponential is expressed as:

$$< \tau >= \frac{\tau}{\beta} \cdot \left(\frac{1}{\beta} - 1\right)! \qquad \textbf{(3.22)}$$

Data composed of an overlap of several relaxation rates can also be analyzed via the inverse Laplace transformation of the electric field autocorrelation function:[107]

$$A(\Gamma) = \frac{1}{2\pi}\int_0^\infty g_1(\tau)\cdot\exp(-\Gamma\tau)d\tau \qquad \textbf{(3.23)}$$

In reality, experimental data contains statistical errors which hamper this operation. The calculation can be accomplished via a regularized procedure of least squares. A common algorithm for this purpose known as CONTIN, was introduced by Provencher.[108]

The method of *cumulants* introduced by Koppel[109] is one of the simplest approaches of data analysis. It is limited to samples of moderate size polydispersity lower than 0.2. The analysis is based on the fitting of the data to a series expansion of the dynamic form factor

$$ln\big(g_1(\tau)\big) = -\kappa_1\tau + \frac{\kappa_2}{2}\tau^2 - \frac{\kappa_3}{6}\tau^3 + \cdots \qquad \textbf{(3.24)}$$

The polydispersity of the diffusion coefficient ($\Delta D/\langle D\rangle$) can be estimated according to:

$$\sigma_D = \frac{\sqrt{\langle D^2\rangle - \langle D\rangle^2}}{\langle D\rangle} = \sqrt{\frac{\kappa_2}{\kappa_1^2}} \qquad \textbf{(3.25)}$$

3.3 Ultramicroscopic particle tracking

Optical microscopy is a very convenient method to study colloids. Under the correct conditions, it is non-disruptive and time resolution observations are possible to evaluate dynamic processes. The resolution of optical microscopy, understood as the possibility to identify two points separated by distance *d*, is limited by the wavelength of light. If the optical system is flawless and no aberrations exist, the theoretical limit is:

$$d = \frac{\lambda}{2NA} \qquad \textbf{(3.26)}$$

where λ is the wavelength. *NA* is the numerical aperture, which refers to the available angular range of observation, and depends on the refractive index *n* of the material. With the use of optical oils to cover the interface of the objective lens, a maximum *NA* value can be obtained.[110]

Ultramicroscopy refers to the possibility to image objects with a size smaller than the wavelength of visible light. Developed by Nobel laureate Richard Adolf Zsigmondy, this technique detects scattered light instead of reflected or transmitted light. This is achieved with an optical arrangement which excludes light which is not scattered (see Figure 3.2). As a result, the image is composed of bright scattering centers in a dark surrounding.

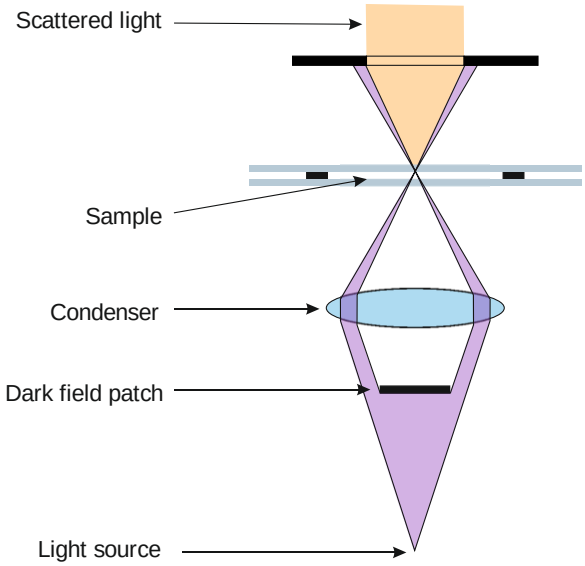

Figure 3.9. Schematic representation of a dark field microscope.

Dark field microscopy allows the time-resolved observation of colloidal particles in motion which are smaller than the wavelength of visible light. It is thus possible to follow the movement of a body which scatters light. In the case of particles in Brownian motion, the recording of the traveled distance as a function of time allows the calculation of the diffusion coefficient and from it, the hydrodynamic radius.[111]

To make valid calculations from ultramicroscopic particle tracking, the sample must be placed in conditions which assure Brownian motion, meaning that no force fields should be present, such as temperature gradients or solvent evaporation. The analysis proceeds with the tracking of the two dimensional projection in the *x*-*y* plane of single scattering objects. This certainly does not mean that the particles move only in two dimensions. Although the sample compartment is narrow in the z direction (collinear with the light beam), the colloidal objects are normally comparably much smaller, and Brownian motion takes place in all three dimensions.

The average squared distance $\langle R^2 \rangle_n$ traveled by particle *n* in a time lapse Δt can be calculated using the following formula:

$$\langle R^2 \rangle_n = \frac{3}{2k_{max}} \sum_{k=1}^{k_{max}} \{[x_n(k\Delta t) - x_n(k\Delta t - \Delta t)]^2 + [y_n(k\Delta t) - y_n(k\Delta t - \Delta t)]^2\} \quad \textbf{(3.27)}$$

where *k* is the number of recorded steps.

The squared length of a vector in three dimensions is equal to the addition of the three squared components along each Cartesian axis. Brownian motion in each of the three dimensions obeys the same statistical principles. Thus, the movement in the z plane is assumed in the formula to be statistically equivalent to that in the other two dimensions, and weighted in the factor multiplying the summation. The difference between the two squared terms in the summation is indicative of the statistical significance of such assumption, so it can be used to evaluate the error in the size determination of each particle. The average squared distance $\langle R^2 \rangle_n$can be used to calculate the corresponding diffusion coefficient D_s, using equation (3.10) and with it, the hydrodynamic radius R_H. using equation (3.11)

3.4 Scanning electron microscopy

Electron microscopy makes use of an electron beam instead of light. The wavelength is controllable by changing the acceleration voltage of the electrons, in accordance to the principles of quantum physics. In this case, magnetic fields act analogous to optical lenses in conventional optic microscopes. For its operation, high vacuum is needed in order to prevent the electrons from being stopped by gas molecules. This limits the operation to dry samples.

In scanning electron microscopy (SEM), a beam of high energy *primary electrons* is focused on the sample, which is placed on a conducting plate. The beam is scanned over the sample in a rectangular pattern by applying deflecting magnetic field which are

perpendicularly oriented. Imaging is based on the emission of *secondary electrons*, which emerge from the atoms which compose the surface of the analyzed sample. These are attracted by a positively charged secondary electron detector. The produced signal is synchronized with the position of the scanning primary electron beam to produce an image (see Figure 3.10). Scanning electron microscopy produces images which depend on the topography of the scanned surface, thus providing three-dimensional information. Typically, the resolution ranges from 1 nm to 10 nm. [110]

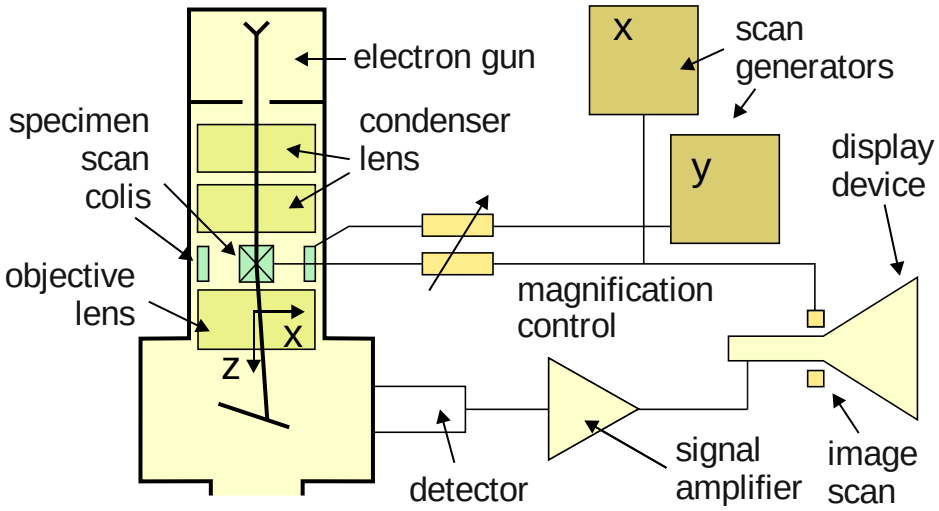

Figure 3.10. Schematic representation of a scanning electron microscope. [110]

The analysis of colloids by SEM has the inherent limitation for dry samples, given the high vacuum conditions which are necessary for the electron beams to travel without disruption. Thus, the analysis of colloidal systems by SEM is mainly advantageous for the structural investigation of the colloidal objects, provided they are stable under vacuum. The three dimensional images represent a valuable tool for the topographical inspection of the colloidal objects. Nevertheless, such topographic imaging implies dimensional distortions or *foreshortenings*, which imply limitations to the use of this characterization method for accurate dimensional analysis. As a consequence, the study of size populations by SEM results in the broadening of the real distribution.[103]

3.5 Turbidimetry

Turbidimetry is the measurement of the attenuation of light after it travels through a specimen. This effect is known as light *extinction*.[112] The measurement can be accomplished with a simple collinear arrangement of a beam of light, the sample, and a photo-detector.

Extinction results from absorption and scattering. Absorption is the main contributor to extinction when the sample is homogeneous. Heterogeneous samples, on the other hand, scatter light more strongly, provided the inhomogeneous domains are in the size range or larger than the wavelength of the incoming light. Scattering takes place on the interface between two materials of differing refraction indexes, which implies that light travels at different speeds in each of these phases. Samples composed of more than one phase of different index of refraction scatter light strongly, which is the case of several colloids.

The extinction of light is defined as:

$$E = \frac{I}{I_0} = exp(-\alpha_{ext} d) \qquad \textbf{(3.28)}$$

where I_0 is the intensity of the incoming light beam, I is the intensity of the attenuated light beam after it travels through the sample, d is the distance the beam travels through the sample, and α_{ext} is an extinction coefficient, which is defined as:

$$\alpha_{ext} = N(C_a + C_s) \qquad \textbf{(3.29)}$$

where C_a and C_s, are the *extinction cross sections* of absorption and scattering respectively, and N is the number of particles per unit volume. An extinction cross section is a hypothetical area which describes the efficiency with which light is extinct by a particle.[112]

3.6 UV/vis spectroscopy

UV/vis spectroscopy refers to the measurement of the absorption of electromagnetic radiation by a sample as a function of wavelength within the ultraviolet to visible range. The resulting absorption spectrum has qualitative and quantitative analytical significance. The absorption of light in the ultraviolet and visible range results in the electronic and vibrational excitation of molecules. An electron in the ground state is promoted by the absorption of a photon, to an unoccupied orbital of higher energy. For this type of transitions, the spectral absorption bands are generally broad, due to the multiple populated vibrational levels which undergo the electronic transition.[113]

The absorbance is experimentally determined in a spectrophotometer (Figure 3.11), which measures the change in the intensity of a monochromatic light beam after it passes through the sample. The absorbance A is defined as:

$$A = log\left(\frac{I_0}{I}\right) \qquad \textbf{(3.30)}$$

where I_0 the intensity of the incoming light beam, and I the intensity of the beam after it travels through the sample. The quantitative significance of this technique is based on the Lambert-Beer law, which is expressed as:

$$A = \epsilon c l \qquad \textbf{(3.31)}$$

where ϵ is the molar extinction coefficient, c is the concentration, and l the path-length traveled by light through the sample. The actual value of the coefficient may vary depending on a series of experimental conditions, such as the solvent.[114]

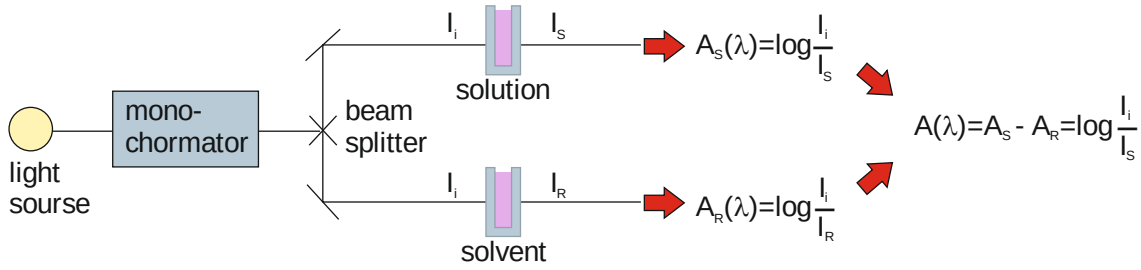

Figure 3.11. Schematic representation of a spectrophotometer.[114]

4 RESULTS AND DISCUSSION

4.1 Synthesis of photo-responsive polymer nanoparticles

4.1.1 Introduction

The present study is centered on functional colloidal nanoparticles which can be reversibly aggregated with light. This chapter describes the synthesis of polymer nanoparticles which are labeled on the surface with responsive molecular structures which undergo associative interactions under light stimulation. Such particles are expected to form the referred light responsive colloidal systems. For this functional purpose, it is necessary that the photo-active functional structures are present right on the interface between the nanoparticles and the continuous phase, with a certain degree of mobility. To fulfill these requirements, it is intended to obtain hard nanospheres with an outer section consisting of pending free chains, carrying the photo-responsive molecule at the free end.

Polymer nanoparticles with a monodisperse size distribution can be conveniently prepared by the miniemulsion technique.[1] The synthesis of copolymers by this technique can be directed towards the deliberate inclusion of certain functional groups over the surface. In miniemulsion systems with an aqueous continuous phase, the more hydrophilic components of the monomer mixture diffuse to the interface of the nano-sized droplets, thus resulting after polymerization in nanospheres with a chemical functionality over the surface which corresponds to the more hydrophilic groups of the monomeric components.[115] In the case of the systems here studied, the selected photo-responsive labels anthracene and pyrene are hydrophobic. Thus, their incorporation to the surface of hydrophobic nanospheres cannot be carried out directly during a miniemulsion polymerization procedure. The functionality of the surface which results from copolymerization in miniemulsion should thus be selected taking in consideration that the hydrophilic component of the monomer mixture (which is expected to migrate to the interface) has chemical properties which are adequate for subsequent post-polymerization synthetic steps leading to the desired labeling.

The overall experimental strategy followed to obtain the desired photo-responsive colloidal systems is described in Figure 4.1. The synthesis of the labeled nanoparticles (up to stage III) is described in section 4.1. The subsequent preparation of aqueous colloidal suspensions of these labeled nanoparticles (samples A through F) is described in sections 4.2 and 4.3, together with the corresponding studies on their photo-responsiveness. The composition of these samples is given in Table 4.1.

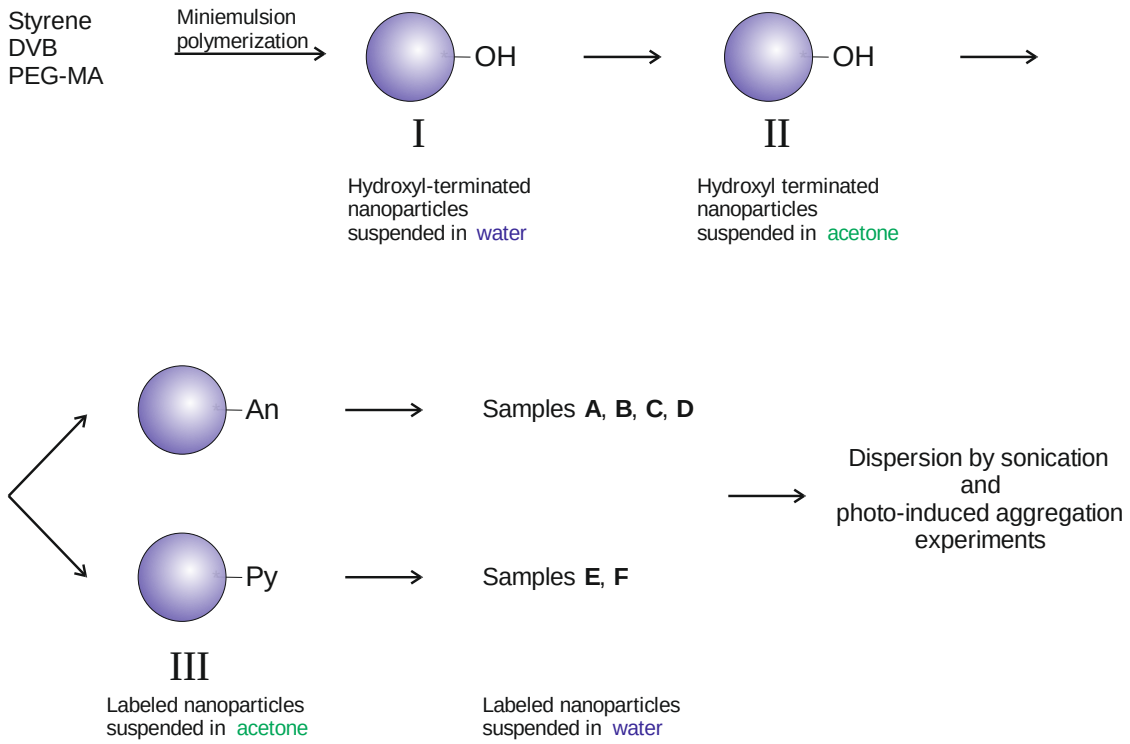

Figure 4.1. Schematic representation of the complete experimental procedures carried on this study.

Table 4.1. Overview of all the samples presented in this study

Sample	Label	Concentration of labeled NPs	Concentration of SDS
A	Anthracene	0.002 g · L^{-1}	0.0012 g · L^{-1} = 0.0005 cmc
B	Anthracene	0.002 g · L^{-1}	0.24 g · L^{-1} = 0.1 cmc
C	Anthracene	0.002 g · L^{-1}	1.2 g · L^{-1} = 0.5 cmc
D	Anthracene	0.002 g · L^{-1}	0.0012 g · L^{-1} = 0.0005 cmc
E	Pyrene	0.002 g · L^{-1}	1.2 g · L^{-1} = 0.5 cmc
F	Pyrene	0.002 g · L^{-1}	2.4 g · L^{-1} = cmc

4.1.2 Preparation of photoactive nanoparticles

The preparation of polystyrene (PS) nanoparticles enriched on the outer interfacial section with poly(ethylene glycol) (PEG) chains carrying photo-active molecular structures on their free ends was carried in two steps: the synthesis of PS-PEG colloidal nanospheres by copolymerization in miniemulsion (stage I in Figure 4.1), and the subsequent chemical labeling in water free conditions (stages II and III in Figure 4.1).

4.1.2.1 Synthesis and characterization of polymer nanoparticles

A master sample of hydroxyl terminated PS-PEG copolymer nanoparticles was produced by direct miniemulsion polymerization (stage I in Figure 4.1). The monomer mixture used for this purpose consisted of styrene, poly(ethylene glycol) methacrylate (PEG-MA), and divinylbenzene (DVB), in weight fractions 0.9, 0.05, and 0.05, respectively. Styrene forms the main core of the particle as it is the largest portion and is highly hydrophobic. DVB is also hydrophobic and readily mixes with styrene. This comonomer was included in the formulation to chemically cross-link the polymer and provide structural stability in organic solvents during the subsequent labeling synthetic step. The amphiphilic comonomer PEG-MA is expected to enrich at the interface between the monomer droplet and the aqueous continuous phase, thus becoming after polymerization the main component of the surface of the nanoparticle. It was included to provide an adequate point for further functionalization out of its terminal hydroxyl groups, which can be chemically bonded with the selected anthracene and pyrene derivatives. Its low molecular weight chains of 360 $g \cdot mol^{-1}$ (6.2 ethylene glycol average repeating units), are expected to provide conformational freedom for the subsequent photo-induced formation of inter-particle bridges.

The size of the produced master sample of nanoparticles was measured by dynamic light scattering (DLS) at multiple angles. The data was evaluated by simple cumulant fit

as introduced by Koppel.[109] The *inverse z average* hydrodynamic radius $[<R_h^{-1}>_z]^{-1}$ was obtained from the *z average* diffusion coefficient, which itself was determined by extrapolation of the corresponding diffusion coefficient values to a squared scattering vector $q^2 \rightarrow 0$ (Figure 4.2). The result of the analysis gave R_h = 59 nm (stage I in Figure 4.1). The cumulant analysis gave a low polydispersity of 0.11. The satisfactory fitting of the data at multiple angles corroborated a monomodal particle size distribution.

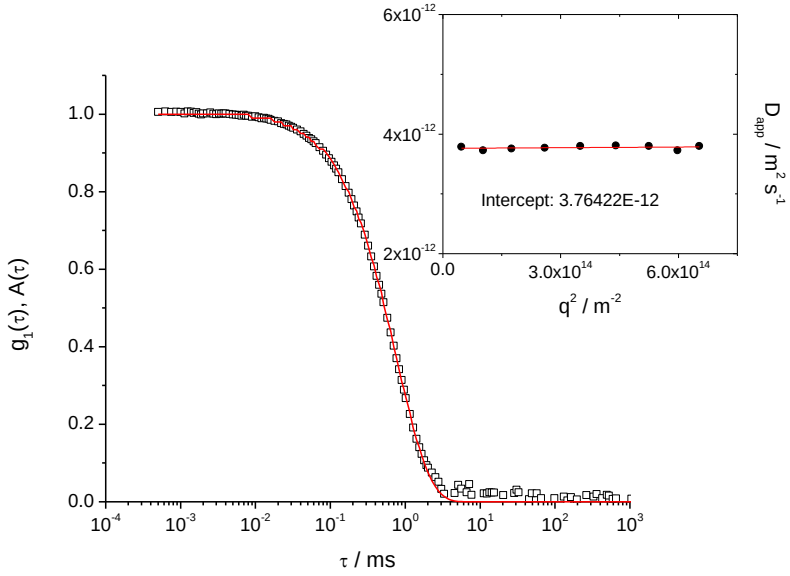

Figure 4.2. Electric field autocorrelation function $g_1(\tau)$ at a scattering angle of 90° analyzed by the method of cumulants. Insert: Extrapolation of the diffusion coefficient values to a squared scattering vecto q^2 of zero. Master suspension of hydroxyl-terminated polymer nanoparticles suspended in water (stage I in Figure 4.1)

The subsequent chemical labeling steps required water free conditions. For this purpose, the particles were transferred from water into dry acetone through several centrifugation and re-dispersion cycles (stage II in Figure 4.1). Acetone was chosen as a suspension medium because it is a bad solvent for polystyrene. Even though the polymer composing the nanoparticles is chemically cross-linked, it is desired to keep swelling in the organic solvent as low as possible to diminish the possibility of any conformational alterations. Acetone is also an adequate choice of solvent because it is miscible with

water, which simplifies the transfer back to aqueous conditions of the nanoparticles after functionalization with the photo-active labels. Stable suspension in acetone could only be obtained at significantly lower solids-content values. The structural stability of the nanoparticles could be corroborated by scanning electron microscopy (Figure 4.3).

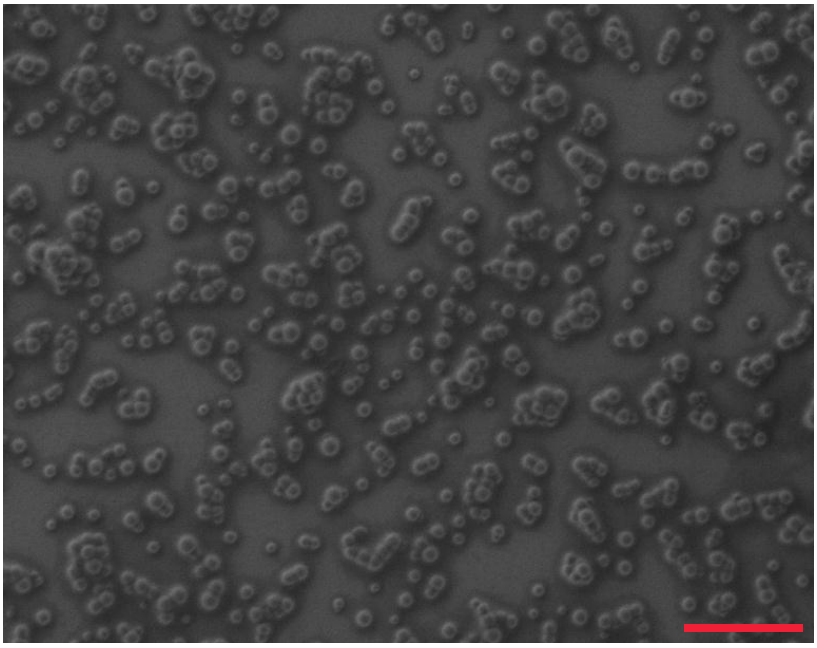

Figure 4.3. Scanning electron microscopy image of the suspension in acetone of PS-PEG copolymer nanoparticles (stage II in Figure 4.1). Scale bar 1 μm.

4.1.2.2 Anthracene labeling

A fraction of the hydroxyl functionalized nanospheres suspended in dry acetone (stage II in Figure 4.1) was labeled with anthracene functionalities (stage III in Figure 4.1) by the esterification reaction of the terminal hydroxyl groups with anthracene carboxylic acid chloride according to the reaction shown in Figure 4.4 (for details, see experimental section).

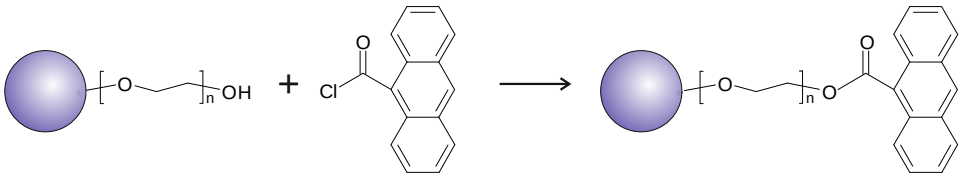

Figure 4.4. Chemical functionalization of the surface of polymer nanoparticles with anthracene carboxylic acid chloride.

After their chemical modification, the nanoparticles were thoroughly washed with acetone through several centrifugation and re-dispersion cycles. The elimination of unreacted anthracene could be evaluated by UV/vis spectroscopy of the continuous phase. Finally, the resulting anthracene-labeled nanoparticles (An-NPs) were kept as a suspension in acetone.

The content of anthracene on the modified nanoparticles was determined by UV vis spectroscopy. A fraction of the suspension in acetone (stage III in Figure 4.1) was dried and re-suspended in tetrahydrofuran (THF), to a final concentration of 3.44 $g \cdot L^{-1}$. This solvent was chosen because it readily dissolves polystyrene. This is expected to diminish light scattering by the nanospheres during the spectroscopic measurement, which ultimately could not be fully avoided.

As shown in Figure 4.5, the characteristic absorption band of anthracene at 383 nm could be identified on An-NPs. The observed high slope of the baseline is characteristic

of strong scattering by the suspended nanoparticles. In order to obtain quantitative information despite scattering, a straight line was traced in between the endpoints of the observed peak. The vertical distance between this imaginary base and the maximum absorption at 383 nm was considered for the analysis. The same type of data handling was carried on the spectra of pure anthracene carboxylic acid solutions in THF of known concentration. The validity of the analysis was confirmed by the observation of a good linear relationship between concentration and absorbance (Figure 4.6), which was determined in the same range of experimental values as that of the An-NP suspension. The content of anthracene in An-NPs was found to an average of 2500 labels per particle (for details, see experimental section).

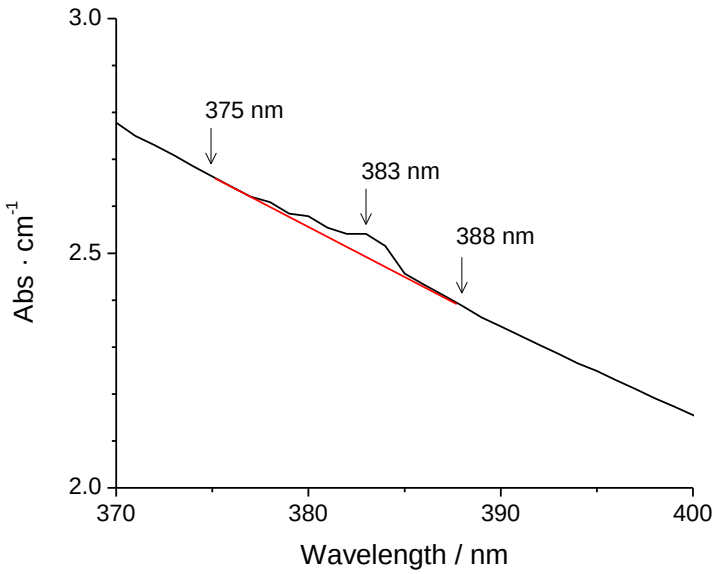

Figure 4.5. UV/vis absorption spectrum of anthracene labeled polymer nanoparticles suspended in THF.

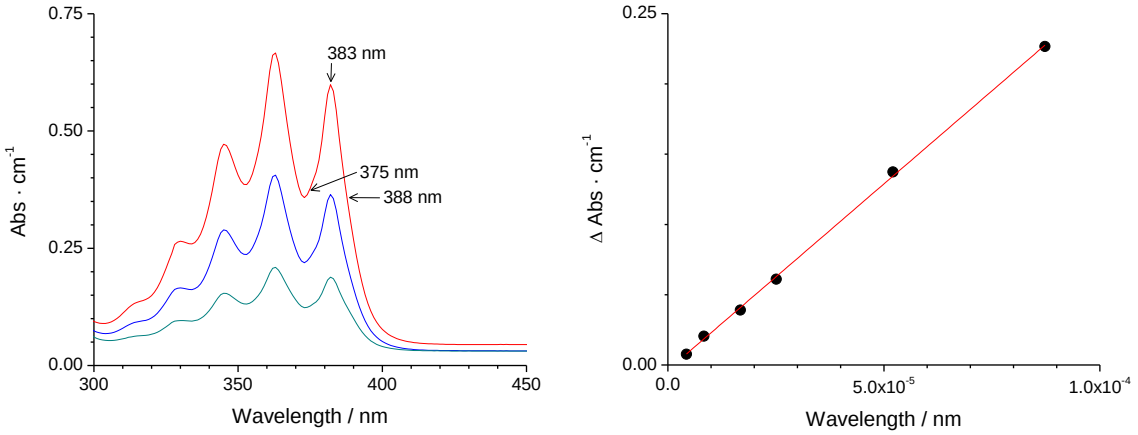

Figure 4.6. Left: Absorption spectra of anthracene carboxylic acid solutions in THF at different concentrations. Right: linear relationship between absorption and concentration, confirming the validity of the Lambert Beer law for this analysis.

4.1.2.3 Pyrene labeling

A second fraction of the hydroxyl-terminated nanospheres suspended in dry acetone (stage II in Figure 4.1) was labeled with pyrene functional structures (stage III in Figure 4.1) by the esterification reaction between the terminal hydroxyl groups with pyrene butyric acid chloride according to the reaction shown in Figure 4.7 (for details, see experimental section).

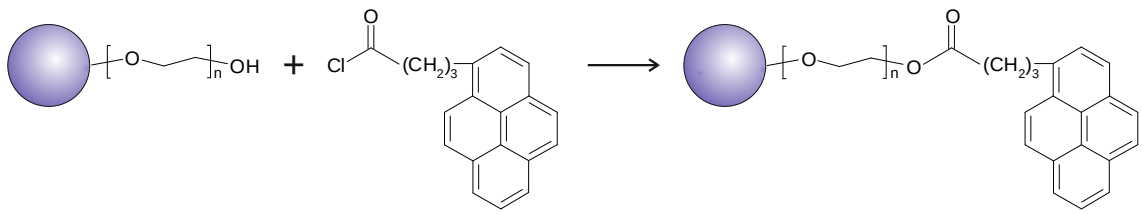

Figure 4.7. Chemical functionalization of the surface of polymer nanoparticles with pyrene butyric acid chloride.

After their chemical modification, the nanoparticles were thoroughly washed with acetone by several centrifugation and re-dispersion cycles. The elimination of unreacted pyrene butyric acid could be evaluated by UV/vis spectroscopic inspection of the continuous phase. The resulting pyrene-labeled nanoparticles (Py-NPs) were finally kept as a suspension in acetone.

The content of pyrene in the modified nanoparticles was evaluated by UV/vis spectroscopy, following the same general procedure previously described for the anthracene-labeled nanoparticles. The UV/vis absorption spectrum of the Py-NPs suspension in THF (11.36 $g \cdot L^{-1}$) is shown in Figure 4.8. It can be observed that the absorption bands of pyrene are fused into a single broad peak. Furthermore, the maximum of this peak is red-shifted with respect to the maximum observed in the absorption spectra of the pure pyrene butyric acid solutions in THF (Figure 4.9). These observations are well known effects of pyrene pre-association,[116] which in this case is indicative of a high density of these labels over the surface of the nanoparticles. The quantitative certainty of the analysis is affected due to pyrene pre-association. Nevertheless, an approximate is accessible through the comparison of the maximum and the minimum to evaluate the corresponding absorbance.[116]

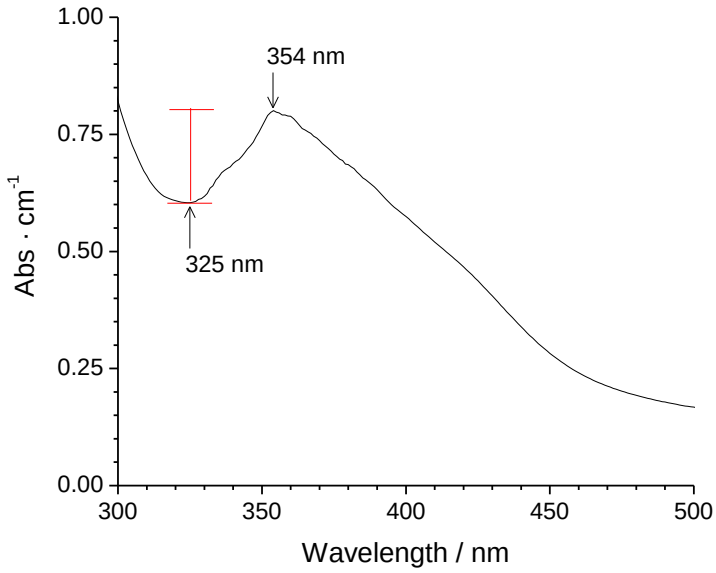

Figure 4.8. UV absorption spectrum of pyrene labeled polymer nanoparticles suspended in THF.

A similar approach was followed for the analysis of the spectra of pure pyrene butyric acid solutions in THF, although due to the red shift effect of pyrene pre-association previously observed, the exact position of the corresponding minimums and maximums was adjusted.

The validity of the analysis was supported by the observation of a good linear relationship between concentration and absorbance (Figure 4.9), which was determined in the same range of experimental absorption values as those of the Py-NP spectra. The analysis indicated an average of over 83000 pyrene labels per nanoparticle, which corresponds to 1.96 molecules per squared nanometer on the surface. This high density is consistent with the highly pre-associated state of pyrene structures which is indicated by the red shift and consequent overlapping of the bands observed in the absorption spectrum of Py-NP (see Figure 4.8)

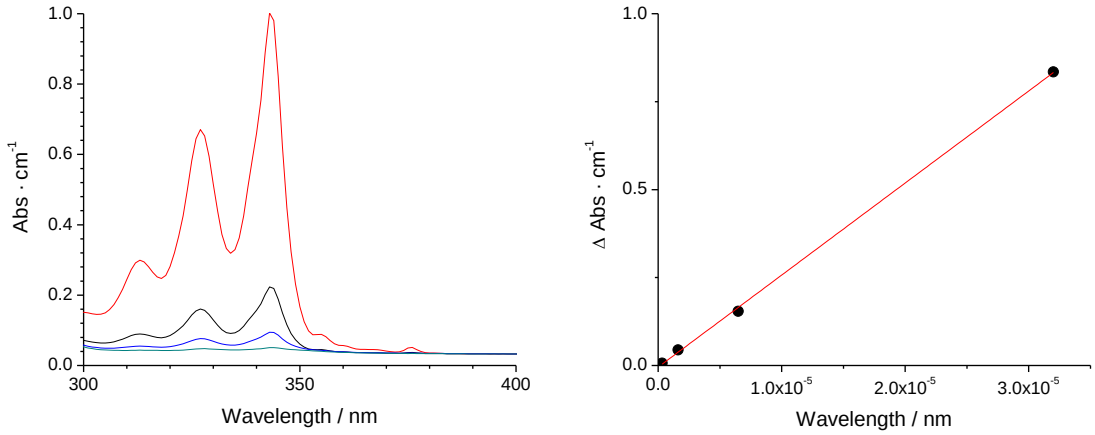

Figure 4.9. Left: Absorption spectra of pyrene butyric acid solutions in THF at different concentrations. Right: linear relationship between absorption and concentration, confirming the validity of the Lambert Beer law for the analysis.

4.2 Photo-induced assembly of anthracene-labeled polymer nanoparticles

4.2.1 Introduction

Anthracene has photo-chemical properties which make it attractive for the development of responsive materials. It forms dimers through a photo-cycloaddition reaction, which is reversible with light of higher energy or when heat is applied.[117] As previously described, anthracene has been successfully used to develop polymer-based responsive materials. Its incorporation to macromolecular building blocks has resulted in systems which can be reversibly cross-linked as a response to photo-irradiation,[63, 93-99] although in most cases reversibility has been achieved only partially.

Nanometer scale responsive materials based on anthracene dimerization have recently been developed. The aggregation of anthracene-labeled gold nanoparticles was reported in lyophilic colloidal conditions, where the solvent toluene readily solubilizes the photo-active anthracene molecular structures. Although the formation of clusters was detected, no detailed quantitative information regarding the systemic aggregation and re-dispersion processes was reported.[100]

The present section documents the study of the reversible assembly of anthracene-labeled polymer nanoparticles suspended in water (Figure 4.10). This system represents a versatile model of a lyophobic colloid consisting of labeled nanoparticles which, because of their size scale and preparation method, can be conveniently adapted to diverse hybrid compositions. Attention is centered in the controlled formation of aggregates and the reversibility of the process.

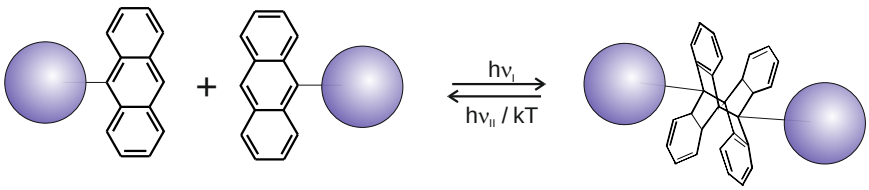

Figure 4.10. Reversible photo-induced dimerization of anthracene-labeled nanoparticles.

4.2.2 Effect of surfactant concentration on the initial state of dispersion and the kinetics of photo-induced aggregation

The content of surfactant is determinant for the stabilization of lyophobic colloids. Given their overall hydrophobic structure, the stability of anthracene-labeled nanoparticles (An-NPs) suspended in water can be expected to strongly depend on the surfactant content. The mechanism for the stabilization of such systems by surfactants is based on the development of repulsive forces between the suspended particles. Thus, the ease to bring these particles together can be anticipated to be strongly influenced by the surfactant.

The initial investigation of the possibility to aggregate An-NPs suspended in water was carried taking into consideration the effects of surfactant concentration. For this purpose, two samples were prepared with the same concentration of nanoparticles, but different concentration of the ionic surfactant sodium dodecyl sulfate (SDS). Both samples were prepared by dilution of aliquots of the same master suspension, which had been previously prepared through the incorporation of An-NPs to an aqueous solution of sodium dodecyl sulfate (SDS) at the critical micelle concentration (cmc) (see experimental section). Both samples appeared clear and homogeneous after preparation. They were further homogenized by simple stirring for a period of over 24 h.

Table 4.2. Composition of aqueous colloidal samples *A* and *B*.

Sample	Concentration of An-NPs	Concentration of SDS
A	0.002 g · L^{-1}	0.0012 g · L^{-1} = 0.0005 cmc
B	0.002 g · L^{-1}	0.24 g · L^{-1} = 0.1 cmc

Samples *A* and *B* were photo-excited under the same experimental conditions for a total of 5 periods of 15 min each (for details see experimental section). The average

hydrodynamic radius was monitored by dynamic light scattering (DLS) measurements carried before and after each photo-excitation period.

The DLS data were initially analyzed using the CONTIN algorithm introduced by Provencher.[108]. It could be observed at low scattering angles that both samples in the initial state presented two main relaxation modes. These were assigned to the diffusion of single nanoparticles and nanoparticle aggregates. In order to properly evaluate the change in the aggregation state of the colloid as photo-irradiation proceeds, it is necessary to obtain quantitatively significant figures which take into consideration the relative content of single particles and of aggregates of different sizes. The average hydrodynamic radius of the entire system is an adequate figure for this purpose. Based on the two bands observed in the initial inspection using the CONTIN algorithm, further analysis of the DLS data was carried out by fitting the experimental intensity correlation function to the sum of two extended exponentials. With the results of such fit at different scattering angles it was possible to obtain the z average diffusion coefficient by extrapolation to zero scattering angle, and from it the *inverse z average* hydrodynamic radius $[<R_h^{-1}>_z]^{-1}$ of the entire system.

To achieve an integral assessment of the system, the average R_h values for each of the analyzed samples are presented along with the corresponding scattered intensity values relative to the initial state (Figure 4.11 and Figure 4.12). This parameter is important in order to evaluate whether the changes in the colloidal size are accompanied by the formation of precipitates. It should be noted that DLS detects only those particles which are in colloidal suspension. The intensity of the scattered light is proportional to the number of scattering objects and to their squared mass. Thus, the analysis of the average hydrodynamic radius in parallel to the relative scattered intensity allows determining whether a change in size can be partially attributed to precipitation.

The initial average R_h value obtained for each sample is a clear indicative of the importance of the surfactant concentration on the stability of the sample. For both samples, this value is considerably higher than the size of the nanoparticles before anthracene labeling ($<R_h>$ = 59 nm), which can be understood in terms of an initial state of partial aggregation. Such an explanation is consistent with the observed initial average size equilibrated at a lower value when the content of SDS is higher (Figure 4.11 and Figure 4.12). The initial equilibration size and its dependence on the

concentration of surfactant are consistent with the lyophobic nature of this colloidal system, due to the overall hydrophobic character of An-NPs.

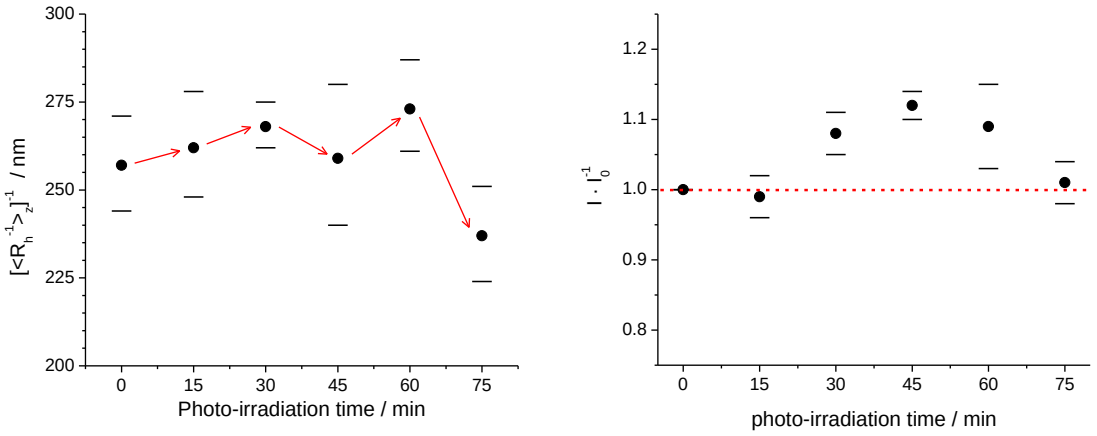

Figure 4.11. Left: average hydrodynamic radii as a function of irradiation time, determined by dynamic light scattering. Right: Relative scattered intensity corresponding to the DLS measurements (a red dotted guideline is presented at a ratio of 1 for comparison purposes). Sample *A* ($c_{\text{An-NP}}$ = 0.002 g · L^{-1}, c_{SDS} = 0.0012 g · L^{-1} = 0.0005 cmc).

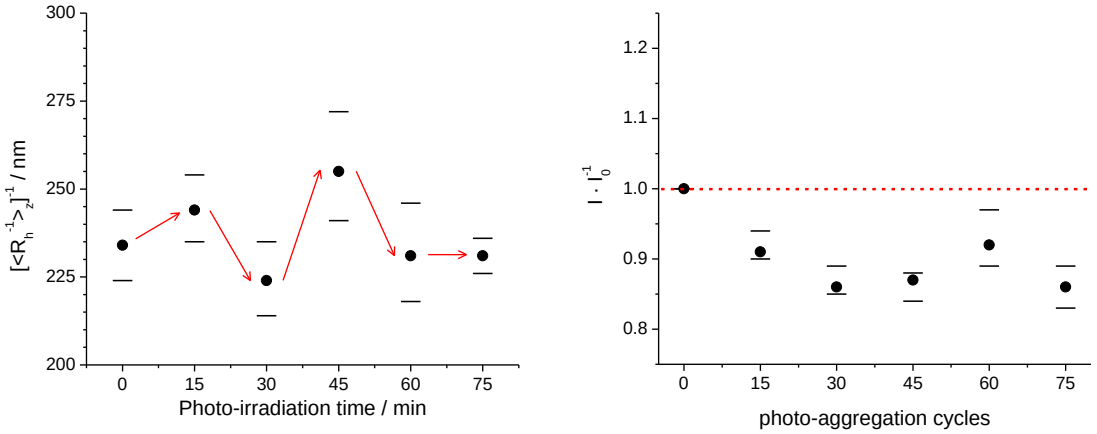

Figure 4.12. Left: average hydrodynamic radii as a function of irradiation time, determined by dynamic light scattering. Right: Relative scattered intensity corresponding to the DLS measurements (a red dotted guideline is presented at a ratio of 1 for comparison purposes). Sample *B* ($c_{\text{An-NP}}$ = 0.002 g · L^{-1}, c_{SDS} = 0.24 g · L^{-1} = 0.1 cmc).

The effect of photo-irradiation on the average size of both samples indicates that it is possible to aggregate colloidal systems of An-NPs with light signaling. Nevertheless, the effect appears to be mild.

Although a consistent increase in average size appears to be the case in sample *A*, this change is observed within the experimental error of the measurement. Still, the likelihood that aggregation is taking place is supported by the observed increase in the relative scattered intensity. The sudden decrease in average size after the last photo-irradiation step can be explained in terms of precipitation, which takes place when progressive aggregation eventually results in the formation of aggregates which are too big to remain stable in the suspension. The resulting precipitation of the larger-sized fraction of the colloid results in a decrease of the average size of the fraction which remains suspended, which is the one that is actually detected by DLS. The proposed formation of precipitate at this final step is consistent with the observed decrease in scattered intensity.

The effect of photo-irradiation on the average size of sample *B* appears to be quite erratic. Nevertheless, it can be found that it matches the observations from sample A if it is considered that the higher content of surfactant has a direct effect on the kinetics of photo-induced aggregation. It can be speculated that the lower surface tension which results from the addition of SDS facilitates the actual contact between the colloidal objects, eventually resulting in a more effective aggregation process which proceed at a faster pace. The formation of precipitate appears to decrease the average size of the colloid every second irradiation step. This explanation is consistent with the constant decrease in scattering intensity, which would be expected after copious precipitation. In that sense, the event of aggregation and subsequent precipitation taking place in sample *A* over a total irradiation time of 75 min, appears to be analogous to the events on sample *B* taking place within 30 min of photo-irradiation.

4.2.3 Detailed analysis of photo-induced aggregation and its reversibility

Further analysis is necessary in order to provide more reliable evidence of the photo-induced aggregation process. It is desired to explain why the effect on the average size appears to be limited. For this purpose, more detailed information is necessary in addition to the average size of the colloidal objects using dynamic light scattering (DLS). The actual distribution of sizes of the colloid can be elucidated using ultramicroscopic particle tracking. Both techniques are highly convenient for the study of aggregation since they are non-disruptive and provide information of the colloid without disrupting it. In order to observe a more pronounced effect of photo-irradiation on the average size of the colloidal objects, it is desirable to have an initial state which is highly dispersed, i.e., with a lower content of aggregates. For this purpose and based on previous results, it was decided to use higher concentrations of surfactant.

Initial dispersed state

A suspension (labeled sample *C*) of anthracene-labeled nanoparticles (An-NP) in aqueous sodium dodecyl sulfate (SDS) was prepared with final concentrations $c_{\text{An-NP}} = 0.002\ \text{g} \cdot \text{L}^{-1}$, and $c_{\text{SDS}} = 1.2\ \text{g} \cdot \text{L}^{-1}$. This concentration of surfactant corresponds to a fraction of 0.5 of the critical micelle concentration (cmc). The suspension appeared clear and homogenous at simple observation. Initial analysis of this suspension by dynamic light scattering gave as a result an average hydrodynamic radius of $R_h = 222$ nm, a value well above that of the original polymer nanoparticles before chemical modification. This value is still in the same range as those observed in the first two samples, despite the substantially higher content of surfactant. In order to promote further re-dispersion, the suspension was treated in a conventional ultrasound bath. Progressive changes in the hydrodynamic radius of the suspension were monitored by DLS. The overall state of aggregation of the system was evaluated through changes in the average hydrodynamic radius. After continued treatment, it was not possible to reach an average size comparable to that of the original unlabeled nanoparticles as determined by DLS. The treatment was prolonged until no significant changes could be

further observed. The sample was left still standing for a period of two weeks, after which DLS was re-measured. The average size of the colloidal objects remained constant within experimental error, with a final value of R_h = 164 nm, thus evidencing the colloidal stability of the system.

In order to understand the difficulty to fully re-disperse the sample into single nanoparticles with an average size in the range of that of single particles, it is important to note that DLS gives an inverse z average hydrodynamic radius, which implies that the obtained value is heavily influenced by the larger-sized fractions of the sample, and may considerably deviate from the number average when the distribution is not monodisperse. For instance, discrete normal distributions with relative standard deviation values greater than 1, will give inverse z average values over 2.8 times larger than the number average (see Figure 4.13). In such cases, the inverse z average hydrodynamic radius given by DLS can be understood as a measurement of the larger end of the distribution of sizes.

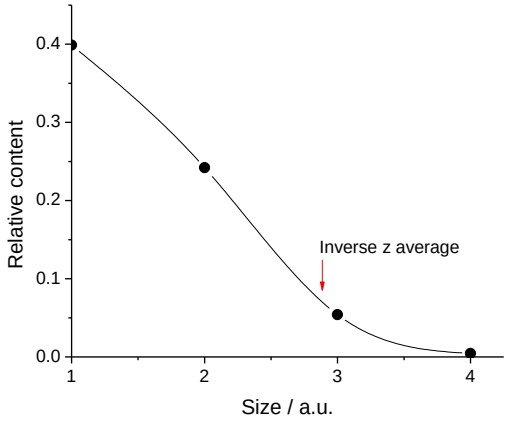

Figure 4.13. Hypothetic normal distribution of sizes, with a value of σ^2=1, and the maximum population at the lowest possible size value of 1.

Sample *C* was analyzed by ultramicroscopic particle tracking to get an insight on the distribution of sizes in the colloid (Figure 4.14). The results revealed that the sample consisted of a mixture of suspended bodies of different sizes, with the majority in the

range of the original un-modified nanoparticles, and a few in a size range which corresponds to aggregates of two of more nanoparticles.

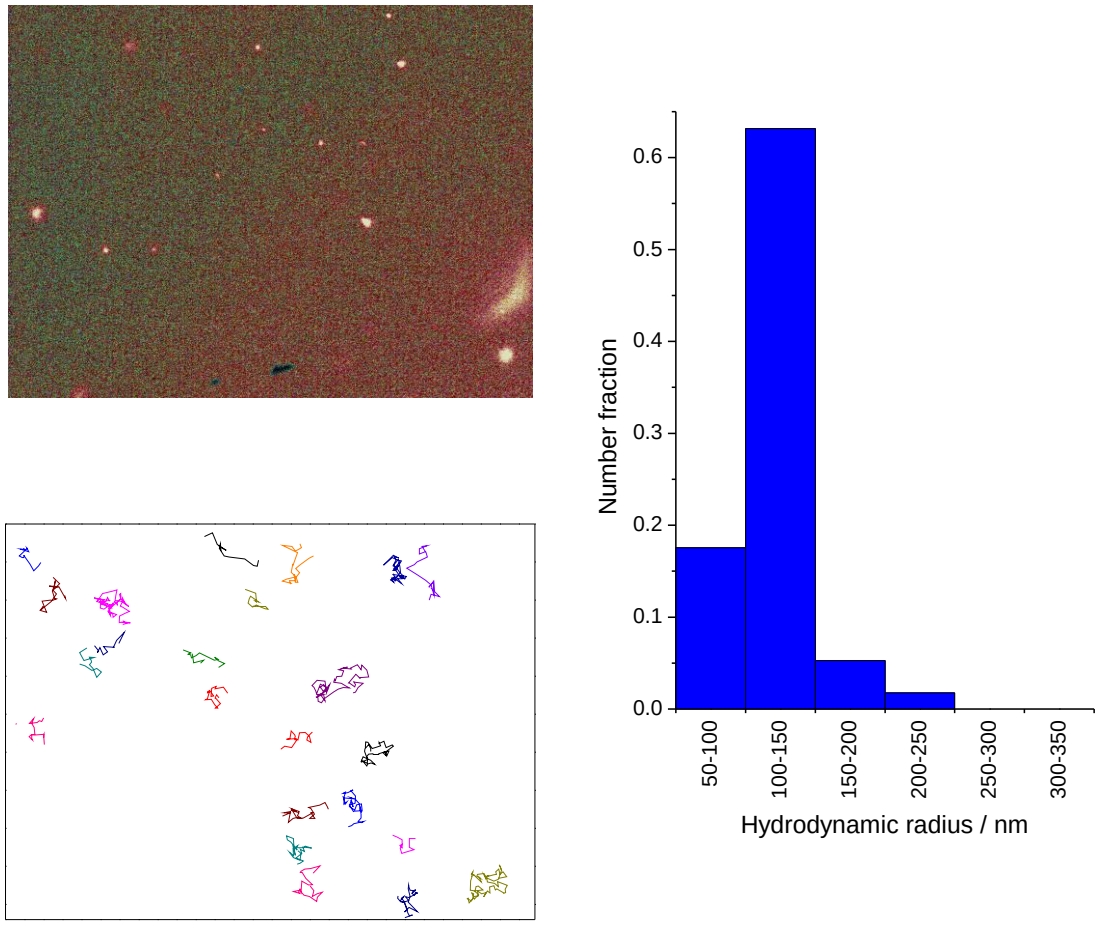

Figure 4.14. Ultramicroscopic particle tracking of the initial dispersed state of sample *C*. Left up: dark field image. Left down: trajectories of the observed particles. Right: Hydrodynamic radii distribution of the tracked colloidal objects.

In general, the shape of the distribution curve is indicative of the history of the colloid. A distribution with a prolonged tail towards smaller sizes indicates that the colloid was formed by nucleation. On the other hand, a distribution of sizes with a prolonged tail towards larger sizes indicates that the colloid was formed by fragmentation. Accordingly, symmetric distributions result as an equilibrium between nucleation and fragmentation processes.[103] In the case of re-dispersed aggregates composed of mono-

sized particles, the size distribution would be expected to have an inherent sharp lower limit at the size of a single particle, and a tail extended towards higher values. Such description complies with the results shown in Figure 4.14.

Further analysis of the sample by scanning electron microscopy confirmed the presence of a majority of single nanoparticles, along with a few aggregates in the range of sizes detected by ultramicroscopy (see Figure 4.15). This corroborates that the higher average size detected by DLS results from a state of partial aggregation. Despite being an analytical technique which disrupts the colloidal state of the sample, it appears that the overall state of aggregation was not heavily distorted by drying during sample preparation, due to the high content of surfactant.

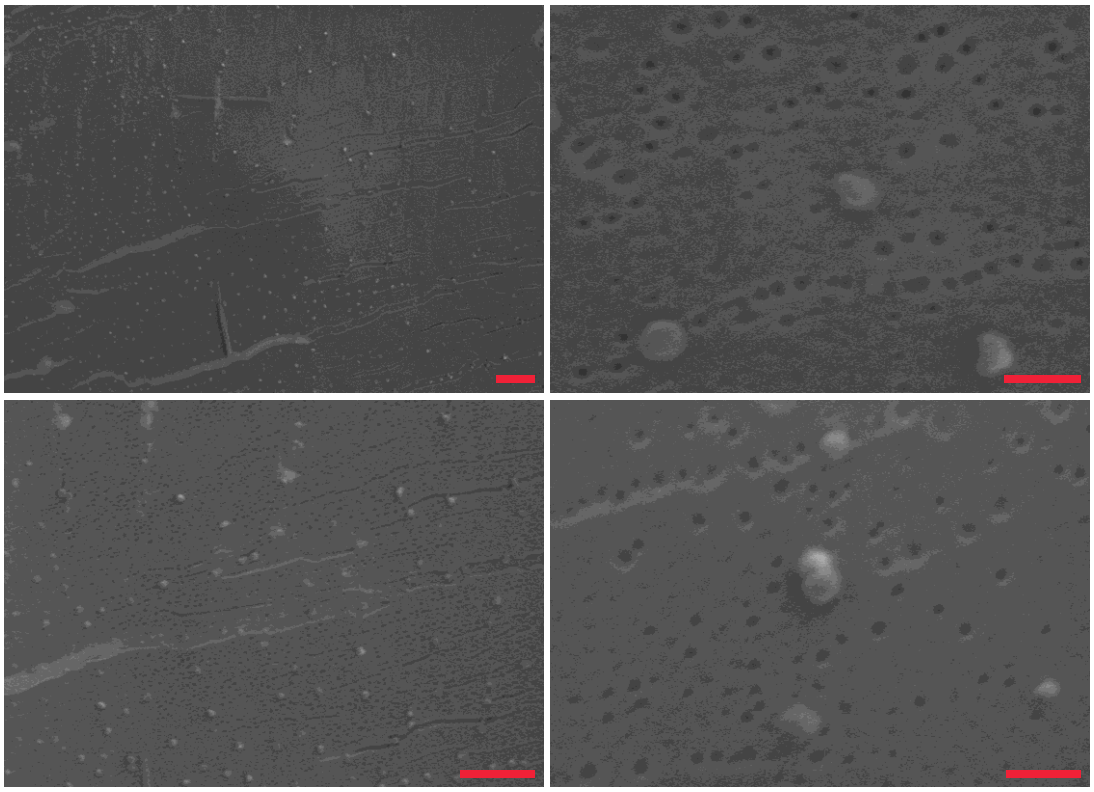

Figure 4.15. Scanning electron microscopy of anthracene-labeled nanoparticles in the initial dispersed state. The nanoparticles can be observed resting over a surfactant-covered surface. Sample *C* ($c_{\text{An-NP}}$ = 0.002 g · L^{-1}, c_{SDS} = 1.2 g · L^{-1} = 0.5 cmc). Scale bars, left: 1μm, right: 200 nm.

The actual state of dispersion of the major portion of the nanoparticles in the system could not be satisfactorily revealed by DLS due to the presence of larger aggregates

which, even though are low in number, strongly influence the measurable inverse z average as previously discussed.

The difficulty to fully re-disperse the entire system can be understood in terms of the decreased hydrophilic character of the nanoparticles. After anthracene labeling, the hydrophilic terminal hydroxyl groups, which are determinant for the aqueous solubility of oligomeric poly(ethylene glycol),[118] were replaced by highly hydrophobic anthracene structures, thus significantly compromising the colloidal stability of the nanoparticles. As a result, full re-dispersion of single nanoparticles in a state of equilibrium appears unlikely.

Photo-induced aggregation

As previously discussed, the stability of the initial state was verified by DLS measurements, which gave a constant average R_h value within experimental error over a period of two weeks. The presence of precipitate at this point was discarded through turbidimetry measurements. Only negligible differences within experimental error were detected in the attenuation of the sample homogenized by stirring, compared to that measured after 24 h of still standing for sedimentation.

In preliminary trials, prolonged photo-excitation was clearly recognized to trigger precipitation, as evidenced even by direct observations at the macroscopic level. It was thus taken care to limit exposure time, aiming to produce colloidally stable aggregates. Figure 4.16 shows the progressive effect of photo-excitation time on the average hydrodynamic radius value of the colloidal system as determined by DLS. A correlation between size and exposure time is observed.

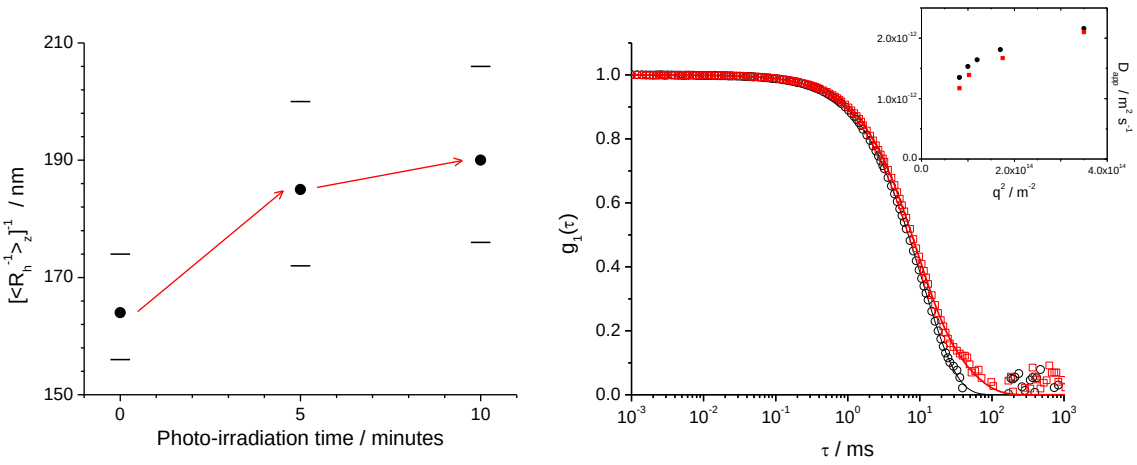

Figure 4.16. Average hydrodynamic radii R_h as a function of irradiation time, determined by dynamic light scattering. Sample *C* ($c_{\text{An-NP}}$ = 0.002 g · L^{-1}, c_{SDS} = 1.2 g · L^{-1} = 0.5 cmc).

The total period of photo-excitation was delivered in two steps. It is noted that the effect of the second step on the average hydrodynamic radius is not as pronounced as that of the first one, which can be understood when a compact arrangement of the aggregates is considered. This can be visualized with the results from scanning electron microscopy on the photo-aggregated sample (Figure 4.17), which shows that the formation of aggregates with compact arrangements results in modest diameter changes even at higher aggregation numbers. Consider the aggregate shown in Figure 4.18, which despite being composed of several nanoparticles, results in a colloidal object with a radius in the range of 100 nm, which is roughly twice that of single particles before chemical functionalization.

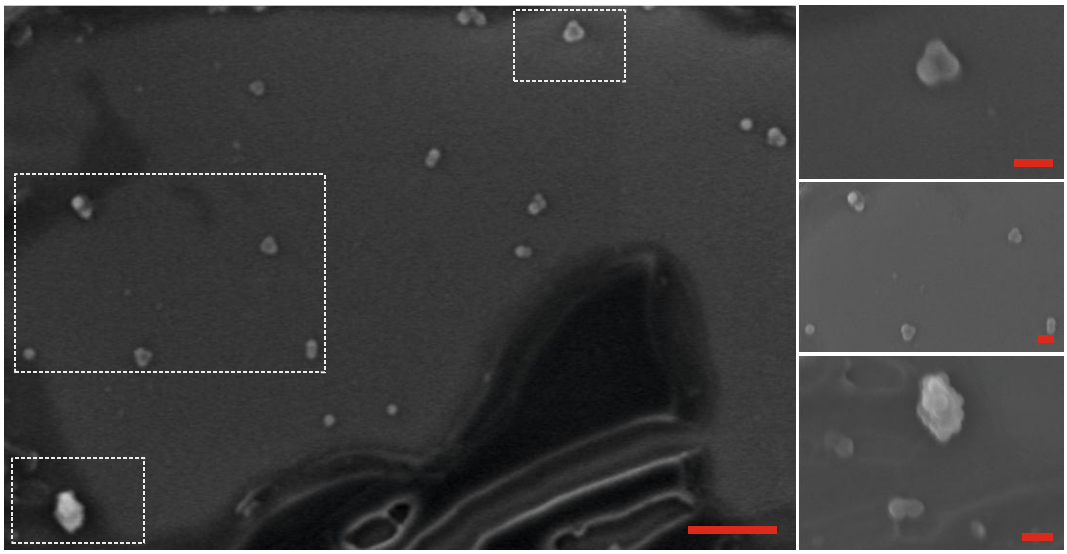

Figure 4.17. Scanning electron microscopy of anthracene-labeled nanoparticles after photo-irradiation. Sample *C* ($c_{An\text{-}NP}$ = 0.002 g · L^{-1}, c_{SDS} = 1.2 g · L^{-1} = 0.5 cmc). Scale bars, left: 1µm, right: 200 nm.

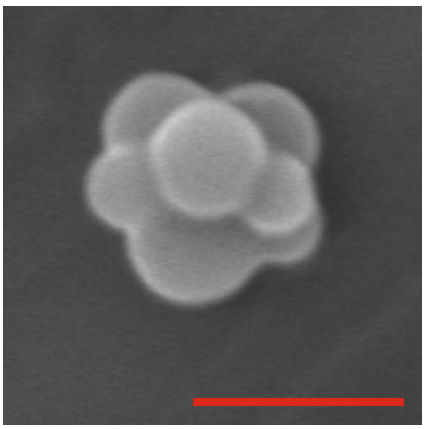

Figure 4.18. Scanning electron microscopy of anthracene-labeled nanoparticles after photo-irradiation. Scale bars, left: 1µm, right: 200 nm. Sample *C* ($c_{An\text{-}NP}$ = 0.002 g · L^{-1}, c_{SDS} = 1.2 g · L^{-1} = 0.5 cmc). Scale bar: 200 nm.

Ultramicroscopic particle tracking of the photo-excited sample showed the displacement of the size distribution towards higher values, with the emergence of aggregates in size ranges well above those corresponding to simple dimers. This confirms aggregation,

and also that the aggregated nanoparticles remain active for further assembling, which may eventually result in the formation of precipitate.

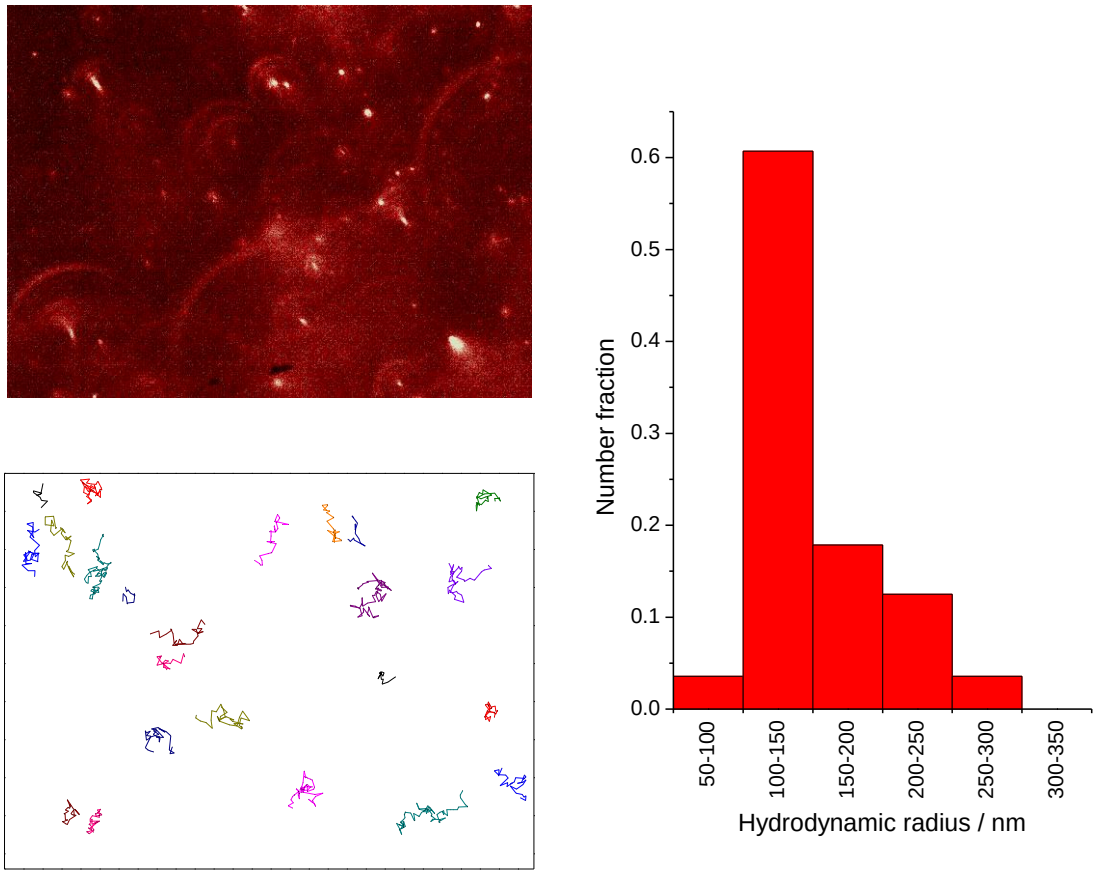

Figure 4.19. Ultramicroscopic particle tracking of sample *C* after photo-irradiation. Left up: dark field image. Left down: trajectories of the observed particles. Right: Hydrodynamic radii distribution of the tracked colloidal objects.

Further analysis of the photo-aggregated sample was carried by turbidimetry. The change in hydrodynamic radius observed by DLS appeared to be in agreement with turbidimetry measurements, showing an increase in attenuation (from 14% to 18.8%) which is expected to result from an increase in the size of the suspended objects. Furthermore, a slight increase in the attenuation of the sample homogenized under stirring, compared to that after a sedimentation period of 24 h, (from 18.8% to 17.3%) indicated the formation of some precipitate.

Re-dispersion of the photo-aggregated state

The photo-aggregated state of sample *C* was sonicated with the aim to induce re-dispersion. Ultrasound is well known to cause cavitation in the continuous aqueous medium, which results in the generation of localized points of high temperature and pressure. Cavitation is prone to occur at interfaces, where there is a sudden change in the mechanical properties which govern sound transmission. To re-disperse this photo-aggregated lyophobic colloid, it is not only necessary to break any formed anthracene photo-dimer bridges, but also to provide energy to mechanically separate the hydrophobic particles, thus allowing the regeneration of the surfactant / solvation shells around them. Ultrasound appears as an adequate instrument to meet both requirements, as it generates localized high temperature points over the interface of the suspended spheres to cleave anthracene dimers, and also provides high energy for the actual separation of the nanoparticles.

Sample *C* was sonicated in a conventional ultrasound bath during 90 min, after which it was analyzed. The results from DLS indicated a decrease in the average size of the suspended fraction of colloidal objects after sonication. The average size determined by DLS decreased from a value of R_h = 190 nm in the photo-aggregated state, down to R_h = 159 nm.

The distribution of sizes of the sonicated sample was analyzed by ultramicroscopic particle tracking. As shown in Figure 4.20, the larger fractions previously detected in the photo-aggregated sample (Figure 4.19), can no longer be observed.

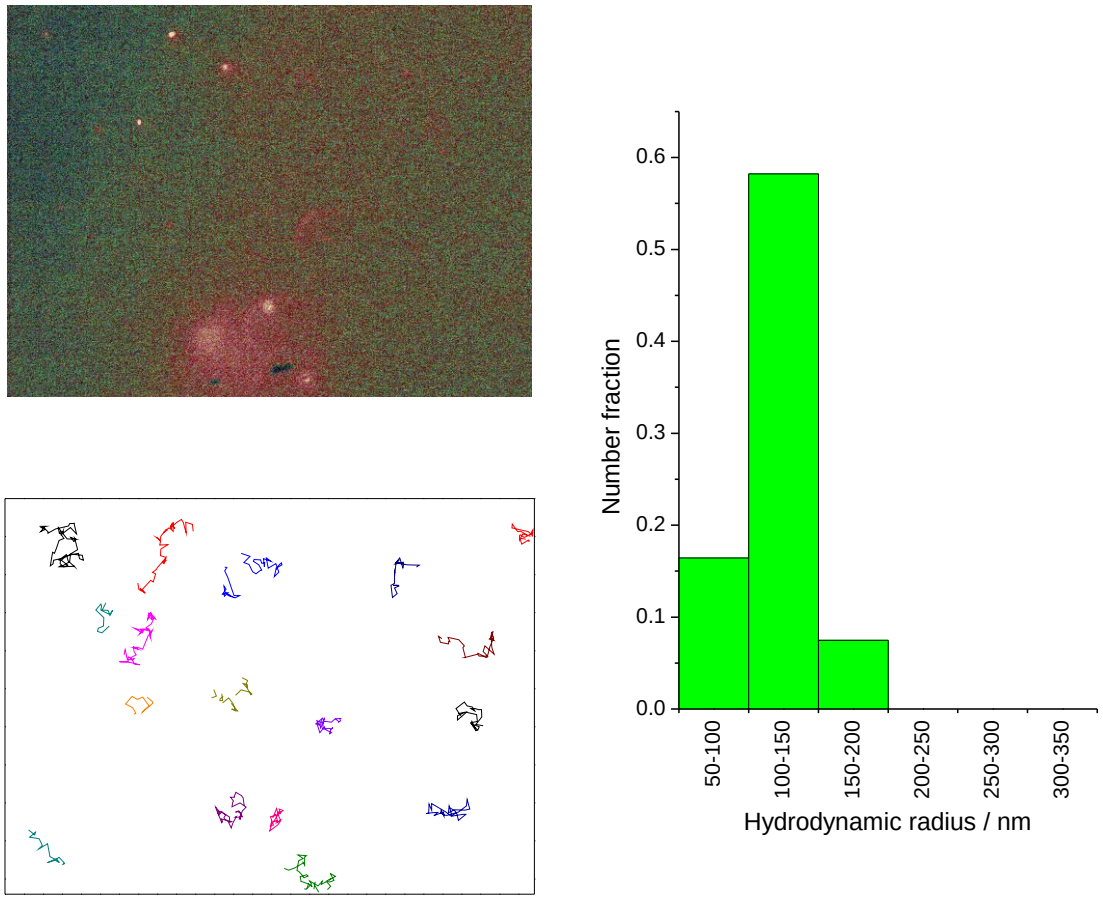

Figure 4.20. Ultramicroscopic particle tracking after sonication, of the previously photo-aggregated sample *C*. Left up: dark field image. Left down: trajectories of the observed particles. Right: hydrodynamic radii distribution of the tracked colloidal objects.

Importantly, turbidimetry indicated the concurrent re-dispersion of some of the particles which had been precipitated under photo-excitation, which is a clear indicative that the decrease in average size of the suspended fraction of colloidal objects detected by DLS and ultramicroscopy is not the result of precipitation but an integral change in the system. A summary of the corresponding turbidimetry measurements on the three investigated states of sample *C* is presented in Table 4.3. After sonication, the attenuation of the homogenized suspension reverted to lower values, implying a systemic decrease in the average size of the objects, including both the precipitated and the suspended fractions. Turbidimetry revealed as well that after sonication a fraction remained precipitated, as indicated by a lower attenuation of light when the

homogenized colloid was allowed to sediment. Altogether, it can be concluded that the state of photo-aggregation can be reverted through sonication.

Table 4.3. Turbidimetry measurements. Sample *C* ($c_{An\text{-}NP}$ = 0.002 g · L^{-1}, c_{SDS} = 1.2 g · L^{-1} = 0.5 cmc).

	Intensity attenuation		
	Initial state	**After irradiation**	**After sonication**
Homogenized (under stirring)	14.0%	18.8%	14.0%
Sedimented (+24 h still standing)	13.6%	17.3%	12.5%

Overview of photo-aggregation and its reversibility

The evaluation (on sample *C*) of the photo-aggregation process and its reversibility has been carried out by comparatively analyzing three states: 1) the initial dispersed equilibrium, 2) the state after photo-excitation, and finally 3) the state after sonication for re-dispersion. A summary of the hydrodynamic radii measurements determined by DLS and ultramicroscopic particle tracking is presented in Table 4.4. The results from ultramicroscopy are presented as a number average $<R_h>_n$, as well as the inverse z average $[<R_h^{-1}>_z]^{-1}$ for comparison purposes with the results from DLS.

Table 4.4. Average hydrodynamic radii determined by Dynamic Light Scattering and Ultramicroscopic Particle Tracking. Sample *C* ($c_{An\text{-}NP}$ = 0.002 g · L^{-1}, c_{SDS} = 1.2 g · L^{-1} = 0.5 cmc).

Method	**Initial state / nm**	**After irradiation / nm**	**After sonication / nm**
$[<R_h^{-1}>_z]^{-1}$ **DLS**	164 ±9	190 ±16	159 ±9
$[<R_h^{-1}>_z]^{-1}$ **Ultramicroscopy**	146 ±44	177 ±39	121 ±26
$<R_h>_n$ **Ultramicroscopy**	76 ±10	101 ±16	73 ±11

The photo-induced increase in average size of the colloid could be simultaneously detected by both techniques. The inverse z average of the results from ultramicroscopic

particle tracking matches, within experimental error, the results from DLS, which adds certainty to the measurements. It is worth noting that, for the ultramicroscopy results, the inverse z average and the number average values differ significantly. As previously discussed, this is indicative of a rather broad distribution of sizes in the colloid, which can be naturally expected from continuous aggregation and re-dispersion processes in a lyophobic colloid. It is relevant to note that the combination of both techniques, DLS and ultramicroscopic particle tracking, provided a convenient way to study the state of aggregation. The inverse z average hydrodynamic radius determined by DLS is highly sensitive to the presence of large bodies, and thus enabled the detection of early stages of the aggregation process, as well as incomplete re-dispersion. Once a change in the state of aggregation could be detected, a more detailed study by ultramicroscopic particle tracking could provide an assessment of the actual distribution of sizes. Importantly, both techniques acquired information of the colloidal state without disrupting it.

4.2.4 Multiple cycles of photo-induced aggregation

A second aggregation cycle for sample *C* was tested and monitored by dynamic light scattering. Initially the stability of the re-dispersed suspension was tested by letting it stand still for two weeks. The average hydrodynamic radius R_h was found to remain constant within experimental error. The sample was irradiated under the same conditions and for the same total period of 10 min, as done in the first cycle. The average hydrodynamic radius R_h increased from 159 (±9) nm to 246 (±8) nm. Interestingly, the increase was remarkably greater than the one observed in the first cycle (Figure 4.21). The average scattered intensity relative to the initial state is presented as a reference. As discussed in previous sections, this parameter is expected to increase with increasing hydrodynamic radii and/or increasing concentration of suspended objects. The relative scattered intensity after the completion of the first cycle is lower than that of the initial state, despite having a very similar average hydrodynamic radius. This is consistent with the previous conclusion that some precipitate persisted after sonication. The starting state of dispersion was not exactly the

same for the first and the second cycles, so they can no longer be directly compared. Due to precipitation, the overall mass concentration at the end of the first cycle should be lower. Thus, the markedly stronger size increase in the second cycle could be the result of a lower optical density, which facilitates the absorption of photons and thus, aggregation.

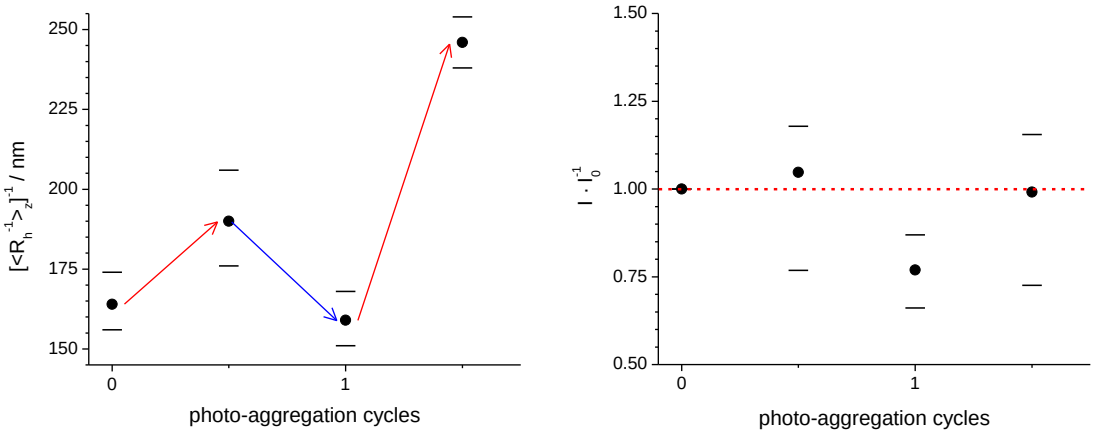

Figure 4.21. Cyclic photo-aggregation (red arrow) and re-dispersion through sonication (blue arrow). Left: average hydrodynamic radii determined by DLS. Right: scattered intensity relative to the initial state (a red dotted guideline is presented at a ratio of 1 for comparison purposes). Sample *C* ($c_{\text{An-NP}}$ = 0.002 g · L^{-1}, c_{SDS} = 1.2 g · L^{-1} = 0.5 cmc).

Cyclic assembly in a surfactant free suspension

Having recognized the difficulty to re-disperse precipitate as a central impediment to achieve multiple photo-aggregation cycles, it was decided to seek conditions under which precipitation is limited. In previous sections, decreasing concentrations of surfactant could be identified to decelerate the kinetics of the photo-aggregation process. At slower aggregation rates, it is easier to control and prevent precipitation. Based on these precepts, a lower concentration of surfactant was tested.

A suspension (labeled sample *D*) was prepared following the same general procedure, with the same concentration of nanoparticles $c_{\text{An-NP}}$ = 0.002 g · L^{-1}, but a substantially lower concentration of surfactant c_{SDS} = 0.0012 g · L^{-1} = 0.0005 cmc (equivalent

concentrations to sample *A*). The suspension appeared clear and homogenous at simple observation.

In contrast with sample *A*, sample *D* was treated in an ultrasound bath to procure homogeneous initial re-dispersion. Progressive changes in the hydrodynamic radius of the suspension were monitored by DLS. The treatment was prolonged until no significant changes could be further observed, reaching a value of R_h = 189 nm.

This equilibration value responds to the expected effects of sonication and surfactant concentration. The obtained average size is lower than the one reached by simple stirring at equivalent concentrations but without sonication (sample *A*). Moreover, the size is larger than the one previously obtained after sonication of a similar suspension at higher concentrations of surfactant (sample *C*). These findings are consistent with the expectation for the re-dispersion of a lyophobic colloid which requires a surfactant to be stabilized.

Sample *D* was subject of three full photo-excitation and sonication cycles. The conditions were the same as those applied on sample *C*, with a total of 10 min of photo-excitation, and 90 min of sonication per cycle. As shown in Figure 4.22, marked aggregation was observed for the first and the third cycles, but not so for the second cycle. At the end of the first cycle, the re-dispersed sample presented an average hydrodynamic radius comparable to that of the initial state. Furthermore, the scattered intensity remained nearly constant within experimental error, thus suggesting that precipitation did not occur. Nevertheless, this was not the case after completion of the second cycle, where the re-dispersed state had an average hydrodynamic size comparable to the initial state, but a notably lower scattered intensity, which is indicative of precipitation. Upon completion of the third cycle, the hydrodynamic radius was slightly higher, with a slightly lower scattering intensity. It can be concluded that mild precipitation persisted upon completion of the third cycle. Altogether, the unexpectedly unequal behavior after each cycle can be understood in terms of a progressive change in the distribution of sizes. This implies that despite very similar inverse z average values, which are mainly indicative of the large-end of the distribution of sizes, the population itself at each size seems to be not fully reverted to the initial state. Cycle after cycle, the distribution seems to be progressively displaced towards

larger values even after sonication, which results in the eventual formation of precipitate.

These results corroborate the previous conclusion that photo-induced aggregation is facilitated at higher contents of surfactant. The enhanced aggregation results in the formation of larger amounts of precipitate, thus making full reversion more complicated in sample *C* compared to sample *D*.

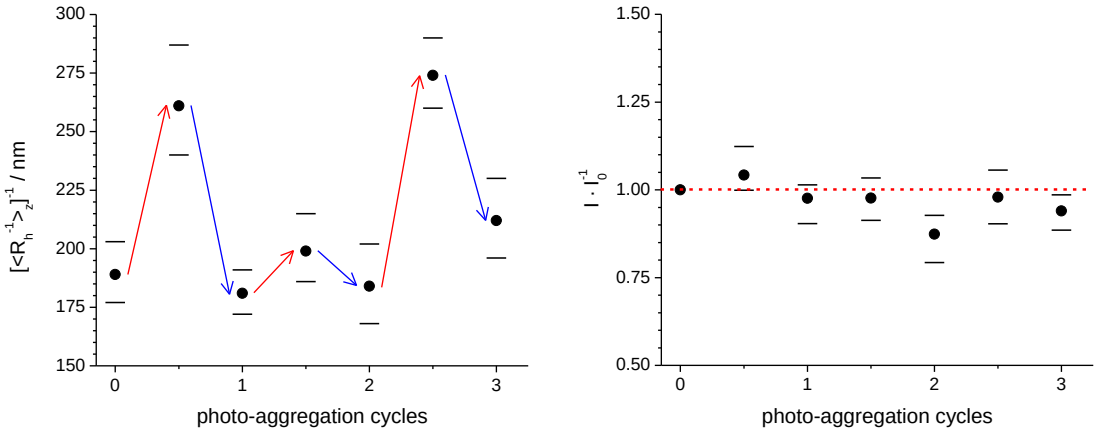

Figure 4.22. Cyclic photo-aggregation (red arrow) and re-dispersion through sonication (blue arrow). Left: average hydrodynamic radii determined by DLS. Right: scattered intensity relative to the initial state (a red dotted guideline is presented at a ratio of 1 for comparison purposes). Sample *D* ($c_{\text{An-NP}}$ = 0.002 g · L^{-1}, c_{SDS} = 0.0012 g · L^{-1} = 0.0005 cmc).

4.2.5 Conclusions

The photo-induced reversible aggregation of colloidal anthracene-labeled nanoparticles has been proven. It has been evidenced that the process results in the assembly of compact nanoparticle clusters. Multiple cycles of aggregation and re-dispersion appear to be possible, nevertheless full reversibility to the exact initial conditions proved to be difficult.

The content of surfactant is determinant for the overall functioning of the system. Higher concentrations of SDS aid re-dispersion, and simultaneously accelerate the

kinetics of the aggregation process. This may ultimately result in heavy precipitation, thus counterbalancing the ease of re-dispersion to the point of obstructing a subsequent cycle. In conclusion, to procure multiple aggregation and re-dispersion cycles, the content of surfactant needs to be cautiously optimized.

The findings on the influence of the surfactant over the kinetics of photo-aggregation provide a relevant insight into the mechanism of the process. At higher concentrations of SDS, the surface tension is lower. It can thus be speculated that under such conditions the disruption of the hydration shell around the interface of the hydrophobic nanoparticles requires less energy, thus facilitating the interaction and ultimately the approach of anthracene labels pending from different nanoparticles, eventually bringing them together. In such a scenario, the breaking of the hydration barrier appears as the pace-making step of the aggregation process.

4.3 Photo-induced assembly of pyrene-labeled polymer nanoparticles

4.3.1 Introduction

The development of responsive materials has been approached by the strategic inclusion in polymeric systems, of molecular functionalities which can form reversible bonds, either covalently or non-covalently.[60] As previously discussed, the inclusion on colloidal nanospheres of functional molecular structures which form inter-particle bridges, permits the assembly of meso-scale aggregates with a rather direct control of the process regarding the extent of aggregation. In the preceding chapter, the use of anthracene molecular structures for this purpose is described with the achievement of reversibility and multiple cycles, although in a limited fashion. These finding comprise the first evidence for the aggregation of colloidal particles in lyophobic conditions controlled by light signaling.

The effectiveness of anthracene in such a system has several implications. Previous work in which nanoparticle suspensions were reported to be successfully aggregated through light-triggered bridging[92, 100] consisted of rather lyophilic colloids in which not only the particles are compatible with the solvent but also the photo-active labels are soluble, thus facilitating the spatial approach of the reactants. In the lyophobic system described in the previous section, photo-active anthracene functionalities pending from different particles are separated, not only by a fluctuating extension of the continuous phase, but also by structured shells built up of surfactant and water molecules which stabilize the colloidal state. This implies that the interaction of the photo-active anthracene labels which precedes the formation of the covalently bonded dimers is strong enough to disrupt and overcome the stabilization shell.

Anthracene is a polycyclic aromatic hydrocarbon (PAH), a type of molecular structures which are prone to form charge-transfer complexes in the excited-state after the absorption of a photon.[119]

A charge-transfer complex is a molecular aggregation of defined stoichiometry, which results from electrostatic interactions that arise in an electronically excited state. They

are generally formed by electron-donor (D) and electron-acceptor counterparts. Charge-transfer complexes formed by two molecules of the same species are known as *excimers*.[119] These complexes are short lived (~ 10^{-8} s) [120] and dissociate after the electronic excited state decays back to the ground state, which may take place either by the emission of a broad red-shifted band, or by a non-radiative process:

$M + h\nu \rightarrow {}^1M^*$ Molecular electronic excitation

${}^1M^* + {}^1M \rightleftarrows {}^1D^*$ Excimer formation

Anthracene is a special case among the polycyclic aromatic hydrocarbons, as its photo-excitation results in covalently bonded dimers which are stable in the ground state. Nevertheless, substantial experimental evidence indicates that under several scenarios the formation of an excimer intermediate precedes the cyclo-addition reaction of the pair of anthracene structures.[117b] On this view, it can be speculated that it is the excimer interaction which is strong enough to disrupt the solvation shell which stabilizes the suspended nanoparticles.

In the preceding chapter, it has been described that the re-dispersion of the studied system is not spontaneous, as it would be expected for such a lyophobic colloidal system. This was the case even when the covalent anthracene-dimer bridges were not present, as evidenced by the difficulties to disperse the labeled nanoparticles in water even prior to the photo-irradiation experiments. Based on these results, it is clear that energy is required to bring apart such hydrophobic components, which can remain dispersed essentially with the aid of surfactant. Given these conditions, the disruption of the solvation stabilization shell should be sufficient to bring the suspended particles together and maintain them assembled, regardless of the formation of a covalent bridge. Furthermore, the re-dispersion of such assemblies can be expected to be comparatively easier when aggregation is not accompanied by the formation of covalent bonds, which in many cases can only be reverted under conditions which also lead to the chemical degradation of the functional molecules, resulting at the end in systems which are not truly reversible.

The present chapter presents the study based on the idea that a surfactant stabilization shell can be disrupted by charge transfer interactions in the electronic excited state which precede the formation of excimers. This implies that a colloidal suspension of hydrophobic nanoparticles labeled on their surface with excimer forming molecules, can be reversibly aggregated by light excitations (see Figure 4.23).

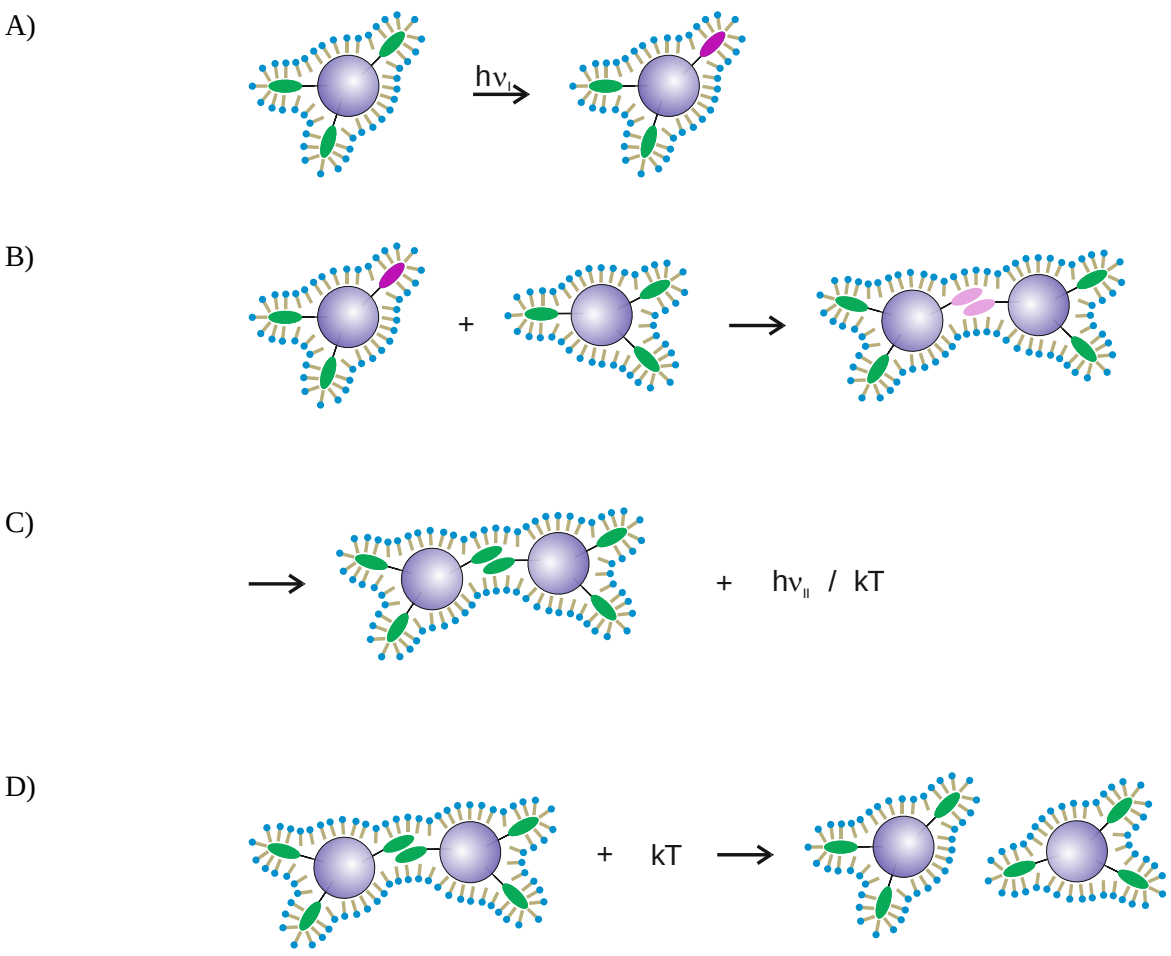

Figure 4.23. Schematic representation of lyophobic nanoparticles labeled with excimer-forming structures and stabilized by a surrounding layer of the surfactant. A) A photon is absorbed by one of the labels. B) The excited label interacts with a ground state label from a neighboring nanoparticle to form an excimer, thus disrupting the surfactant shell. C) The excimer decays back to the ground state by the emission of a photon (with $\nu_{II} < \nu_{I}$), or by a radiationless process. The two nanoparticles remain associated due to hydrophobic interactions. D) The particles can easily be dissociated by thermal energy.

The investigated system corresponds to polystyrene nanoparticles labeled with pyrene molecules on the surface, suspended in water with sodium dodecyl sulfate as the stabilizing surfactant.

4.3.2 Cyclic assembly of pyrene-labeled nanoparticles

The cyclic assembly of pyrene-labeled nanoparticles was initially tested under the same general conditions as those observed to work for anthracene labeled nanoparticles (An-NPs). A suspension (labeled sample *E*) of pyrene-labeled nanoparticles (Py-NPs) in aqueous sodium dodecyl sulfate (SDS) was prepared with final concentrations $c_{\text{An-NP}} = 0.002$ g · L^{-1}, and $c_{\text{SDS}} = 1.2$ g · L^{-1}. This concentration of surfactant corresponds to a fraction of 0.5 of the critical micelle concentration (cmc). The suspension appeared clear and homogenous at simple observation.

Sample *E* was treated in an ultrasound bath to procure homogeneous initial re-dispersion. Progressive changes in the average hydrodynamic radius of the suspension were monitored by DLS. Based on the results from previous samples, the data was analyzed by fitting the experimental autocorrelation function to a sum of two extended exponentials.

The sonication treatment was prolonged until no significant changes could be further observed, reaching an average hydrodynamic radius R_h = 227 ±25 nm. Like in the case of An-NPs samples, this value is substantially higher than that of the non-functionalized nanoparticles of R_h = 59 nm (stage I in Figure 4.1). Moreover, the equilibration average size value for this sample of Py-NPs is substantially higher than its An-NPs counterpart at the same concentration and equilibrated as well using ultrasound. This can be understood in terms of the overall higher hydrophobicity of Py-NPs compared to An-NPs. Pyrene has a higher molecular weight than anthracene. Furthermore, as described in section 4.1, the level of functionalization of the used sample is considerably high.

The sample was subject of two cycles of photo-irradiation (5 min) and sonication. In contrast with previous attempts, the sonication of this sample was periodically

monitored by DLS and prolonged until further decrease in the average hydrodynamic radius could not be detected.

As shown in Figure 4.24, the photo-induced aggregation of colloidal Py-NPs could be observed by an increase in the average hydrodynamic radius of the system well over the error range of the measurement. Furthermore, sonication effectively decreased the average size of the colloid, although the effect appeared incomplete. This observation can be taken to explain the unexpected behavior on the second cycle, during which photo-irradiation was not observed to trigger further aggregation, and even sonication resulted in an increase of the average size of the colloidal objects. It is noted that the scattered intensity was sustained nearly constant until the last sonication step, in which an evident increase in intensity matches the observed increase in average size. This final increase of size due to sonication can be understood in terms of the re-dispersion of precipitate which might have been formed during the first cycle.

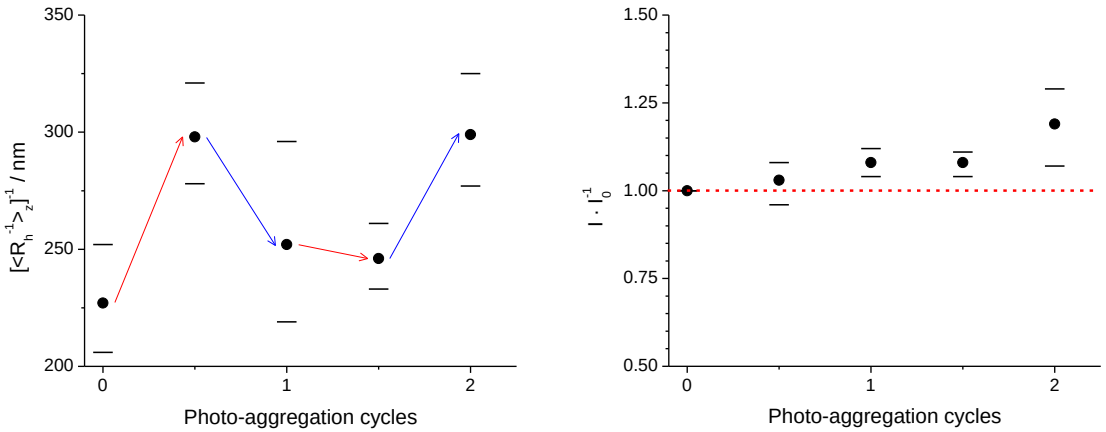

Figure 4.24. Cyclic photo-aggregation (red arrow) and re-dispersion through sonication (blue arrow). Left: average hydrodynamic radii determined by DLS. Right: scattered intensity relative to the initial state (a red dotted guideline is presented at a ratio of 1 for comparison purposes). Sample *E* ($c_{\text{An-NP}}$ = 0.002 g · L^{-1}, c_{SDS} = 1.2 g · L^{-1} = 0.5 cmc).

Attempt at higher concentration of surfactant

Given the difficulty to re-disperse the photo-aggregated state of colloidal Py-NPs, a higher concentration of surfactant was tested. Py-NPs were suspended in aqueous sodium dodecyl sulfate (SDS), with final concentrations $c_{\text{An-NP}} = 0.002\ \text{g} \cdot \text{L}^{-1}$, and $c_{\text{SDS}} = 2.4\ \text{g} \cdot \text{L}^{-1}$. This content of SDS corresponds to the critical micelle concentration. The suspension appeared clear and homogeneous at simple sight. This sample (labeled *F*) was treated in an ultrasound bath to procure an initial dispersed state. Progressive changes in the aggregation state, as indicated by the average hydrodynamic radius of the system, were monitored by DLS. Based on the results from previous samples, the data was analyzed by fitting the experimental autocorrelation function to a sum of two extended exponentials. The sonication treatment was prolonged until no further changes could be detected in the average hydrodynamic radius, which remained constant at a value of $R_h = 266 \pm 25$ nm. Surprisingly this value is, within experimental error, in the same range as the one determined for Py-NPs at a lower concentration of surfactant. Thus, it appears that Py-NPs are too hydrophobic to be further dispersed at this concentration and by this surfactant.

Sample *F* was subject to three cycles of photo-irradiation (5 min) and sonication. In line with the previous Py-NPs sample, the sonication of this sample was periodically monitored by DLS and prolonged until further decrease in average hydrodynamic radius could not be detected. As shown in Figure 4.25, the photo-induced aggregation of colloidal Py-NPs could be detected by an increase of the average hydrodynamic radius of the system, well over the error range of the measurement for the first and the third cycles, but not so for the second cycle. On the other hand, sonication appeared to re-disperse the photo-aggregated state more effectively, although apparently still incompletely for the first cycle. Yet, in contrast with sample *E*, photo-induced aggregation was observed for two subsequent cycles. On the other hand, sonication effectively decreased the average size of the colloid, although the effect appeared incomplete in the first cycle. After completion of the first cycle, the scattered intensity was observed to increase markedly. Nevertheless, along the second and third cycles, the value fluctuates moderately. For this sample, three photo-induced aggregation cycles could be detected. Altogether it appears that re-dispersion is also a difficulty for this sample, although to a lower extent when compared to sample *E*.

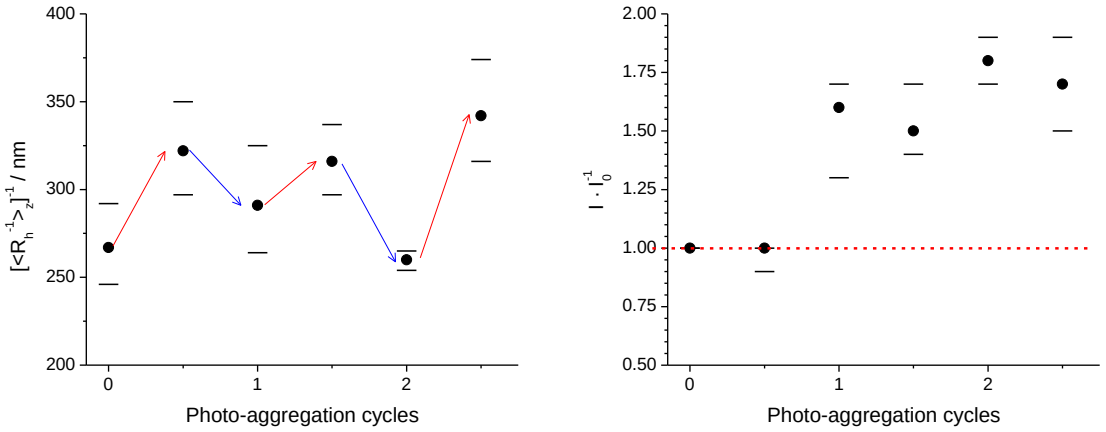

Figure 4.25. Cyclic photo-aggregation (red arrow) and re-dispersion through sonication (blue arrow). Left: average hydrodynamic radii determined by DLS. Right: scattered intensity relative to the initial state (a red dotted guideline is presented at a ratio of 1 for comparison purposes). Sample *F* ($c_{\text{An-NP}}$ = 0.002 g · L^{-1}, c_{SDS} = 2.4 g · L^{-1} = cmc).

Further analysis was carried on the *initial* and the *final* state of this sample. Sub-samples were collected before the first photo-irradiation cycle, and after the last photo-irradiation step. These were analyzed by ultramicroscopic particle tracking. The hydrodynamic radius distribution graphs are presented together with a table displaying the number average, as well as the inverse z average for comparison purposes with the results from DLS.

The distribution of sizes of the initial state is shown in Figure 4.26. The majority of the observed particles had a size in the range of the original unlabeled nanoparticles. Importantly, a few larger-sized objects in the range of 200-300 nm could be detected, which is in agreement with the results from DLS. The distribution has an inherent sharp lower limit at the size of single particles, and a tail extended towards larger values, which is expected from re-dispersed colloids composed of mono-sized nanoparticles. The corresponding average hydrodynamic radius values presented in Table 4.5 show a good agreement within experimental error between DLS and ultramicroscopy, thus providing additional certainty to the measurements.

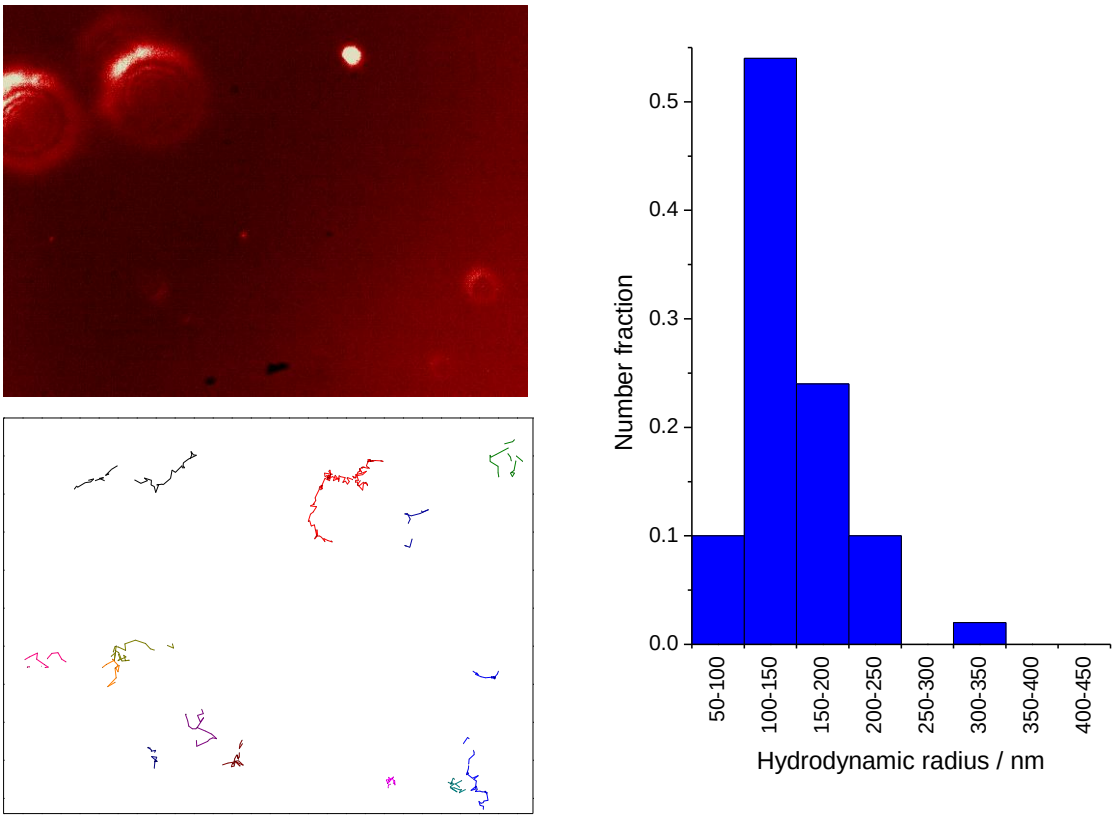

Figure 4.26. Ultramicroscopic particle tracking of the dispersed initial state (sample *F*). Left-up, dark field image. Left-down, trajectory of the moving particles. Right, histogram of the determined hydrodynamic radii.

Table 4.5. Average hydrodynamic radii of the initial state (sample *F*).

Method	**Hydrodynamic radius of the initial state / nm**
$\langle R_h \rangle_n$ Ultra-microscopy	94±26
$[\langle R_h^{-1} \rangle_z]^{-1}$ Ultra-microscopy	210±53
$[\langle R_h^{-1} \rangle_z]^{-1}$ DLS	256±25

The distribution of sizes of the final photo-aggregated state as determined by ultramicroscopy is shown in Figure 4.27. A clear displacement of the distribution maximum towards larger sizes is observed, showing the detection of objects well above

the sizes present in the initial state. The corresponding average hydrodynamic radius values presented in Table 4.5 show a good agreement within experimental error, between DLS and ultramicroscopy, thus providing additional certainty to the measurements.

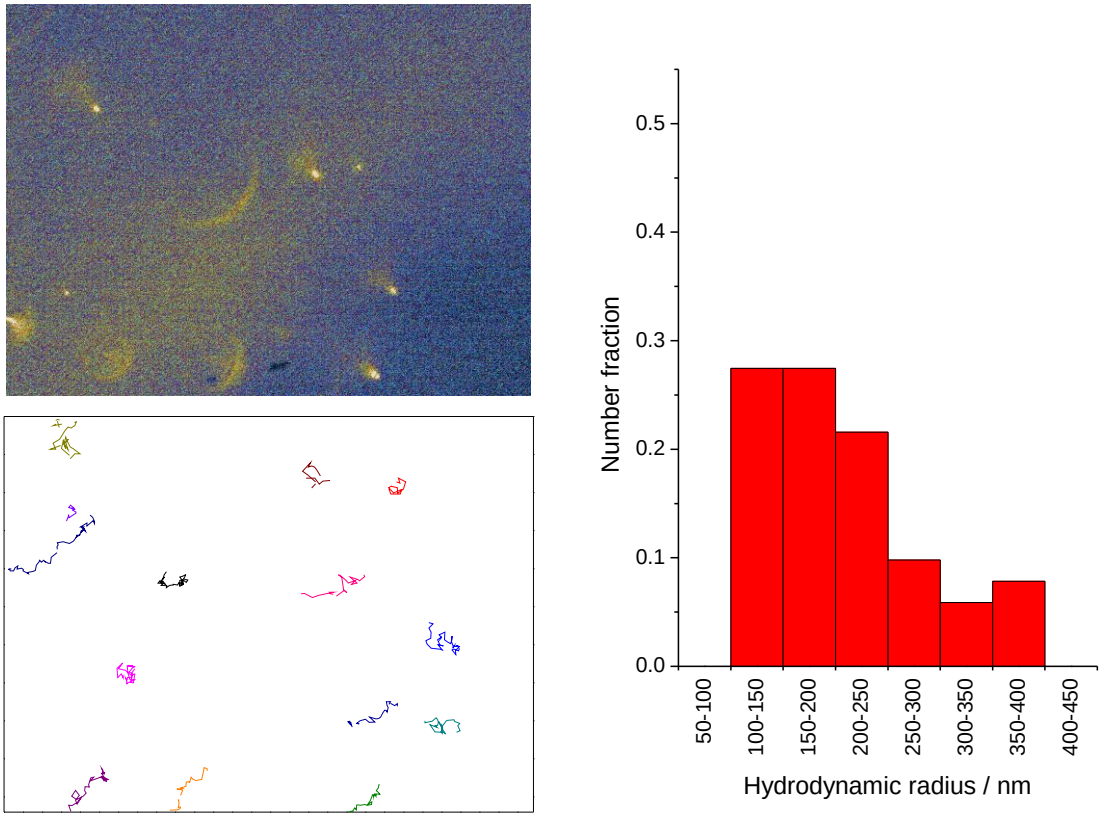

Figure 4.27. Ultramicroscopic particle tracking of the final photo-aggregated state (sample *F*). Left-up, dark field image. Left-down, trajectory of the moving particles. Right, histogram of the determined hydrodynamic radii.

Table 4.6. Average hydrodynamic radii of the final aggregated state after the third photo-irradiation cycle (sample *F*).

Method	**Hydrodynamic radius of the final photo-aggregated state / nm**
$\langle R_h \rangle_n$ **Ultra-microscopy**	155±26
$[\langle R_h^{-1} \rangle_z]^{-1}$ **Ultra-microscopy**	299±40
$[\langle R_h^{-1} \rangle_z]^{-1}$ **DLS**	346±31

4.3.3 Conclusions

As initially speculated the excited state interaction leading to the formation of pyrene excimers is strong enough to break the solvation shell which surrounds and stabilizes the nanoparticles composing a lyophobic colloid. This leads to the generation of light-responsive nanoparticles which can be reversibly assembled in a colloidal system.

Given the nature of the system, reversion of the aggregated state could only be hindered by the lyophobic nature of the colloid, since no bonded bridging is ever formed between the nanoparticles. Thus, the difficulty to fully revert the system to the initial state after photo-induced aggregation can be understood in terms of the actual distribution of sizes. As previously discussed, the distribution of sizes in a colloid responds to the history behind its formation. It has also been recognized that the full re-dispersion of a partially aggregated lyophobic colloid is challenging. Altogether, it appears unlikely to achieve full reversion to the same exact distribution of sizes. As a result, increasing differences emerge as progressive aggregation and re-dispersion cycles take place.

It has been evidenced that a lyophobic colloid can be aggregated in a controlled fashion by non-covalent bridging. The achievement of a system which is fully reversible over several cycles under this mechanism should then respond to the fine-tuning of the lyophobic character of the system, which itself depends on the type and concentration of surfactant and the overall lyophobic character of the labeled nanoparticles in suspension.

4.4 Experimental section

Materials

Divinylbenzene (mixture of isomers, Fulka), and poly(ethylene glycol) methacrylate, *Mn* ~ 360 (Aldrich), were used without further purification. Styrene (Merk) was distilled before use. Sodium dodecyl sulfate (Merk), Hexadecane 99% (Aldrich), 9-anthracenecarboxylic acid (Aldrich), and the hydrophobic initiator 2,2'-azobis(2-methylbutyronitrile) (V59) from Wako Chemicals, Japan, were used as received. Dimethylformamide (extra dry, Acros), thionyl chloride, tetrahydrofuran, and acetone (Aldrich), were also used as received. Na_2SO_4 (anhydrous, Riedel-de Haën) was further dried under vacuum at a temperature of 150 °C. The photo-responsive labels 9-anthracenecarboxylic acid (99%, from Aldrich) and 1-pyrenebutyric acid (99%, from Acros), were used without further purification.

High purity sodium dodecyl sulfate (Biomol) and ultrapure water (MilliQ system) were used to prepare the colloidal suspensions of the labeled nanoparticles used in the photo-aggregation experiments.

Synthesis of photo-active polymer nanoparticles

Synthesis of polystyrene nanoparticles

A colloidal suspension of polymer nanoparticles was prepared by the polymerization in miniemulsion of a monomer mixture consisting of styrene, poly(ethylene glycol) methacrylate (PEG-MA), and divinylbenzene (DVB), in weight fractions 0.9, 0.05, 0.05, respectively. A total of 6 g of monomers were mixed with 250 mg of the hydrophobe hexadecane and 100 mg of the initiator V59. This hydrophobic fraction was added to 24 g of water premixed with 60 mg of sodium dodecyl sulfate (SDS). The biphasic mixture was emulsified by simple stirring during 1 h. Afterwards a miniemulsion was formed by ultrasonication during 2 min at 90% intensity with a

Branson Sonfier 405W, 0.5” tip. The mixture was then placed in an oil bath at 72°C under stirring and allowed to react for 24 h.

To perform the subsequent labeling reaction under the required water free conditions, the polymer nanoparticles were transferred into dry acetone as a suspension medium through several cycles of centrifugation (14,000 rpm during 90 min) and re-dispersion in water-free acetone aided by sonication.

Labeling of nanoparticles

Anthracene carboxylic acid and pyrene butyric acid were coupled to separate batches of the nanoparticles through equal procedures. The acidic dyes were bonded to the terminal hydroxyl groups of the nanoparticles by an esterification reaction via the intermediate preparation of the corresponding acid chloride in a one pot procedure.

0.15 g of the acidic dye were placed in a brown flask and arranged for reflux in a N_2 purged environment. 5 ml of $SOCl_2$ and subsequently a few drops of anhydrous dimethylformamide (DMF) were added through a septum fitted to the system. DMF triggered the full dissolution of the solid. The reaction mixture was stirred for 24 h at a temperature of 60 °C. Excess $SOCl_2$ was then evaporated under reduced pressure, and the product was used without characterization.

An aliquot of 20 mL of the suspension of nanoparticles in dry acetone, accounting for approximately 0.5 g of polymer, was further dried with the addition of 4 g of anhydrous Na_2SO_4. The water free suspension was then added through a septum to the flask containing the acid chloride of the dye, while keeping the system under N_2 atmosphere. The reaction mixture was stirred at a temperature of 60 °C during 35 h. Afterwards, the resultant labeled nanoparticles were washed through several cycles of centrifugation (14,000 rpm for 90 min) and re-dispersion in pure acetone. The elimination of the unreacted dye was monitored by UV/vis spectroscopy measurements of the discarded solvent.

Determination of label content by UV/vis spectroscopy

A suspension of dye-labeled nanoparticles in tetrahydrofuran (THF) was prepared in order to swell the cross-linked polymer and reduce light scattering for spectroscopic analysis. An aliquot of the suspension in acetone was allowed to evaporate and THF was added to the remaining solid. The mixture was sonicated extensively and stepwise diluted in THF until a stable suspension was obtained. The solids content of the resultant suspension was determined gravimetrically.

The content of dye in the suspension was determined using a UV/vis spectrophotometer Lambda 25 from Perkin Elmer. Calculations on the amount of labels per particle were carried considering the average size of the nanoparticles as measured by Dynamic Light Scattering (DLS) previous to the labeling procedure. The total surface area per mass was determined considering the density of the nanoparticles to be that of polystyrene in the bulk.

Sample preparation and handling

A master suspension of labeled nanoparticles in water was prepared by the drop-wise addition of the suspension in acetone, into an aqueous solution of sodium dodecyl sulfate (SDS) at the critical micelle concentration (2.4 $g \cdot L^{-1}$). The mixture was sonicated and subsequently bubbled with N_2 to eliminate the acetone, taking care that water is not lost. The suspension was filtered with a 5 μm pore-size PTFE syringe filter (Millipore) and the content of solids was determined gravimetrically. To determine the portion of solids corresponding to polymer nanoparticles, the final concentration of SDS in the master suspension was assumed to be at cmc.

Aliquots of the master suspension were diluted with water and/or aqueous SDS to the desired final concentrations in a dust-free quartz cell for light scattering (Hellma), and sealed with a septum-fitted cap. The suspensions were then bubbled through the septum with N_2 during 30 min to displace O_2, and kept inside the sealed cells at all times for light scattering measurements, photo-excitation, and sonication procedures. Small sub-samples were taken for microscopy through the septum without disruption of the N_2

atmosphere. The photo-irradiation of the samples was carried with a 100 W high pressure Hg lamp (Muller Elektronic LXH100 fitted with an HBO 100W/2 short arc lamp from Osram). A long-pass filter with cut at λ = 295 nm was used.

Analysis and instrumentation

Dynamic light scattering

Light scattering measurements were carried using a multi-tau full-digital ALV-5000 (ALV GmbH, Langen) correlator with 320 channels (10^{-7} s ≤ t ≤ 10^{3} s) and a HeNe laser (Uniphase) of λ = 632.8 nm and output power of 25 mW. The quartz cells containing the samples were submerged in a toluene bath of matching refractive index, and held at a constant temperature of 20 °C. The time autocorrelation function of the scattered intensity was measured at varying angles with a detector mounted on a goniometer.

Data analysis for the measurements on the original well dispersed nanoparticle suspension (prior to the chemical labeling procedure) was carried by simple cumulant fit as introduced by Koppel.[109] In the case of the more complex -partially aggregated- suspension of the labeled nanoparticles, an initial analysis was carried using the CONTIN algorithm by Provencher.[108] Further detailed analysis was carried by fitting (using the Levenberg-Marquardt algorithm) the experimental intensity correlation functions to a sum of tow extended exponential

$$\boldsymbol{G}(t) - 1 = c_0 + \left(c_1 * e^{-(t/\tau_1)^{\beta 1}} + c_2 * e^{-(t/\tau_{12})^{\beta 2}}\right)^2 \qquad \textbf{(4.1)}$$

τ_1 and τ_2 each represent the central position of a distribution of relaxation times. The β parameter, which determines the corresponding width of the distribution curve, was

allowed to vary within the range of ($0 < \beta \leq 1$).[107] The average relaxation time of each extended exponential was calculated using equation (3.22). All the relaxations detected in the measurements corresponding to complex multi-component systems could be adequately quantified by this combination of two extended exponential functions, which provided a broadening distribution band for each: higher aggregates and singly-dispersed nanoparticles. The system average was calculated by weighing the relaxation rates $\Gamma = 1/\tau$ with their corresponding coefficients c_1 and c_2.

All measurements were carried at multiple scattering angles θ ranging from 30° to 150° ($3.3 \cdot 10^{13}$ $m^{-2} \leq q^2 \leq . 6.5 \cdot 10^{14}$ m^{-2}). The z average diffusion coefficient was obtained by linear extrapolation of the squared scattering vector $q^2(\theta)$ to zero. The statistical error in the *y* intercept of the linear fit was used to calculate the error range of the measurement.

Ultramicroscopic particle tracking

The hydrodynamic radius of the colloidal nanoparticles was determined by ultramicroscopic particle tracking. Time dependent imaging was carried on an optical microscope (Zeiss) fitted with a dark-field illumination set (Cyto Viva fixed with X-cite series 120 light source). A magnification lens of 100x (Zeiss) and immersion oil (518C, Zeiss) were used.

Samples were handled in a way which assures that Brownian motion is not disrupted by flow or solvent evaporation during observation. A compartment of defined dimensions was formed by fixing a glass cover slide (#1 Menzel-Gläser) rested over a spacer (0.16 mm), to a coplanar base slide by sealing the perimeter, leaving a small stretch uncovered to feed the sample.

Stacks of 200 images taken every 0.14 s were collected. The position of the imaged particles was tracked by recording the coordinates of their projection on the x-y plane for a minimum of 10 steps.

The average squared mean-displacement of each particle was calculated using equation (3.27). The difference between the two squared terms in the summation was used to evaluate the error in the size determination of each particle. The hydrodynamic radius

was calculated from the mean squared displacement using equations (3.10) and (3.11).

A minimum of 50 particles were screened for each sample, taking care that the trajectories of each of them did not cross over along the entire image stack. To compare the results with those from dynamic light scattering (DLS), the inverse z average hydrodynamic radius was calculated using to the following equation:

$$\left[\langle R_h^{-1}\rangle_z\right]^{-1} = \frac{\sum n_i M_i^2}{\sum n_i M_i^2 R_h^{-1}} = \frac{\sum n_i R_h^6}{\sum n_i R_h^5} \qquad \textbf{(4.2)}$$

Turbidimetry

Turbidimetry measurements were carried using an in-house built set-up consisting of a HeNe laser (Uniphase) with λ = 632.8 nm and output power of 25 mW, and an aligned photomultiplier detector. Samples were positioned in between, and stirred in place for the measurement. For sedimentation measurements, the samples were kept still standing in place for a period of 24 h.

Scanning electron microscopy

Scanning Electron Microscopy was carried on a Zeiss Gemini 1530 using an InLens detector. The suspensions were diluted to different concentrations to minimize the masking of the nanoparticles by surfactant. Sample droplets were then evaporated on silicon wafers.

5 GENERAL CONCLUSIONS AND OUTLOOK

The photo-induced assembly of nanospheres to form compact clusters out of lyophobic colloidal conditions, was achieved via the incorporation over their surface of responsive labels which give rise to attractive inter-particle bridging interactions in the electronic excited state. These labels correspond to anthracene, which forms covalently bonded dimers, and also pyrene, which forms short-lived excited state dimers that showed to be effective to disrupt the stability of the lyophobic colloid, to form clusters which hold together by hydrophobic interactions.

A correlation between photo-excitation time and the degree of aggregation was identified, thus establishing the direct control of the process of cluster growth. The effect proved to be reversible, as the state of photo-induced aggregation could be re-dispersed by sonication. In contrast with other systems which have been reported, the colloidal nanoparticles here studied could be photo-aggregated in consecutive cycles, which is indicative that the re-dispersion process does not degrade the system. The reversibility nevertheless appeared to be incomplete, as evidenced by the accumulation of precipitate as the cycles of photo-aggregation and re-dispersion proceeded.

In the case of anthracene-labeled nanoparticles (An-NPs), the lack of full reversibility can be partially attributed to an incomplete cleavage of anthracene-dimer inter-particle bridges. Nevertheless, the difficulty to fully re-disperse the photo-aggregated state was also observed for pyrene-labeled nanoparticles (Py-NPs), which are held together only by hydrophobic forces without any covalent bridges being formed. This uncovers the hydrophobicity of the nanoparticles as a crucial hindrance to reach full reversibility.

The development of light-responsive colloidal nanoparticles presented in this dissertation is relevant for a series of purposes spanning from synthetic strategies at the nano and meso scales, to more intricate responsive or *smart* systems.

The established processes for the controlled aggregation and re-dispersion of colloidal nanoparticles can be combined in an iterative way as an approach for the facile mass production of well-defined mesoscale assemblies of nanoparticles. This synthetic outcome is flexible and of broad reach given the characteristics of the selected nanoparticles, which have a size range and overall architecture that makes them an adequate model system for the application of the general methodology here presented

towards the controlled assembly at different levels, of diverse materials which can be included within photo-responsive hybrid nanoparticles thanks to the versatility of the miniemulsion polymerization process which was used.[1]

The development of responsive *smart* systems is also a potential application of relevance. For instance, the reversible aggregation of colloidal nanoparticles can trigger changes in viscosity or osmotic pressure. The possibility to generate these changes by facile light signaling brings the opportunity to study microscopically enclosed systems which are otherwise hardly accessible. It is also relevant to note that under the right conditions and arrangement, mechanical work could as well be carried in a controlled manner within such spaces.

It is also relevant to identify the implications of the results here presented in relation to electronic excited state interactions and colloidal stability. The use of the excimer effect to trigger inter-particle bridging brings great advantages and opens many possibilities for applications. Since it is a non-covalent association, reversibility is attainable without the input of high energy, thus minimizing the risk for degradation and enhancing the possibility of multiple cycles. Another transcendental advantage is related to the vast variety of molecular structures which undergo associations in the electronic excited. This has important implications in the accessible spectrum of different wavelengths which could be used to trigger the reversible assembly of these responsive colloidal nanoparticles. Potentially, multi-response systems sensitive to light signals of different wavelengths, could be achieved using labels with well differentiated excimer excitation spectra.

Based on the results here presented, it can be concluded that further studies with the aim to improve the reversibility and the continuous functionality over several cycles of these type of photo-responsive nanoparticles, should be directed towards the control of the *lyophobicity* of the system.

As previously discussed, the *lyophobicity* of the system and its inherent difficulty to form homogeneous suspensions of fully dispersed nanoparticles could be recognized as a parameter which directly determines the operability of these responsive colloids over multiple cycles. Thus, alternative systems should consider the regulation of the overall

hydrophobic character of the labeled nanoparticles. For instance, hydrophilic moieties could be included on the surface of the nanoparticles in an alternate manner along with the hydrophobic labels. For this purpose, ionizable groups are an interesting choice due to the repulsive inter-particle charges which arise. Adversely, the use such photo-active nanoparticles with a lower hydrophobic character might result in a milder aggregation effect; particularly in those systems based in non-covalently bonded bridges triggered by the excimer effect.

REFERENCES

[1] K. Landfester, *Angewandte Chemie-International Edition* **2009**, *48*, 4488-4507.
[2] B. A. Grzybowski, C. E. Wilmer, J. Kim, K. P. Browne, K. J. M. Bishop, *Soft Matter* **2009**, *5*, 1110-1128.
[3] M. Grzelczak, J. Vermant, E. M. Furst, L. M. Liz-Marzan, *ACS Nano* **2010**, *4*, 3591-3605.
[4] R. Klajn, K. J. M. Bishop, B. A. Grzybowski, *Proceedings of the National Academy of Sciences of the United States of America* **2007**, *104*, 10305-10309.
[5] X. Yuan, M. Schnell, S. Muth, W. Schartl, *Langmuir* **2008**, *24*, 5299-5305.
[6] D. Peer, J. M. Karp, S. Hong, O. C. FaroKhzad, R. Margalit, R. Langer, *Nature Nanotechnology* **2007**, *2*, 751-760.
[7] J. Dobson, *Nature Nanotechnology* **2008**, *3*, 139-143.
[8] T. Dvir, B. P. Timko, D. S. Kohane, R. Langer, *Nature Nanotechnology* **2011**, *6*, 13-22.
[9] C. Rutherglen, D. Jain, P. Burke, *Nature Nanotechnology* **2009**, *4*, 811-819.
[10] F. Schwierz, *Nature Nanotechnology* **2010**, *5*, 487-496.
[11] a) A. G. Cano-Marquez, F. J. Rodriguez-Macias, J. Campos-Delgado, C. G. Espinosa-Gonzalez, F. Tristan-Lopez, D. Ramirez-Gonzalez, D. A. Cullen, D. J. Smith, M. Terrones, Y. I. Vega-Cantu, *Nano Lett.* **2009**, *9*, 1527-1533; b) D. V. Kosynkin, A. L. Higginbotham, A. Sinitskii, J. R. Lomeda, A. Dimiev, B. K. Price, J. M. Tour, *Nature* **2009**, *458*, 872-876.
[12] L. Dossel, L. Gherghel, X. L. Feng, K. Mullen, *Angewandte Chemie-International Edition* **2011**, *50*, 2540-2543.
[13] J. S. Wu, W. Pisula, K. Mullen, *Chemical Reviews* **2007**, *107*, 718-747.
[14] S. Park, R. S. Ruoff, *Nature Nanotechnology* **2009**, *4*, 217-224.
[15] G. D. Scholes, G. Rumbles, *Nature Materials* **2006**, *5*, 683-696.
[16] J. L. Bredas, J. E. Norton, J. Cornil, V. Coropceanu, *Accounts Chem. Res.* **2009**, *42*, 1691-1699.
[17] A. Goel, V. Vogel, *Nature Nanotechnology* **2008**, *3*, 465-475.
[18] W. R. Browne, B. L. Feringa, *Nature Nanotechnology* **2006**, *1*, 25-35.
[19] P. M. Ajayan, L. S. Schadler, P. V. Braun, *Nanocomposite science and technology*, Wiley-VCH, **2003**.
[20] B. Njuguna, K. Pielichowski, *Advanced Engineering Materials* **2003**, *5*, 769-778.
[21] S. R. Bakshi, D. Lahiri, A. Agarwal, *International Materials Reviews* **2010**, *55*, 41-64.
[22] W. Sparreboom, A. van den Berg, J. C. T. Eijkel, *Nature Nanotechnology* **2009**, *4*, 713-720.
[23] M. Auffan, J. Rose, J. Y. Bottero, G. V. Lowry, J. P. Jolivet, M. R. Wiesner, *Nature Nanotechnology* **2009**, *4*, 634-641.
[24] G. Schmid, *Nanoparticles: From Theory to Application*, John Wiley & Sons, **2010**.
[25] M. C. Daniel, D. Astruc, *Chemical Reviews* **2004**, *104*, 293-346.
[26] A. K. Geim, K. S. Novoselov, *Nature Materials* **2007**, *6*, 183-191.
[27] a) K. S. Novoselov, A. K. Geim, S. V. Morozov, D. Jiang, Y. Zhang, S. V. Dubonos, I. V. Grigorieva, A. A. Firsov, *Science* **2004**, *306*, 666-669; b) Y. B. Zhang, Y. W. Tan, H. L. Stormer, P. Kim, *Nature* **2005**, *438*, 201-204.

[28] H. W. Kroto, J. R. Heath, S. C. Obrien, R. F. Curl, R. E. Smalley, *Nature* **1985**, *318*, 162-163.
[29] S. Iijima, *Nature* **1991**, *354*, 56-58.
[30] M. C. Hersam, *Nature Nanotechnology* **2008**, *3*, 387-394.
[31] S. N. Baker, G. A. Baker, *Angewandte Chemie-International Edition* **2010**, *49*, 6726-6744.
[32] A. Krueger, *Advanced Materials* **2008**, *20*, 2445-+.
[33] E. Kwon, H. Oikawa, H. Kasai, H. Nakanishi, *Crystal Growth & Design* **2007**, *7*, 600-602.
[34] T. Ishi-i, S. Shinkai, in *Supermolecular Dye Chemistry, Vol. 258*, Springer-Verlag Berlin, Berlin, **2005**, pp. 119-160.
[35] G. O. Lloyd, J. W. Steed, *Nature Chemistry* **2009**, *1*, 437-442.
[36] a) M. Antonietti, C. Goltner, *Angewandte Chemie-International Edition in English* **1997**, *36*, 910-928; b) C. F. J. Faul, M. Antionietti, *Chemistry-a European Journal* **2002**, *8*, 2764-2768; c) Y. Guan, M. Antonietti, C. F. J. Faul, *Langmuir* **2002**, *18*, 5939-5945.
[37] F. Grohn, *Macromol. Chem. Phys.* **2008**, *209*, 2295-2301.
[38] A. F. Thunemann, M. Muller, H. Dautzenberg, J. F. O. Joanny, H. Lowne, in *Polyelectrolytes with Defined Molecular Architecture Ii, Vol. 166*, Springer-Verlag Berlin, Berlin, **2004**, pp. 113-171.
[39] F. Ganachaud, J. L. Katz, *ChemPhysChem* **2005**, *6*, 209-216.
[40] P. A. Lovell, M. S. El-Aasser, *Emulsion polymerization and emulsion polymers*, J. Wiley, **1997**.
[41] G. M. Whitesides, M. Boncheva, *Proceedings of the National Academy of Sciences of the United States of America* **2002**, *99*, 4769-4774.
[42] a) Z. H. Nie, A. Petukhova, E. Kumacheva, *Nature Nanotechnology* **2010**, *5*, 15-25; b) C. Sonnichsen, B. M. Reinhard, J. Liphardt, A. P. Alivisatos, *Nature Biotechnology* **2005**, *23*, 741-745.
[43] D. M. Eigler, E. K. Schweizer, *Nature* **1990**, *344*, 524-526.
[44] O. Custance, R. Perez, S. Morita, *Nature Nanotechnology* **2009**, *4*, 803-810.
[45] C. D. Onal, O. Ozcan, M. Sitti, *IEEE Transactions on Nanotechnology* **2011**, *10*, 472-481.
[46] A. Ashkin, J. M. Dziedzic, J. E. Bjorkholm, S. Chu, *Optics Letters* **1986**, *11*, 288-290.
[47] F. Li, D. P. Josephson, A. Stein, *Angewandte Chemie-International Edition* **2011**, *50*, 360-388.
[48] Y. J. Min, M. Akbulut, K. Kristiansen, Y. Golan, J. Israelachvili, *Nature Materials* **2008**, *7*, 527-538.
[49] S. C. Glotzer, M. J. Solomon, *Nature Materials* **2007**, *6*, 557-562.
[50] P. X. Guo, *Nature Nanotechnology* **2010**, *5*, 833-842.
[51] H. Colfen, S. Mann, *Angewandte Chemie-International Edition* **2003**, *42*, 2350-2365.
[52] a) C. S. Wagner, B. Fischer, M. May, A. Wittemann, *Colloid and Polymer Science* **2010**, *288*, 487-498; b) V. N. Manoharan, M. T. Elsesser, D. J. Pine, *Science* **2003**, *301*, 483-487.
[53] G. Kostorz, *Phase transformations in materials*, Wiley-VCH, **2001**.
[54] M. Shahinpoor, H. J. Schneider, *Intelligent materials*, RSC Publishing, **2008**.
[55] S. Kobatake, S. Takami, H. Muto, T. Ishikawa, M. Irie, *Nature* **2007**, *446*, 778-781.

[56] M. Das, H. Zhang, E. Kumacheva, *Annual Review of Materials Research* **2006**, *36*, 117-142.
[57] C. J. F. Rijcken, O. Soga, W. E. Hennink, C. F. van Nostrum, *Journal of Controlled Release* **2007**, *120*, 131-148.
[58] E. W. Edwards, M. Chanana, D. Wang, H. Moehwald, *Angewandte Chemie-International Edition* **2008**, *47*, 320-323.
[59] a) F. Ercole, T. P. Davis, R. A. Evans, *Polymer Chemistry* **2010**, *1*, 37-54; bS. Das, S. Varghese, N. S. S. Kumar, *Langmuir* **2010**, *26*, 1598-1609.
[60] R. J. Wojtecki, M. A. Meador, S. J. Rowan, *Nature Materials* **2011**, *10*, 14-27.
[61] S. Yagai, A. Kitamura, *Chemical Society Reviews* **2008**, *37*, 1520-1529.
[62] J. Eastoe, A. Vesperinas, *Soft Matter* **2005**, *1*, 338-347.
[63] L. A. Connal, R. Vestberg, C. J. Hawker, G. G. Qiao, *Advanced Functional Materials* **2008**, *18*, 3315-3322.
[64] T. Seki, *Curr. Opin. Solid State Mat. Sci.* **2006**, *10*, 241-248.
[65] a) M. H. Li, P. Keller, *Soft Matter* **2009**, *5*, 927-937; b) Y. Zhao, *J. Mater. Chem.* **2009**, *19*, 4887-4895.
[66] Y. Zhao, *Chemical Record* **2007**, *7*, 286-294.
[67] T. Ikeda, J. Mamiya, Y. L. Yu, *Angewandte Chemie-International Edition* **2007**, *46*, 506-528.
[68] O. J. Cayre, N. Chagneux, S. Biggs, *Soft Matter* **2011**, *7*, 2211-2234.
[69] R. Pelton, *Advances in Colloid and Interface Science* **2000**, *85*, 1-33.
[70] B. H. Tan, K. C. Tam, *Advances in Colloid and Interface Science* **2008**, *136*, 25-44.
[71] D. Klinger, K. Landfester, *Soft Matter* **2011**, *7*, 1426-1440.
[72] a) J. M. Schumers, C. A. Fustin, J. F. Gohy, *Macromol. Rapid Commun.* **2010**, *31*, 1588-1607; b) E. Cabane, V. Malinova, W. Meier, *Macromol. Chem. Phys.* **2010**, *211*, 1847-1856.
[73] E. M. Rosenbauer, M. Wagner, A. Musyanovych, K. Landfester, *Macromolecules* **2010**, *43*, 5083-5093.
[74] M. Bradley, B. Vincent, N. Warren, J. Eastoe, A. Vesperinas, *Langmuir* **2006**, *22*, 101-105.
[75] H. Y. Koo, H. J. Lee, J. K. Kim, W. S. Choi, *J. Mater. Chem.* **2010**, *20*, 3932-3937.
[76] K. S. Sun, R. Kumar, D. E. Falvey, S. R. Raghavan, *J. Am. Chem. Soc.* **2009**, *131*, 7135-7141.
[77] F. A. Plamper, A. Walther, A. H. E. Muller, M. Ballauff, *Nano Lett.* **2007**, *7*, 167-171.
[78] A. Shiotani, T. Mori, T. Niidome, Y. Niidome, Y. Katayama, *Langmuir* **2007**, *23*, 4012-4018.
[79] S. Lena, P. Neviani, S. Masiero, S. Pieraccini, G. P. Spada, *Angewandte Chemie-International Edition* **2010**, *49*, 3657-3660.
[80] C. Wang, Q. Chen, F. Sun, D. Q. Zhang, G. X. Zhang, Y. Y. Huang, R. Zhao, D. B. Zhu, *J. Am. Chem. Soc.* **2010**, *132*, 3092-3096.
[81] F. P. Hubbard, N. L. Abbott, *Langmuir* **2007**, *23*, 4819-4829.
[82] A. M. Ketner, R. Kumar, T. S. Davies, P. W. Elder, S. R. Raghavan, *J. Am. Chem. Soc.* **2007**, *129*, 1553-1559.
[83] D. Chen, H. Liu, T. Kobayashi, H. F. Yu, *J. Mater. Chem.* **2010**, *20*, 3610-3614.
[84] I. Willerich, F. Grohn, *Angew Chem Int Ed Engl* **2010**, *49*, 8104-8108.
[85] M. R. Banghart, A. Mourot, D. L. Fortin, J. Z. Yao, R. H. Kramer, D. Trauner, *Angewandte Chemie-International Edition* **2009**, *48*, 9097-9101.

[86] Q. A. Jin, G. Y. Liu, J. A. Ji, *J. Polym. Sci. Pol. Chem.* **2010**, *48*, 2855-2861.
[87] A. Szilagyi, K. Sumaru, S. Sugiura, T. Takagi, T. Shinbo, M. Zrinyi, T. Kanamori, *Chem. Mat.* **2007**, *19*, 2730-2732.
[88] Y. G. Jiang, Y. P. Wang, N. Ma, Z. Q. Wang, M. Smet, X. Zhang, *Langmuir* **2007**, *23*, 4029-4034.
[89] J. Q. Jiang, Q. Z. Shu, X. Chen, Y. Q. Yang, C. L. Yi, X. Q. Song, X. Y. Liu, M. Q. Chen, *Langmuir* **2010**, *26*, 14247-14254.
[90] J. He, X. Tong, Y. Zhao, *Macromolecules* **2009**, *42*, 4845-4852.
[91] D. J. Shi, M. Matsusaki, T. Kaneko, M. Akashi, *Macromolecules* **2008**, *41*, 8167-8172.
[92] X. F. Yuan, K. Fischer, W. Scharl, *Advanced Functional Materials* **2004**, *14*, 457-463.
[93] a) J. W. Fu, Z. P. Cheng, N. C. Zhou, J. Zhu, W. Zhang, X. L. Zhu, *Polymer* **2008**, *49*, 5431-5438; b) M. Coursan, J. P. Desvergne, A. Deffieux, *Macromol. Chem. Phys.* **1996**, *197*, 1599-1608.
[94] Y. J. Zheng, M. Mieie, S. V. Mello, M. Mabrouki, F. M. Andreopoulos, V. Konka, S. M. Pham, R. M. Leblanc, *Macromolecules* **2002**, *35*, 5228-5234.
[95] C. Mengel, W. H. Meyer, G. Wegner, *Macromol. Chem. Phys.* **2001**, *202*, 1138-1149.
[96] J. R. Jones, C. L. Liotta, D. M. Collard, D. A. Schiraldi, *Macromolecules* **2000**, *33*, 1640-1645.
[97] Y. Chujo, K. Sada, R. Nomura, A. Naka, T. Saegusa, *Macromolecules* **1993**, *26*, 5611-5614.
[98] J. T. Goldbach, K. A. Lavery, J. Penelle, T. P. Russell, *Macromolecules* **2004**, *37*, 9639-9645.
[99] H. Morikawa, Y. Kotaki, R. Mihara, Y. Kiraku, S. Ichimura, S. Motokucho, *Chemistry Letters* **2010**, *39*, 682-683.
[100] A. R. Smith, D. F. Watson, *Chem. Mat.* **2010**, *22*, 294-304.
[101] R. J. Hunter, *Foundations of colloid science*, Oxford University Press, **2001**.
[102] A. A. Baran, *Uspekhi Khimii* **1985**, *54*, 1100-1126.
[103] J. W. Goodwin, *Colloids and interfaces with surfactants and polymers: an introduction*, J. Wiley, **2004**.
[104] R. Newburgh, J. Peidle, W. Rueckner, *American Journal of Physics* **2006**, *74*, 478-481.
[105] R. Pecora, *Dynamic light scattering: applications of photon correlation spectroscopy*, Plenum Press, **1985**.
[106] W. Schärtl, *Light scattering from polymer solutions and nanoparticle dispersions*, Springer, **2007**.
[107] W. Brown, *Dynamic light scattering: the method and some applications*, Clarendon Press, **1993**.
[108] S. W. Provencher, *Computer Physics Communications* **1982**, *27*, 229-242.
[109] D. E. Koppel, *J. Chem. Phys.* **1972**, *57*, 4814-&.
[110] R. F. Egerton, *Physical principles of electron microscopy: an introduction to TEM, SEM, and AEM*, Springer Science+Business Media, **2005**.
[111] a) W. Schaertl, H. Sillescu, *Journal of Colloid and Interface Science* **1993**, *155*, 313-318; b) C. Finder, M. Wohlgemuth, C. Mayer, *Particle & Particle Systems Characterization* **2004**, *21*, 372-378.
[112] C. F. Bohren, D. R. Huffman, *Absorption and scattering of light by small particles*, Wiley, **1983**.

[113] B. Valeur, *Molecular fluorescence: principles and applications*, Wiley-VCH, **2002**.
[114] G. Gauglitz, T. Vo-Dinh, *Handbook of spectroscopy*, Wiley-VCH, **2003**.
[115] a) K. Landfester, *Annual Review of Materials Research* **2006**, *36*, 231-279; b) A. Musyanovych, R. Rossmanith, C. Tontsch, K. Landfester, *Langmuir* **2007**, *23*, 5367-5376.
[116] F. M. Winnik, *Chemical Reviews* **1993**, *93*, 587-614.
[117] a) H. Bouas-Laurent, A. Castellan, J. P. Desvergne, R. Lapouyade, *Chemical Society Reviews* **2000**, *29*, 43-55; b) H. Bouas-Laurent, A. Castellan, J. P. Desvergne, R. Lapouyade, *Chemical Society Reviews* **2001**, *30*, 248-263.
[118] M. Spitzer, E. Sabadini, W. Loh, *J. Braz. Chem. Soc.* **2002**, *13*, 7-9.
[119] J. B. Birks, *Rep. Prog. Phys.* **1975**, *38*, 903-974.
[120] A. Weller, *Progress in Reaction Kinetics and Mechanism* **1961**, *1*, 187-214.

LIST OF ABBREVIATIONS

An	anthracene
An-NPs	anthracene-labeled nanoparticles
CMC	critical micelle concentration
DLS	dynamic light scattering
DVD	divinylbenzene
PAMAM	poly(amido amine)
PEG	poly(ethylene glycol)
PEG-MA	poly(ethylene glycol) methacrylate
PS	polystyrene
Py	pyrene
Py-NPs	pyrene-labeled nanoparticles
R_h	hydrodynamic radius
$[<R_h^{-1}>]^{-1}$	inverse z average hydrodynamic radius
SDS	sodium dodecyl sulfate
SEM	scanning electron microscope
PAH	polycyclic Aromatic Hydrocarbon
RPM	revolutions per minute
UV	ultraviolet